UNIVERSITY OF CRETE
DEPARTMENT OF CHEMISTRY

General Postgraduate Program

BIOINORGANIC LABORATORY

Master of Science Thesis

Hybrid Porphyrin Complexes with Ruthenium for Catalytic Oxidations.

Sofia Margiola

Master Thesis Supervisor: Athanassios G. Coutsolelos

HERAKLION 2016

ΠΑΝΕΠΙΣΤΗΜΙΟ ΚΡΗΤΗΣ
ΤΜΗΜΑ ΧΗΜΕΙΑΣ

Γενικό Μεταπτυχιακό Πρόγραμμα

ΕΡΓΑΣΤΗΡΙΟ ΒΙΟΑΝΟΡΓΑΝΗΣ

ΜΕΤΑΠΤΥΧΙΑΚΟ ΔΙΠΛΩΜΑ ΕΙΔΙΚΕΥΣΗΣ

Υβριδικά Πορφυρινικά Σύμπλοκα με Ρουθήνιο για Καταλυτικές Οξειδώσεις.

Σοφία Μαργιώλα

Υπεύθυνος Καθηγητής: Αθανάσιος Γ. Κουτσολέλος

ΗΡΑΚΛΕΙΟ 2016

Examination Committee

Athanassios G. Coutsolelos

Professor, Department of Chemistry, University of Crete

Constantinos J. Milios

Professor, Department of Chemistry, University of Crete

Thierry Tron

Researcher A, Research Director, University of Marseille

To my beloved ones…

Acknowledgments

I would first like to thank my thesis advisor Prof. Athanassios G. Coutsolelos of the Department of Chemistry at University of Crete. The door to Prof. Coutsolelos' office was always open whenever I ran into a trouble spot or had a question about my research or writing. He consistently allowed this paper to be my own work, but steered me in the right the direction whenever he thought I needed it.

I would also like to thank the experts who were involved in the validation survey for this research project: Dr. George Charalambidis and Prof. Ally Aukauloo. Without their passionate participation and input, the validation survey could not have been successfully conducted.

I would like to acknowledge Prof. Constantinos J. Milios of the Department of Chemistry at University of Crete and Dr. Thierry Tron Research Director, University of Marseille as committee members, and I am gratefully indebted to them for their very valuable comments on this thesis.

I would like also to thank the members of Bioinorganic Laboratory for their friendship and support, and for creating a cordial working environment.

Finally, I must express my very profound gratitude to my family and to my loved ones for providing me with unfailing support and continuous encouragement throughout my years of study and through the process of researching and writing this thesis. This accomplishment would not have been possible without them. Thank you.

Abstract

The sustainable production of clean energy constitutes one of the most important scientific challenges of the 21st century. Currently, the major part of the global energy supply is provided by carbon-based energy sources, which are connected to severe environmental issues, such as air pollution and the greenhouse effect. Consequently, it is crucial to turn to clean and environmentally friendly carbon-neutral alternatives that have the potential to meet the needs of present and future generations. In fact, every hour the sun provides our planet with more energy than what is consumed during a whole year. This fact has mesmerized researchers and makes the conversion of solar energy into fuel and electricity one of the most promising solutions to this problem.

Photosynthetic organisms are ubiquitous in nature; they are responsible for the development and sustenance of all life on Earth. They may be quite different, but all of them use the same basic strategy, in which light is initially absorbed by antenna proteins containing many chromophores, followed by energy transfer to a specialized reaction center protein, in which the captured energy is converted into chemical energy by means of electron-transfer reactions. However, for an artificial system, a more practical approach would be to use solar energy to split H_2O into molecular oxygen and hydrogen. This process requires the coupling of the two half-reactions: (i) oxidation of H_2O to generate the reducing equivalents (electrons) and (ii) reduction of protons to molecular hydrogen. Harnessing solar energy for the photoproduction of renewable fuels therefore requires interfacing several fundamental but challenging photophysical steps with complicated catalytic transformations.

In this thesis, the synthesis of a porphyrin–RuII polypyridine complexes where the porphyrin acts as a photoactive unit and the RuII polypyridine as a catalytic precursor is described. Comparatively, the free base porphyrin was found to outperform the ruthenium based chromophore in the yield of light induced electron transfer. Mechanistic insights indicate the occurrence of a ping-pong energy transfer from the ^{1}LC excited state of the porphyrin chromophore to the ^{3}MCLT state of the catalyst and back to the ^{3}LC excited state of the porphyrin unit. The latter, triplet–triplet energy transfer back to the chromophore, efficiently competes with fast radiationless deactivation of the excited state at the catalyst site. The energy thus recovered by the chromophore allows improved yield of formation of the oxidized form of the chromophore and concomitantly of the oxidation of the catalytic unit by intramolecular charge transfer. Also the catalytic properties of the dyads were investigated through photocatalytic reactions, using organic compounds as substrates for oxidative reactions.

Περίληψη

Η οικονομικά βιώσιμη παραγωγή καθαρής ενέργειας αποτελεί μία από τις σημαντικότερες επιστημονικές προκλήσεις του 21ου αιώνα. Στις μέρες μας, η πλειοψηφία του παγκόσμιου ενεργειακού εφοδιασμού παρέχεται από πηγές ενέργειας με βάση τον άνθρακα, γεγονός που συνδέεται με σοβαρά περιβαλλοντικά ζητήματα, όπως η ατμοσφαιρική ρύπανση και το φαινόμενο του θερμοκηπίου. Ως εκ τούτου, είναι ανάγκη ζωτικής σημασίας να στραφούμε σε καθαρές και φιλικές προς το περιβάλλον εναλλακτικές λύσεις, που έχουν τη δυνατότητα να καλύψουν τις ανάγκες των σημερινών και των μελλοντικών γενεών. Στην πραγματικότητα, κάθε ώρα ο ήλιος παρέχει στον πλανήτη μας με περισσότερη ενέργεια από ό, τι καταναλώνεται κατά τη διάρκεια ολόκληρου του έτους. Το γεγονός αυτό οδήγησε την επιστημονική κοινότητα σε εκτενείς μελέτες με σκοπό την μετατροπή της ηλιακής ενέργειας σε καύσιμα και σε ηλεκτρική ενέργεια.

Φωτοσυνθετικοί οργανισμοί υπάρχουν παντού στη φύση, είναι υπεύθυνοι για την ανάπτυξη και τη διατήρηση της ζωής στη Γη. Αν και διαφέρουν σε μεγάλο βαθμό, όλοι χρησιμοποιούν την ίδια βασική στρατηγική, στην οποία το φως αρχικά απορροφάται από πρωτεΐνες κεραίες που περιέχουν πολλά χρωμοφόρα, ακολουθεί μεταφορά ενέργειας σε ένα εξειδικευμένο πρωτεϊνικό κέντρο, στο οποίο η δεσμευμένη ενέργεια μετατρέπεται σε χημική ενέργεια μέσω των αντιδράσεων μεταφοράς ηλεκτρονίων. Ωστόσο, για ένα τεχνητό σύστημα, μια πιο πρακτική προσέγγιση θα ήταν η χρήση της ηλιακής ενέργειας για να διασπάσει το νερό σε μοριακό οξυγόνο και υδρογόνο. Αυτή η διαδικασία απαιτεί τη σύζευξη των δύο ημιαντιδράσεων: (i) οξείδωση του H_2O για να δημιουργηθούν τα αναγωγικά ισοδύναμα (ηλεκτρόνια) και (ii) αναγωγή των πρωτονίων σε μοριακού υδρογόνου. Η αξιοποίηση της ηλιακής ενέργειας για την φωτοπαραγωγή των ανανεώσιμων καυσίμων απαιτεί το συνδυασμό διαφόρων θεμελιωδών αλλά και απαιτητικών φωτοφυσικών διαδικασιών με περίπλοκες καταλυτικούς μετασχηματισμούς.

Σε αυτήν την εργασία, περιγράφεται η σύνθεση δυάδων προφυρίνης και πολυπυριδινικών συμπλόκων του ρουθηνίου, όπου η πορφυρίνη δρα ως χρωμοφόρο και το σύμπλοκο του RuII ως πρόδρομη καταλυτική μονάδα. Συγκριτικά, η ελεύθερη πορφυρίνη βρέθηκε να έχει καλύτερη απόδοση από χρωμοφόρα του ρουθηνίου όσο αναφορά την επαγόμενη από το φώς, μεταφορά ηλεκτρονίων. Οι μελέτες για το μηχανισμό, δείχνουν την εμφάνιση μιας πινγκ-πονγκ μεταφοράς ενέργειας από την ^{1}LC διεγερμένη κατάσταση του χρωμοφόρου πορφυρίνης στην κατάσταση ^{3}MCLT του καταλύτη και πίσω στο ^{3}LC διεγερμένη κατάσταση της μονάδας πορφυρίνης. Αυτή η triplet-triplet ενεργειακή μεταφορά πίσω στο χρωμοφόρο, ανταγωνίζεται αποτελεσματικά τη γρήγορη απενεργοποίηση της διεγερμένης κατάστασης του καταλύτη. Ως εκ τούτου, η ενέργεια που ανακτάται από τον χρωμοφόρο επιτρέπει τη βελτιωμένη απόδοση του σχηματισμού της οξειδωμένης μορφής του χρωμοφόρου, και ταυτόχρονα, της οξείδωσης της καταλυτικής μονάδας από ενδομοριακή μεταφορά φορτίου. Επιπλέον, οι καταλυτικές ιδιότητες των δυάδων ερευνήθηκαν μέσω φωτοκαταλυτικών πειραμάτων, με τη χρήση οργανικών ενώσεων σαν υποστρώματα για οξειδωτικές αντιδράσεις.

Table of Contents

1 Introduction

1.1 Porphyrin

1.1.1 General

The porphyrins and their derivatives have captured the interest of the scientific community since the 19th century due to their biological significance and their exceptional photophysical properties.[1] The porphyrin ring is heterocyclic macrocycle organic structure, composed of four modified pyrrole subunits interconnected at their α carbon atoms via methine bridges (=CH−). (Fig. 1.1)

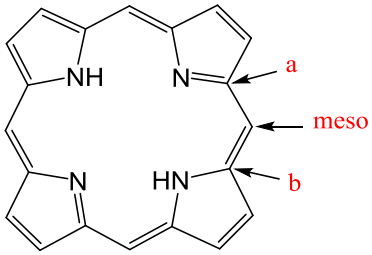

Figure 1.1: Structure of a Porphyrin.

The porphyrin ring is a conjugated system, constituted by 18 out of 26 π electrons in total, that participate in a delocalized system, agreeing with the Hückel rule for aromaticity.

The four N atoms of the porphyrin ring are sp^2 hybridized, with two of them forming a σ bond with hydrogen atoms while the other two do not. (Fig. 1.2). In the first two N atoms, every sp^2 orbital has an electron that forms a σ bond with two carbon atoms and one hydrogen atom. The lone pair of electrons occupies the p orbital (1) perpendicular to the plane of the porphyrin ring, thus, each nitrogen will contribute two electrons in the conjugated system. In the case of the N atoms which do not form bonds with hydrogen, (4) they are sp^2 hybridized as well. The lone pair of electrons is available for coordination with a metal. In perpendicular to the porphyrin ring, there is the p orbital (3) with an electron which forms a π bond with the adjacent carbon.

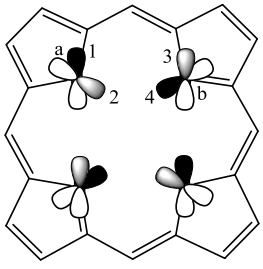

Figure 1.2: Porphyrin ring with N orbitals.

In ^{1}H NMR spectroscopy, porphyrins have a very characteristic pattern, because of the anisotropic effect of the porphyrin ring protection, the N-H protons appear at high fields (-2, -4 ppm). In contrast, the peripheral protons occur at low fields (8,10 ppm), because of the deprotection which exist as a result of the phenomenon called aromatic ring current.[2] (Fig. 1.3)

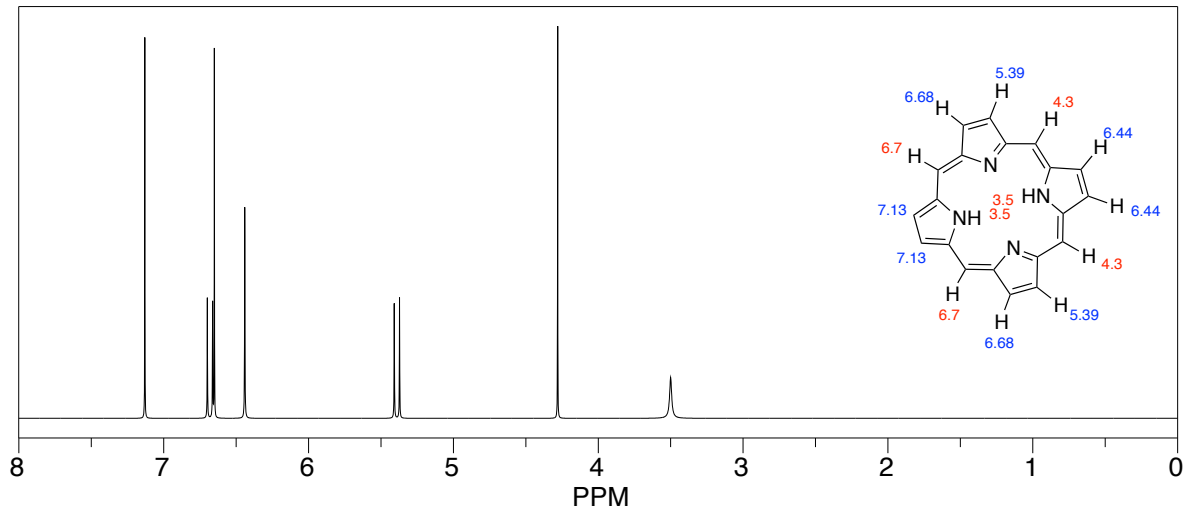

Figure1.3: 1H NMR prediction by ChemDraw Ultra.

In the visible spectrum, porphyrins have an intense absorption band at 400nm called Soret Band[3], which is a result of the delocalization of the porphyrin ring current. In the 450-800nm region, four weaker bands appear which are responsible for the rich color of porphyrins, known as Q Bands.

The porphyrins can participate in both electrophilic and radical reactions due to the aromatic nature of the porphyrin ring. The meso- positions have a higher electron density, making it more reactive. However, when the meso- positions are occupied, beta- positions can participate in electrophilic reactions.[3]

The porphyrin rings are generally stable under strong acidic or basic conditions. Strong bases such as alkoxides can remove two protons (Pka ~ 16) by the internal N atoms to form a dianion, while the two free atoms of N (Pka ~ 9) can be protonated by acids such as trifluoro acetic acid (TFA) to form a dication. The inner protons may also be replaced by a metal. There are a variety of metals (Zn, Cu, Ni, Sn) that can be introduced into the porphyrin cavity by using various metal salts.[1] The metallization can be reversible, and treatment with acid can achieve the demetallization of the porphyrin ring. The demetallization demands different types of acids and acidities for the removal of each type of metal.

Aromatic molecules such as porphyrins were always considering as planar, but references in a number of publications have proven that this assumption was indeed incorrect. The planar structure of porphyrin can be affected either by the metal ion or the peripheral ligands.[4,5] Macrocycle compounds, like the porphyrin rings, are very selective in relation to the size of the coordinated metal and offer them a very high stability because of the conjugated system. Structural studies and computer models have shown that ions with a spherical radius of 60-70pm are located directly in the central cavity of porphyrin rings,

while ions greater than 70pm, such as lanthanides (85-106pm) are located outside of the plane, defining the four nitrogen atoms of the porphyrin ring. (Fig. 1.4)

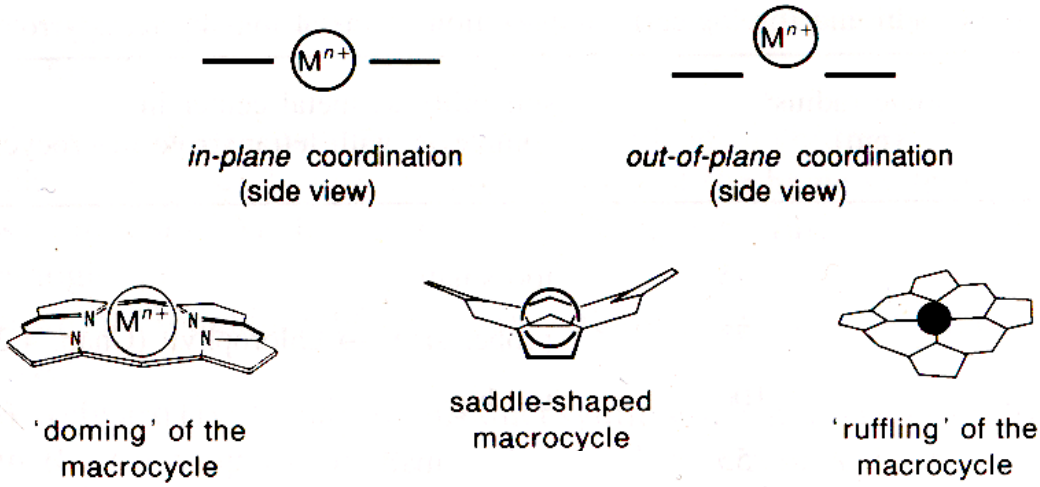

Figure 1.4: Typical geometrical configurations of metallated porphyrin ring.

The porphyrin rings are capable of "taking" and "giving" electrons, and thus, the processes of the first oxidation and the first reduction can be achieved with great ease. The formed anions or cations are considered quite stable. These abilities of light absorption and their easy redox make them the best energy transducers in biological systems.

1.1.2 The porphyrins in biological systems

Many significant biological processes occur because of porphyrin complexes and their properties, with one of the most important being photosynthesis. However, other porphyrin derivatives exist in major protein systems such as hemoglobin, myoglobin, cytochromes and peroxidases and catalases.

1.1.2.1 Chlorophyll

Photosynthesis is the only way our planet is able to capture solar energy and transform it into chemical energy. It takes place in photosynthetic centres of most plants and algae, as well as in active centers of cyanobacteria. Photosynthesis occurs in the chloroplasts of plants where the principal receptor is chlorophyll a. Chlorophyll a is a substituted porphyrin, specifically where the four nitrogen atoms of the porphyrin ring create a bond with the magnesium ion to form a porphyrin magnesium. (Fig. 1.5)

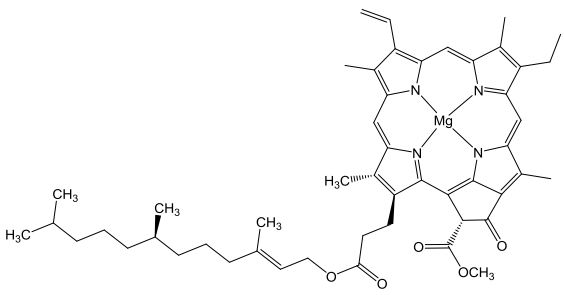

Figure 1.5: Stucture of chlorophyll a.

1.1.2.2 Heme

Hemoproteins is a family of metalloproteins called hemes, that are cofactors consisted by porphyrin derivatives metallated with Iron (Fe^{2+}). Hemes are most commonly recognized as components of hemoglobin, the red pigment in blood, but are also found in a number of other biologically important hemoproteins such as hemoglobin, myoglobin and cytochromes.

Hemoglobin

Hemoglobin is a protein compound of red blood cells, which carry oxygen from the respiratory organs to the rest of the body. It is formed by two different pairs of protein chains and four hemes as prosthetic groups. (Fig. 1.6). The active centre is the protoporphyrin IX, which is linked to the protein through a histidine imidazole. These prosthetic groups have such a crucial role in life due to the presence of iron, which binds oxygen and transfers it to all the tissues. Haemoglobin is also able to bind other gases such as carbon dioxide, giving it an additional role to oxygenating all the body's tissue. As haemoglobin carries carbon dioxide, this allows for the safe transfer and disposal of this gas during respiration.

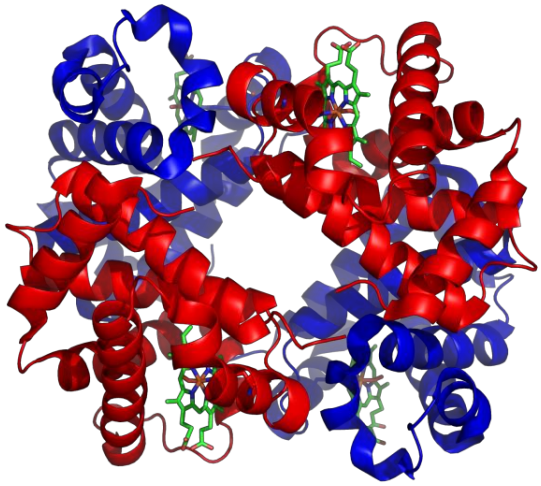

Figure 1.6: Structure of human hemoglobin. The proteins α and β subunits are in red and blue, and the iron-containing heme groups in green.

Myoglobin

Myoglobin belongs to hemoproteins family; it is an iron- and oxygen-binding protein which resembles hemoglobin as it consists of α-, β-, γ- and δ- chains. Despite the structural and role similarities, myoglobin exists only as a monomer, thus, its molecular weight is ¼ to that of hemoglobin. (Fig. 1.7) Also as a monomer, myoglobin only has one binding site for oxygen on its one heme group, which leads to its affinity for that oxygen being very high compared to hemoglobin. (Fig 1.7b). This high affinity affects the release of oxygen, which can take place only at extremely low oxygen partial pressures. Increased concentration of myoglobin is seen in the serum after trauma to either skeletal or cardiac muscle.

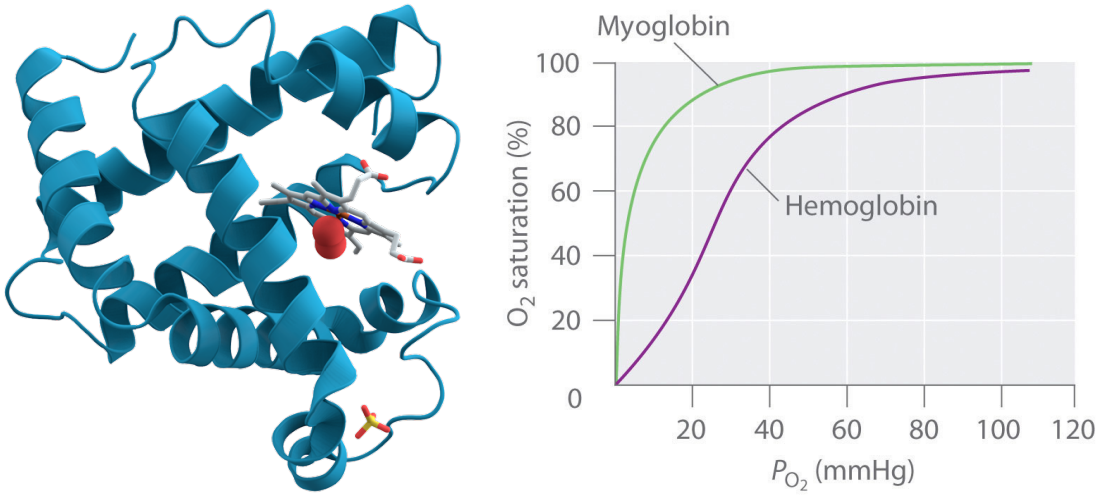

Figure 1.7: Structure of myoglobin(left),Myoglobin and haemoglobin oxygen affinities(right).

1.1.2.3 Cytochrome Complexes

Cytochromes consist a different family of hemeproteins, which participate in the electron transfer chain in mitochondria. The electron transfer is related to the presence of the redox couple Fe (III) -Fe (II). The cytochromes have the ability to directly react in the nitrogen cycle and enzymatic reactions associated with photosynthesis. Among the 50 identified cytochromes, the cytochrome c is the most studied. The cytochromes can be classified by both the nature of the system of the porphyrin ring and the spectroscopic data of pyrido- derivatives. (Tab. 1.1)

Cytochrome type	Prosthetic group (Fig. 1.8)	Band a in UV-Vis. spectra
Cytochrome a	Heme A	>570 nm
Cytochrome b	Protoporphyrin IX	555-560 nm
Cytochrome c	Protoporphyrin IX	548-552 nm

Table 1.1: *Spectroscopy of Pyrido-derivatives*

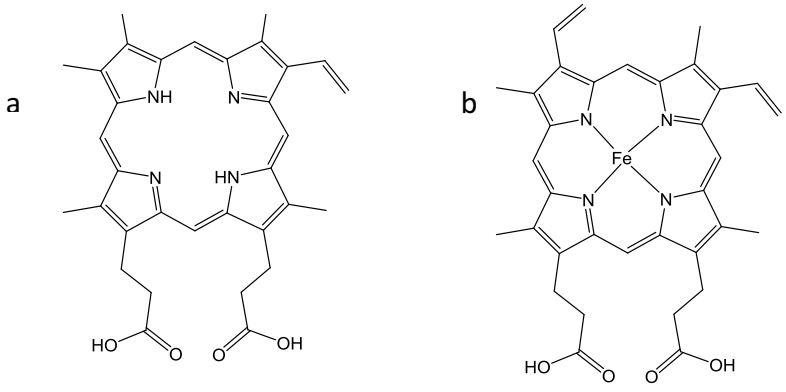

Figure 1.8: Stucture of Protoporphyrin IX (a) and Heme A (b).

Cytochrome C

The cytochrome C is comprised of a heme group which is covalently linked to the protein via a thioether bridge. (Fig.1.9) Most types of cytochromes c are low spin, while the axial substituents are histidine (His-18) and methionine (Met-80) (cytochromes c and c2) or histidine (cytochrome c3). The protein contains a cysteine which is coordinated along vinyl bonds. The crystal studies of cytochrome demonstrate that the binding of the heme to the polypeptide chain takes place via covalent bonds between cysteines 14 and 17. The cytochrome c is an enzyme, which is very stable in both temperature and pH changes while it can easily be reduced by sulphite and ascorbic acid.

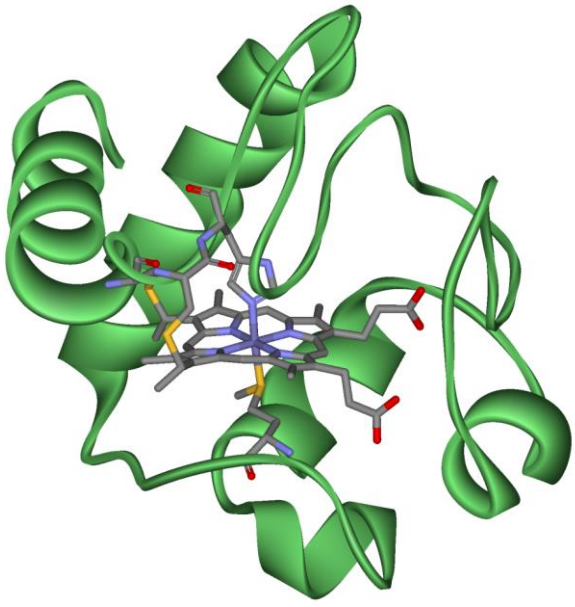

Figure 1.9: Structure of cytochrome c

Cytochrome 450

Cytochrome 450 is another family of hemeproteins which means they containing heme as a cofactor. Cytochromes 450 are able to use either small or large molecules as substrates in enzymatic reactions. They are monooxygenases, which means that carrying an oxygen atom, and catalyse the hydroxylation of RH substrate with molecular oxygen by reductive cleavage of the bond C-C. The term P450 is obtained from the spectrophotometric peak at the wavelength of the absorption maximum of the enzyme (450 nm) when it is in the reduced state and complexed with carbon monoxide.

1.1.3 Nomenclature of Porphyrins

The porphyrins, as previously mentioned, are consisted of four modified pyrrole subunits interconnected at their α carbon atoms via methine bridges (=CH−). In total, a porphyrin ring has 20 carbon and four nitrogen atoms and is a conjugated system of 18 π electrons.

A porphyrin ring has the α-positions (1,4,6,9,11,14,16,19) the β-positions (2,3,7,8,12,13,17,18) and meso-positions (5,10,15,20). The positions of nitrogen atoms are named according to the numbers seen below 21, 22, 23, 24. (Fig. 1.10) The number of substituents which may be present on the porphyrin ring are denoted by the numerical prefixes di-, tri-, etc.

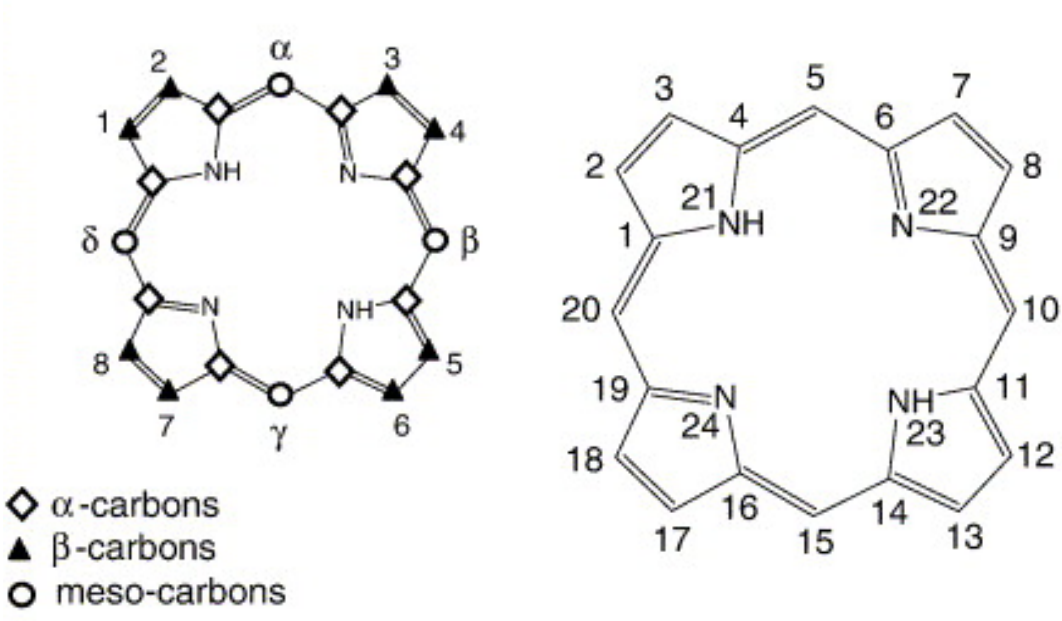

Figure 1.10: Porphyrin ring numbered according to IUPAC.

The cis, trans prefixes are used to denote the configuration of the porphyrin in space. The axial ligands can also be characterized when we ascertained the layouts with the letters a and b, (where 'a' denotes below the planar of the porphyrin, while 'b' denotes above it).

1.1.4 Applications

As discussed in section 1.2, the porphyrins and their derivatives have a crucial role in the most important biological processes. Additional applications in different fields may be found because of their low toxicity, their stability under harsh conditions (temperature and pH) and their photophysical properties. [4]

The porphyrin systems can be broadly used in Medical and Pharmaceutical chemistry as molecular sensors, in molecular recognition in photodynamic therapy (Photo Dynamic Therapy, PDT), as antiviral drugs, molecular information storage and non-linear optics. [6,7]

Another field that has gained great interest by the scientific community is the development of DSSs (Dye-sensitized solar cell)[8]. Porphyrins are widely used as photosensitizers in these photoelectrochemical systems, both in p-type and n-type DSSs. The DSSs can operate as a photoanode (n-DSC), where photocurrents result from electron injection by the sensitized dye and as photocathodes (p-DSCs)[9,10] where dye-excitation is followed by rapid electron transfer from a p-type semiconductor to the dye (dye-sensitized hole injection, instead of electron injection). Such p-DSCs and n-DSCs can also be combined to construct tandem solar cells (pn-DSCs).

The porphyrins and metalloporphyrins are also ideal for studying light harvesting systems), electron transfer and catalytic oxidation and redox reactions.[11] They may have both the roles of the chromophore and the catalyst or be the photosensitizer coupled to a catalytic moiety or to protein with catalytic properties[12]. Currently it is paramount to comprehend the "communication" between the moieties which participate in these catalytic systems. The factors which can affect the catalytic ability of a system are the distance, the arrangement and the geometry because this controls the inner communication of the moieties.

1.1.5 Synthesis

Over the last century, the synthetic procedure of porphyrins has undergone great changes[13]. It is currently possible to synthesize any desirable porphyrin ring through different methodologies and techniques depending on their symmetry features. For example, the simple polymerization of monopyrroles, the MacDonald route, using two dipyrromethanes (the [2+2] approach) and one of its variants (the [3+1] method). Other synthetic procedures involve cyclization of an open-chain tetrapyrrole (the so-called a,c-biladienes) which possesses no symmetry restrictions.[14,15]

1.1.5.1 Porphyrins via Monopyrrole Tetramerization

The tetra-aryl porphyrins are synthetic porphyrins which have various applications. The easiest way to synthesize symmetrical porphyrins is the condensation of pyrrole and the corresponding aldehyde under acidic conditions. This process was first developed by Rothemund[17] and then modified by Alder and Longo.[16,17] The final optimization of the method came from Lindsey's group which succeeded in a high yield by using a high dilution two-step reaction between arylaldehydes and pyrrole, in presence of a Lewis acid catalyst (usually BF_3-etherate) and using a quinone such as 2,3-dichloro-5,6-dicyanobenzoquinone (DDQ) to oxidize the porphyrinogen to porphyrin.[18,19] (Fig. 1.11)

1.1.5.2 Porphyrins via MacDonald [2+2] synthesis

The development of the so-called MacDonald[20] synthesis was a game-changer for porphyrin synthesis, with the key to this success being the synthesis of dipyrromethane. The method is a condensation of two dipyrromethanes with appropriate bridging carbons which results in two porphyrin products, as the dipyrromethanes can react in either of two orientations related by a 180° rotation of one of the dipyrromethanes. (Fig. 1.12)

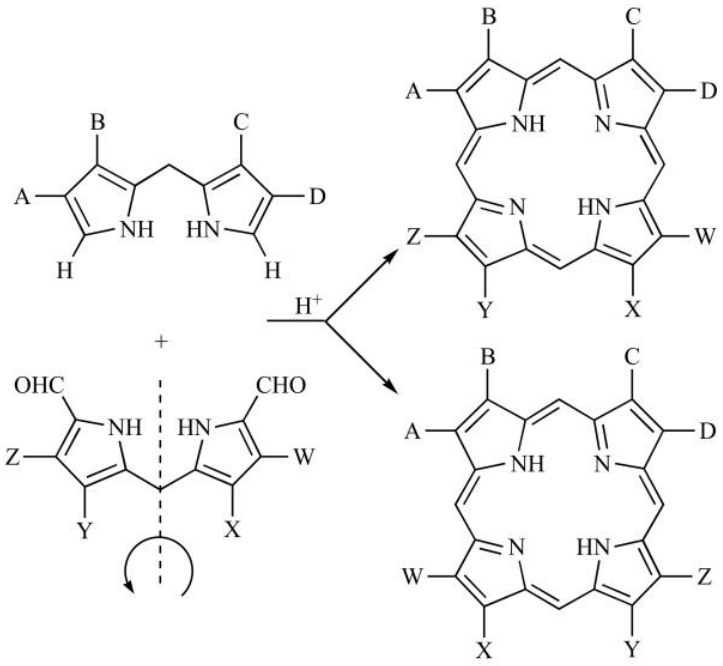

Figure 1.11: Synthesis of a porphyrin (MacDonald [2+2]).

1.1.5.3 Porphyrins via MacDonald [3+1] synthesis

The [3+1] synthetic procedure is based on that already developed by the MacDonald approach. However, instead of condensing two dipyrromethanes (hence [2+2]), a tripyrrane is reacting with a monopyrrole bearing the two "bridging" carbon atoms.[21,22] (Fig. 1.13)

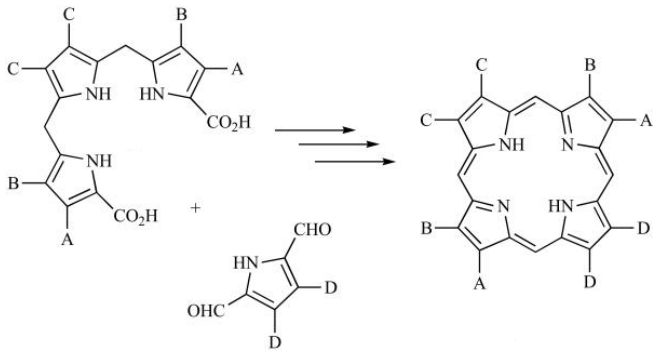

Figure 1.12: Synthesis of a porphyrin (MacDonald [2+2]).

1.1.5.4 *Porphyrins via a,c-biladiene salts synthesis*

The synthesis of a porphyrin with a completely unsymmetrical array of substituents must progress through open-chain tetrapyrrolic intermediates[23]. The most commonly used open-chain precursors of choice have been shown to be 1,19-dimethyl-a,c-biladiene salts. Fig. 1.14

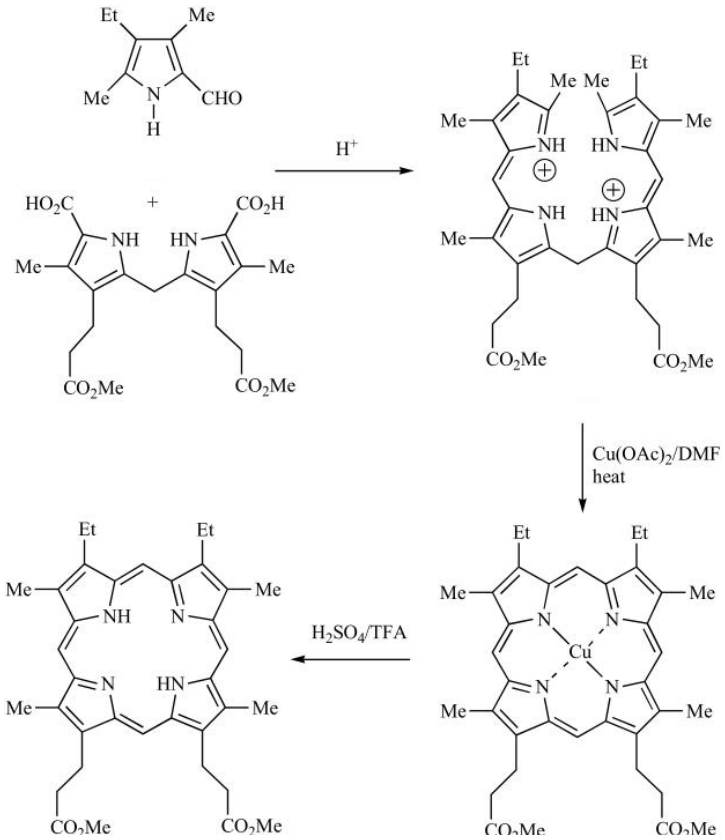

Figure 1.13: Synthesis of a porphyrin via a,c-biladiene salts.

1.1.5.5 *Porphyrins via synthesis with different meso- substituents in aqueous media*

The current synthetic procedures for non-symmetrical porphyrins which are gaining much interest in the scientific community are taking place in aqueous media, a method that was developed by two groups: Gryko's and Balaban's[15]. Their method is very useful for synthesizing various substituted porphyrins under mild conditions that avoids scrambling and has been a long sought after reaction for the past two decades. This method , in aqueous media, is also an environmentally friendly and avoids the use of rather hazardous reagents. It is an effective method to prepare trans-A_2B_2-, A_3B-and trans-AB_2C-porphyrins and offers good yields of porphyrins (9–25%). During this method, the reaction conditions make it possible to direct the cascade of acid-promoted Friedel–Crafts reactions between dipyrromethanes and aldehydes towards the intermediate porphyrinogens. This is being oxidized by a quinone such as 2,3-dichloro-5,6-dicyanobenzoquinone (DDQ) or Tetrachloro-1,4-benzoquinone (p-chloranyl). (Fig.1.15)

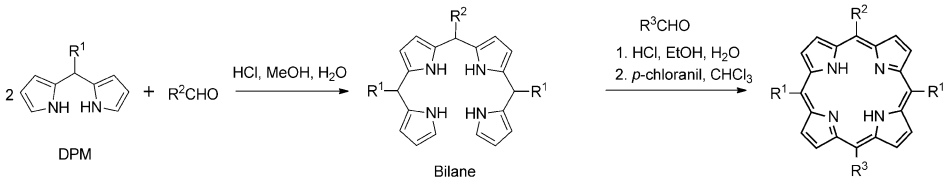

Figure 1.14: Synthesis of a porphyrin (Gryko and Balaban).

1.2 Ruthenium-Polypiridyl Complexes

1.2.1 General

Over the last few decades, the ruthenium-polypiridyl complexes captured the interest of the scientific community because of their remarkable chemical stability and photophysical properties[24,25]. Ruthenium(II) trisbipyridyl complexes have especially been thoroughly studied and are known as chromophores in a wide range of applications in different areas, such as solar energy related research[26–31], molecular wires[32–34], sensors and switches[35] as well as therapeutic agents[36].

1.2.2 Absorption of $[Ru(bpy)_3]^{2+}$

The well-studied $[Ru(bpy)_3]^{2+}$ has octahedral geometry of D3 symmetry. (Fig. 2.1) At the UV-region, the absorption spectrum is dominated by ligand-centered (LC) $\pi \rightarrow \pi^*$ transition at 285 nm (ε ~ 8×104 $M^{-1}cm^{-1}$). The spectrum in the visible region has a characteristic intense metal-to-ligand charge transfer (^{1}MLCT) band at 450 nm (ε ~ 104 $M^{-1}cm^{-1}$), caused by the transition from a dπ metal orbital to a ligand based orbital (π_L^*)[26]

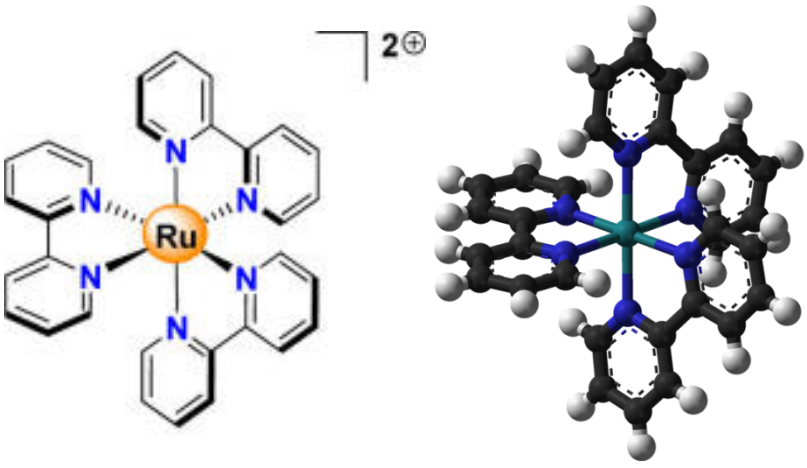

Figure 2. 1: Structure of [Ru(bpy)3]2+.

1.2.3 Cyclic Voltammetry

In the cyclic voltammogram (CV) of $[Ru(bpy)_3]^{2+}$ (Fig. 2.2), a reversible oxidation involving a metal-centered orbital (dπ) appears at 0.88 V and three closely spaced ligand-localized reductions at –1.74, −1.93 and –2.17 V, where each added electron is localized on a single ligand.[24,25] In the ^{3}MLCT excited state, formally $[Ru^{III}(bpy)_2(bpy^{\bullet-})]^{2+}$, the metal is oxidized and one ligand is reduced, and the complex is therefore both a strong reductant and oxidant.

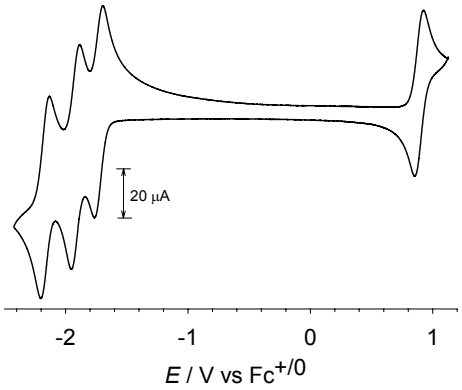

Figure 2. 2: Cyclic voltammogram of $[Ru(bpy)_3]^{2+}$.

1.2.4 Photo-induced Electron Transfer

As previously mentioned, $[Ru(bpy)_3]^{2+}$ type complexes have a distinct absorption in the visible region (λmax ≈ 450 nm), and upon illumination, one electron in a metal- centered t_{2g} orbital is excited to a ligand-centered π* orbital.

In this metal-to-ligand charge transfer state (MLCT), the ruthenium centre has formally been photo-oxidized to RuIII, while the bpy ligand backbone has undergone a single electron reduction. The initially photo-generated state, which is the lowest excited singlet state ($^1[Ru(bpy)_3]^{2+}$*), is short-lived and undergoes rapid intersystem crossing to yield a long-lived triplet state, $^3[Ru(bpy)^3]^{2+}$*, that has the potential to engage in single- electron transfer. The electronic configuration of this excited state can thus be described as a $^3[(d\pi)^5(\pi bpy^*)^1]$ with almost exclusively triplet character. This excited triplet state has a long lifetime because the conversion to the singlet state is spin- forbidden and decays to the ground state on the microsecond time-scale. The excited state is therefore sufficiently long-lived to partake in bimolecular electron-transfer reactions, which can compete with deactivation pathways. The photo-excited state has the ability of being both more oxidizing and more reducing than the ground state of $[Ru(bpy)_3]^{2+}$, and this dual nature of the excited state enables it to serve either as a single-electron oxidant or as a reductant.[24,25,37–39] (Fig 2.3)

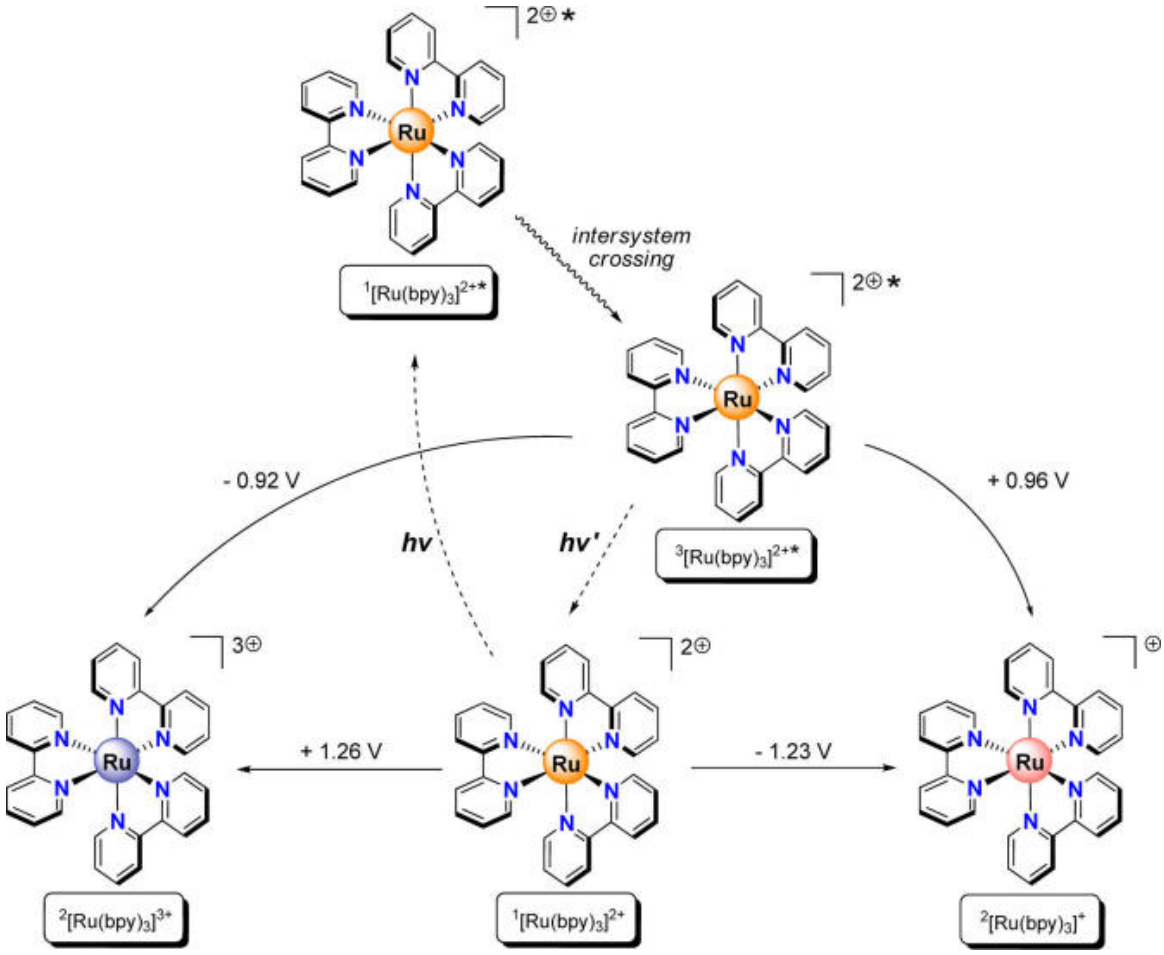

Figure 2. 3: Simplified Picture of the Photochemistry of $[Ru(bpy)_3]^{2+}$.

1.1.5 Synthesis

1.2.5 $[Ru(bpy)_3]^{2+}$ type complexes

The most common synthetic approach to ruthenium(II) polypyridyl complexes starts from $RuCl_3 \cdot xH2O$. The first part is a reflux of $RuCl3 \cdot xH2O$ in DMF with a thermally insensitive bipyridyl (bpy) ligand, transforming it into cis-$Ru(bpy)_2Cl_2$.[40] A third chelate is then easily introduced to give the bisheteroleptic $[Ru(bpy)2(bpy')]^{2+}$ complex. With heat-sensitive ligands, $Ru(DMSO)_4Cl_2$[41] or $Ru(CH_3CN)_4Cl_2$[42] are convenient intermediates, since the synthesis is performed under less vigorous conditions.

The spectroscopic and redox properties of the ground state and excited state of the ruthenium(II) polypyridyl complexes can be modified with the incorporation of three different pp ligands into the coordination sphere. Several synthetic routes for the preparation of trisheteroleptic $[Ru(bpy)(bpy')(bpy'')]^{2+}$ complexes have been developed the last few years.

One of the most popular and widely studied methods was developed by Meyer and co-workers, starting from $[Ru(CO)_2Cl_2]_n$.[43–45] Another interesting approach was recently presented by Mann's group[46], suggesting the use of the easy photochemical displacement of benzene in [(benzene)Ru(bpy)Cl] Cl to give $[Ru(bpy)(CH_3CN)_3(Cl)]Cl$ and $Ru(bpy)(CH_3CN)_2Cl_2$. As a result, the insertion of two additional bidentate ligands can be achieved. The most popular method starting from $Ru(DMSO)_4Cl_2$ was developed by Grätzel and co-workers.[47] The first bipyridyl ligand is introduced in refluxing chloroform. The choice of solvent is crucial since protic solvents (methanol or ethanol) or high boiling solvents (DMF or DMSO) were reported to give mixtures of mono- and bis-substituted products.

1.2.6 Synthesis of oligopyridines

The synthesis of 2,2'-bipyridine and 2':6',2''-terpyridine as well as the coordination chemistry of these and other oligopyridines has been extensively investigated. They captured scientific interest because of their redox stability, ease of functionalization and capability to complex metal ions. All of these properties enabled their wide applications in chemistry.

Nowadays, there is a large variety of synthetic procedures for both 2,2'-bipyridine and 2',2': 6',2''-terpyridine.[48,49] Different coupling methods have been applied in the preparation of 2,2′-bipyridines, such as oxidative coupling of pyridines using raney nickel or palladium on charcoal.[50] The yield of 2,2′-bipyridine, however, is small and only minor amounts of 2,2′:6′,2′′-terpyridine are formed. Other methods such as the copper mediated Ullmann coupling of halopyridines also showed low yields.[51]

High yields were achieved through the use of nickel catalyzed couplings of halopyridines[52], or the ipso-substitution on sulfoxide-pyridyl compounds by 2-pyridyllithium.[53] More recent coupling strategies for the preparation of oligopyridines have relied on the palladium catalyzed cross-coupling reactions of pyridyl-boron (Suzuki)[54], pyridyl-tin (Stille)[55], and pyridyl-zinc (Negishi)[56] reagents.

Various synthetic approaches[48] have also been suggested for 2':6',2''-terpyridine, most of them are multistep syntheses have been developed by the groups of Kröhnke[57], Potts[58,59] and Jameson[60] (Fig. 2.4). They all depend on the isolation of a suitably substituted enone. Subsequent reaction with the enolate of acetylpyridine in the presence of NH_4OAc gives the corresponding 2,2′:6′,2′′-terpyridine. The advantages of these methods lie in the opportunity to introduce asymmetry in the terpyridyl ligand.

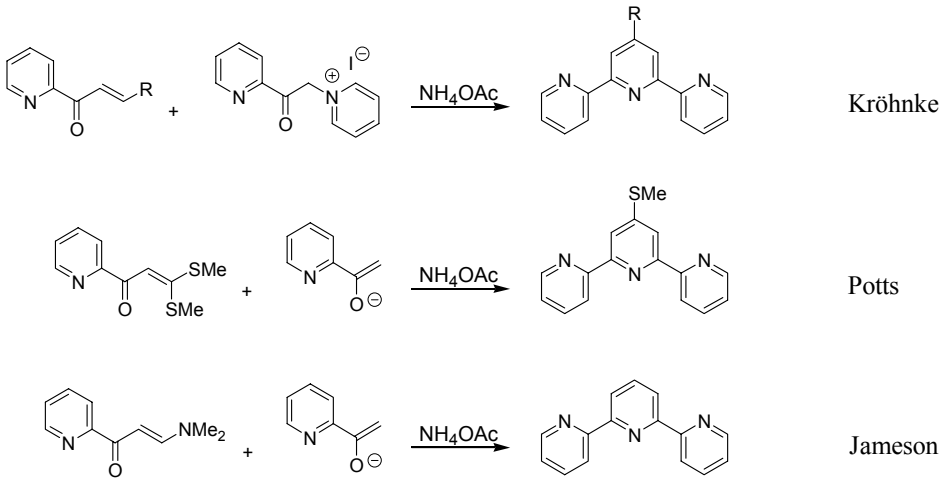

Figure 2. 4: Synthesis of 2,2′:6′,2′′-terpyridine

1.3 Artificial Photosynthesis

Rising levels of atmospheric carbon dioxide and the related rise in global temperature, which in part is due to the use of fossil fuels, have caused great worry to the world. Scientists have been calling for attention to this issue because it is not only a progressing environmental problem, since the global average surface temperature continue to rise, but as the human population and the global energy consumption also grow, the energy crisis comes to surface.[61–63] For this reason, it is crucial to develop environmentally sustainable energy systems. Among the various available renewable sources, the sun is the most available and abundant energy source which indicates that solar energy will play an increasingly important role in the future.

1.3.1 Photosynthesis in nature

Photosynthesis is the natural process where solar energy converts to chemical energy through photo-induced oxidation of water. The enzyme responsible for this process is the Photosystem II where are two functional moieties: a chromophore, where photo-excitation produces charge-separation resulting in a reductant and a strong oxidant on either side of the membrane; and a catalyst, capable of accumulating sufficient charge and oxidizing power to oxidize two water molecules into oxygen, protons, and reducing equivalents.[64,65] After a photonic excitation of the chlorophylls is indicated, the sequence of electron transfer begins.[66] (Fig. 3.1)

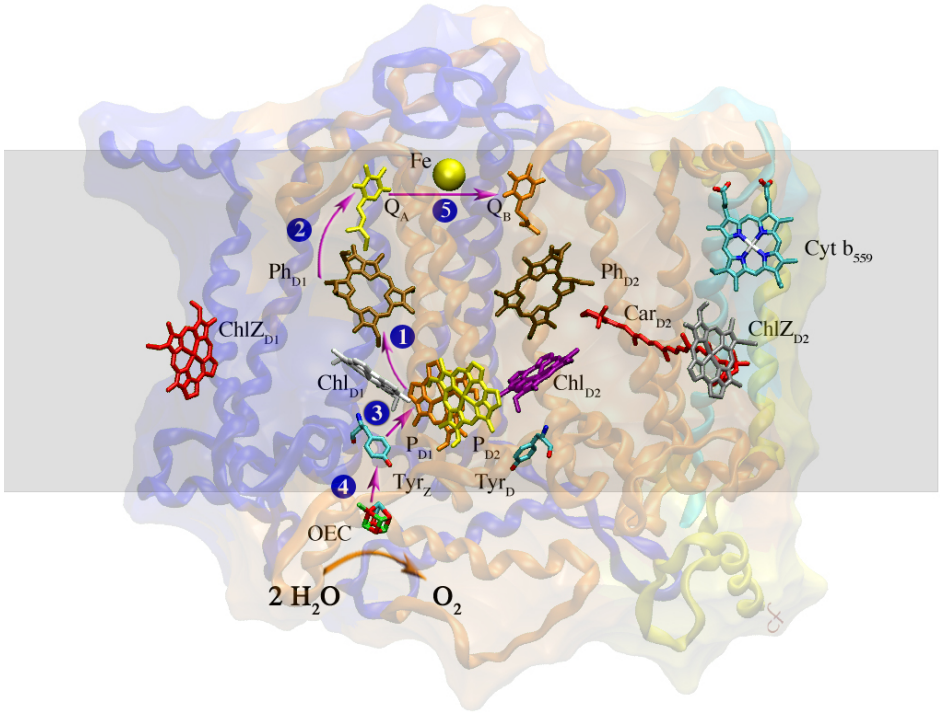

Figure 3 1: Map of the main cofactors of PSII. The arrows show the electron transfer steps.

Step 1: Light induced charge separation: charge separation takes place between pigment molecules very rapidly after excitation of the chlorophylls in the enzyme. A radical pair is detected a few picoseconds after excitation and this appears to form a chlorophyll (PD1) cation and a pheophytin (PhD1) anion.

Step 2: The pheophytin anion radical rapidly donates an electron to a quinone (QA) thereby stabilizing the charge-separated state.

Step 3: The highly oxidizing chlorophyll cation extracts an electron from a tyrosine residue (TyrZ). The tyrosine's phenolic carbonyl group loses a proton as the tyrosyl radical forms.

Step 4: The neutral tyrosyl radical then goes on to oxidize the Mn ions of the Mn complex.

Step 5: The semiquinone anion formed is further stabilized by a lateral electron transfer step to a second quinone, QB.

After one round of excitation, the plastoquinone is only partially reduced and the Mn cluster has increased in valence. This step occurs with a quantum yield of 90% and results in a relatively stable intermediate that is stable for tens of seconds to minutes. In order to complete the reduction of plastoquinone, another photo-excitation must take

place. The oxidation of water, however, takes a full four photo-excitation cycles. Photosystem II performs the difficult work of coupling one-electron reactions (the photo-excitation), to multi-electron reactions such as the reduction of plastoquinone (2 e^-) and the oxidation of water (4 e^-).

The reducing equivalents are transported by redox couples and ultimately used to generate transmembrane proton gradients and synthesize adenosine triphosphate (ATP, a biological energy carrier that is used by many enzymes) and to synthesize the biological two-electron reducing agent β-nicotinamide adenine dinucleotide phosphate (NADPH).

1.3.2 Water Oxidation in Photosystem II

Water oxidation in nature is catalyzed by the oxygen evolving complex (OEC) in Photosystem II (PS II) driven by light. Protons and electrons extracted from water are then delivered to Photosystem I (PS I) for the reduction of CO_2 to carbohydrates.

The manganese cluster, known as the oxygen evolving complex (OEC) catalyzes the water oxidation reaction. It is composed of four manganese ions, bridged by oxo- ligands. Calcium chloride and carbonate ions are known to be present at the OEC but their roles are unclear as of yet. The mechanism for the removal of four electrons and four protons from two substrate water molecules is still subject to speculations.[67] The main obstacle to the understanding of this mechanism is the lack of knowledge concerning the structure of the OEC. (Fig. 3.2) Recent X-Ray diffraction structures[68,69] are impeded by lack of resolution and by the reduction of the high valence Mn ions back to MnII by the X-ray beam.[70] While the electronic structure of the different S-states, substrate binding, calcium/chloride binding, and function of amino acid side chains are still a matter of debate, it is widely accepted that the substrate waters undergo deprotonation as the valence state of the Mn cluster increases[71,72], compensating for charge accumulation and preventing large increases in the redox potential. Different possible pathways for the eventual formation of the oxygen–oxygen bond have been proposed.

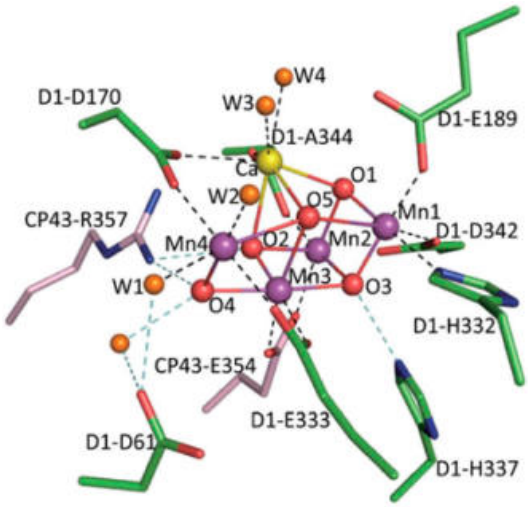

Figure 3 2: Structure of the manganese calcium cubane, Mn_4Ca, located in the OEC.

1.3.3 Mimicking photosynthesis

The photosynthetic process has inspired many research groups over the last few decades. The investigation of natural photosynthesis and the understanding of its basic principles at a molecular level[73] led to the concept of artificial photosynthesis, defined as the conversion of solar energy into fuels.

The most basic molecular device relevant to natural photochemical processes should be composed of a photosensitizer linked to an electron donor on one side and to an electron acceptor on another side. For an artificial photosynthetic system to be efficient, it must be capable of absorbing a photon by a chromophore (photosensitizer)(1), forming a charge-separated state by transferring the electron to a reduction catalyst, usually via a primary acceptor(2), accepting and accumulating two consecutive electrons at the reduction catalyst. This subsequently uses these to reduce two protons to molecular hydrogen(3), allowing regeneration of the chromophore by transfer of an electron from the oxidation catalyst, generally via a primary donor(4). After the transferring of four consecutive electrons, one by one, from the oxidation catalyst, the oxidation catalyst is regenerated by a formal one-step transfer of four electrons from two molecules of H_2O to generate one molecule of O_2 and four protons(5).[64,74]

Coupling two catalytic reactions can be a very complex procedure. In this case it involves the same number of electrons on a single molecule, requiring the rates for the catalytic reactions to be faster than the recombination rates. Furthermore, it is considerably more challenging when the two reactions performed do not involve the same number of electrons. Water splitting belongs to the latter case. In particular, this reaction requires the coupling of a $2e^-$ reduction (H+ reduction) and a $4e^-$ oxidation reaction (H_2O oxidation). After accumulating two charges, proton reduction occurs, while the oxidation of water would still require two more oxidizing equivalents. However, charge accumulation must be compensated for in order to maintain the efficiency of the primary photophysical events, regardless of the redox state of the system. Similarly, the conditions for the reduction reaction and the oxidation reaction might be different and must be accounted for in the final device.

A sophisticated technique to avoid this obstacle was developed recently by designing a photochemical cell in which the oxidation and reduction reactions are separated. In such a system we could imagine the oxidation catalyst (Cat_{ox}) linked by a photosensitizer to an anode and a reduction catalyst (Cat_{red}) grafted to a cathode (Fig. 3.3). [66] The electrons from the oxidation half-cell could be transferred through an electrical connection between the electrodes, to the reduction half-cell, while protons move in the opposite direction through a selective membrane. The efficiency of a photoactive molecular catalyst demands the five requirements previously mentioned, even in the case of a compartmentalized photochemical cell. However, the use of two separated compartments with surface-bound catalysts prevents intermolecular short-circuiting reactions between the photo-catalysts and

between the photo-catalysts and the reaction products. Other benefits inherent to tethering catalysts to surfaces are the preclusion of diffusion and being able to take advantage of well-researched semiconductor surfaces. Large band-gap semiconductor surfaces like TiO_2 offer very fast injection rates for electrons from the excited state of attached chromophores to their conduction band contributing to the necessary control of directionality of electron transfer.

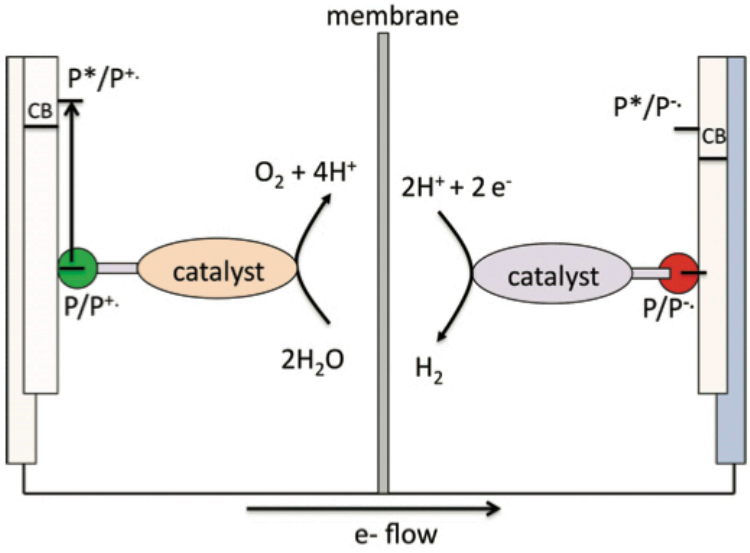

Figure 3 3: Schematic view of a photoelectrochemical cell for water splitting using molecular based materials fixed on semiconducting electrodes

1.3.4 The Water Oxidation Catalyst (WOC)

At a first glance, the oxidation of H_2O seems to be a straightforward transformation, because of its structural simplicity of starting material and products. However, this procedure is definitely not an easy accomplishment because although the majority of redox processes in nature are single- or two-electron processes, the oxidation of H_2O requires the transfer of four electrons and additionally rearrangement of multiple bonds and formation of the O−O bond.

Because of the complexity and the high oxidation potential required to oxidize H_2O, this half reaction is currently considered to be crucial in the development of a sustainable artificial solar fuel system. It is necessary for the catalyst to be capable of accumulating four oxidizing equivalents and operating close to the thermodynamic potential of H_2O oxidation. Also, the formation of damaging high-energy intermediates needs to be avoided as they can reduce the longevity of the WOC. An ideal WOC should therefore be fast, amenable to interfacing with photosensitizing materials, and stable to oxidative, hydrolytic, and thermal degradation during turnover.[75]

Multi-electron-transfer catalysis can be facilitated by synchronizing proton and electron-transfer events, via proton-coupled electron transfer (PCET), and is essential in many biological and chemical processes. PCET permits the total charge of a chemical species to remain unchanged, whereas just single electron transfer, without the loss of a proton, leads to charge accumulation and high-energy intermediates. Coupling electron transfer to proton transfer may also allow the accumulation of multiple redox equivalents and influence reaction pathways and energetics of a certain chemical reaction. This is an essential feature in realizing the four-electron oxidation of H_2O in artificial photosynthesis.[76–78]

1.3.5 Insight into Artifical Water Oxidation Catalysts mechanism

There is an existing requirement on WOCs to produce stable high- valent metal–oxo species at low redox potentials, to be able to partake in the complicated process of multi-electron oxidation of H_2O. To enable the rational design of molecular complexes that can fulfill this requirement, extensive research has been directed toward elucidating and understanding the fundamental steps of H_2O oxidation. One step in particular that needs to be better understood is the mechanism(s) for the O–O bond formation. Despite the experimental difficulties in determining the reaction mechanisms, some progress has been made, which has yielded two major mechanistic pathways for H2O oxidation (Fig. 3.4): (i) solvent water nucleophilic attack (WNA) and (ii) interaction of two M–O units (I2M).[39]

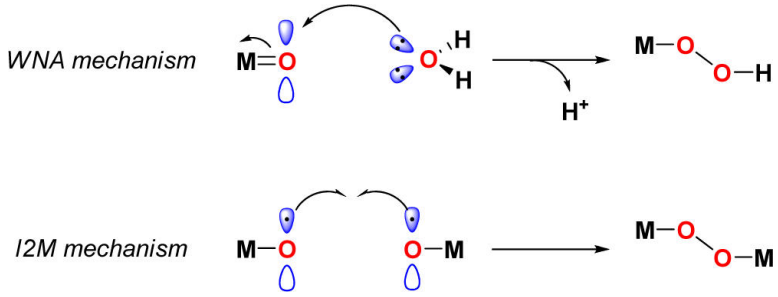

Figure 3 4: Schematic Representation of the Two Mechanistic Pathways for O–O Bond Formation for Single- Site and Dinuclear Artificial WOCs.

However, despite this mechanistic progress, there still exists a need for the development of a better understanding regarding the ligand-dependent preferences of the two mechanisms, and the parameters that favour one mechanism over the other.

The first complex capable of mediating the four-electron-four-proton oxidation of H_2O was reported by Meyer's group in 80s.[79,80] The complex responsible for this breakthrough was a dinuclear µ-oxo-bridged ruthenium complex, commonly known as the "blue dimer" due to its characteristic blue color (Fig 3.5). Although the turnover number (TON; defined as moles of produced product per mole of catalyst, nO_2/ncat), 13.2[81], and TOF, 4.2×10^{-3} s^{-1} [82], were moderate when using Ce^{IV} as oxidant, this seminal study proved that the demanding multi-electron oxidation of H_2O to O_2 was indeed possible. Since then, a variety of dinuclear Ruthenium complexes have been synthesized and studied as WOCs.

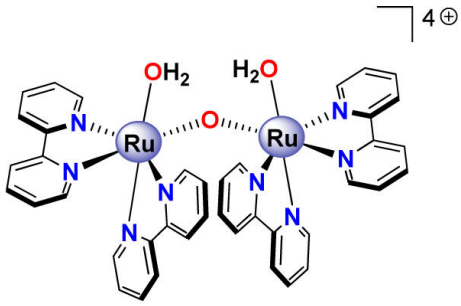

Figure 3 5: Molecular structure of the so-called "blue dimer", cis,cis- $[(bpy)_2(H_2O)Ru(\mu\text{-}O)Ru(H_2O)(bpy)_2]^{4+}$.

Because of the multi-metallic core of the OEC, it was long considered that artificial molecular WOCs must accommodate multiple metal centres to cope with the accumulation of the four oxidizing equivalents needed for H_2O oxidation. The initial lack of reports on single-site WOCs led to the creation of a paradigm, which claimed that at least two metal centres were required for H_2O oxidation to occur. However, this early belief has now been disproven, and today there are variety of single-site catalysts that can mediate the four-electron oxidation of H_2O.

The first evidence that the four- electron oxidation of H_2O was possible on single-site metal complexes was provided by the group of Thummel in 2005. Their ruthenium complexes' ligands were a tridentate polypyridyl type ligand, 2,6-di(1,8- naphthyridin-2-yl)pyridine, with uncoordinated naphthyridine nitrogens (Fig. 3.5). The uncoordinated nitrogens interact with the aqua ligand through hydrogen bonding, thus, stabilizing the single-site aqua complexes.[83] Presently, a diversity of mono-nuclear WOCs have been synthesized as well.

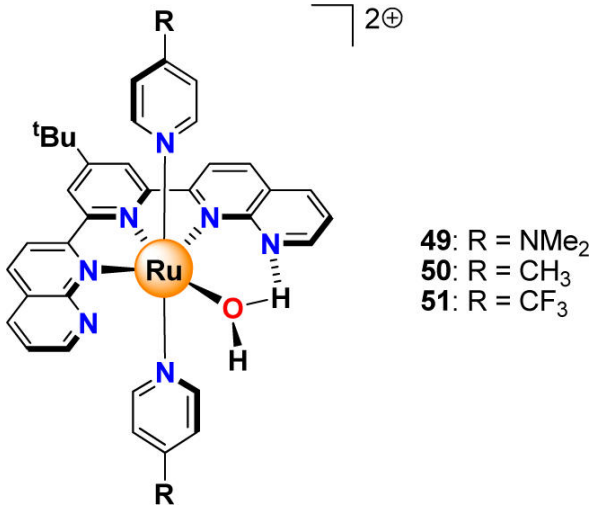

Figure 3 6: Molecular structures of the single-site ruthenium complexes

Molecular single-site catalysts offer the possibility of straightforward ligand design, synthesis, and characterization. It is relatively easy to tune ligand environment in these molecular systems, both electronically and sterically, which make them ideal for structure−activity relationship studies. Advantages are also offered when conducting detailed mechanistic studies, from both an experimental and a theoretical point of view. However, the relative ease with which these molecular mononuclear catalysts can be developed and thoroughly studied is not solely the fundamental objective to be pursued. The incorporation and/or attachment of these catalysts to viable supramolecular assemblies, for example, linking them to a chromophore for light-absorption, for H_2O splitting, is also greatly facilitated.[39]

1.3.6 Light activation of Water Oxidation Catalysts

The first step in an artificial photosynthetic system is light-harvesting by a chromophore, that is, a light-absorbing component analogous to the photosynthetic pigments. This chromophore should efficiently absorb and convert the incoming solar energy into an excited state that can transfer an electron to an acceptor for the creation of a charge-separated state, thereby generating the required thermodynamic driving force for the desired chemical reactions. Both photoactive molecular dyes and semiconductors can induce electron transfer and have the potential of being used as light-harvesting chromophores in a future artificial device for H_2O splitting.

The most well studied molecular photosensitizers for electron-transfer processes are the $[Ru(bpy)_3]^{2+}$-type complexes, after the discovery in the early 1970s that they could undergo electron transfer from their excited states to a sacrificial electron acceptor[51,52]. Although different pigments have been investigated over the last few years, porphyrins are an excellent candidate due to their properties.[12]

The porphyrin ring has been extensively studied as a synthetic model of its natural chlorophyll counterparts. A vast amount of work was primarily devoted to the synthesis and characterization of sensitizer-donor or acceptor dyads with the target being to understand the primary events in the photosynthetic process, such as the formation of charge-separated states, their lifetime, and the recombination process.[12] Porphyrin dyes are also currently being developed for their potential use in nanocrystalline TiO_2 Grätzel cells. A wide variety of differently substituted porphyrin derivatives, both free-base and metallated have been synthesized and tested as dyes for replacing ruthenium-based chromophores. An encouraging efficiency of 4.2% has been reached indicating the need for more in-depth investigation of the parameters affecting the light harvesting ability of porphyrins.[84]

The use of porphyrins as chromophores to harvest light and induce the electron transfer process to ultimately activate a catalytic module via different electron mediators will be investigated. One of the main assets of porphyrinic systems over other chromophores such as $[Ru(bpy)_3]^{2+}$ type complexes, is their absorption properties, which can be extended to the near-IR region, while the ruthenium complex MLCT absorption band that initiates the formation of the triplet state lies more in the blue region (450 nm). Importantly, the absorption bands of porphyrins exhibit high molar extinction coefficients, an important parameter in the light capture process.

There are a few examples of porphyrin derivatives used as photosensitizers for the activation of catalytic moieties, both oxidative and reductive. Tetrapyrrolic derivatives were used as a sensitizer to activate a rhenium-based catalyst for the reduction of CO_2[85], cobaloximes[86,87] and hydrogenase models[88,89] for hydrogen production.

2 Scope of this thesis

This thesis was inspired by previous literature references studying porphyrin derivatives as photosensitizers in photo-activation of catalytic complexes. This includes work by Rocha's group who used $[(tpy)Ru(tppz)Ru(bpy)(L)]^{n+}$ (where L is Cl or H_2O, tpy and bpy are the terminal ligands 2,2':6',2''-terpyridine and 2,2'-bipyridine, and tppz is the bridging backbone 2,3,5,6-tetrakis(2-pyridyl)pyrazine) for catalytic photo-oxidation of alcohols.(Fig. 2.5)

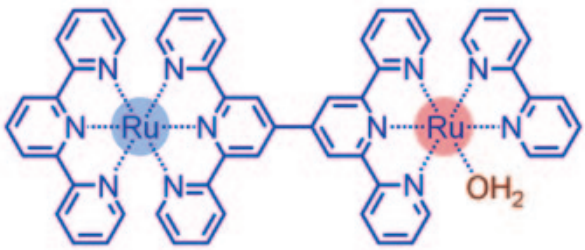

Figure 2. 5: Structure of $[(tpy)Ru(tppz)Ru(bpy)(L)]^{n+}$

This thesis' purpose was to synthesize porphyrin derivatives, covalently linked through an amide bond, to ruthenium polypyridyl complexes. Furthermore, they were fully characterized through MALDI-tof and NMR along with photophysical and electrochemistry studies. Eight dyads were synthesized and studied which can be divided into two groups according to the position of their anchoring group. The idea was to use the porphyrin as a photosensitizer and study the possibility of activating the ruthenium complex as a catalyst through irradiation. (Scheme 2.1)

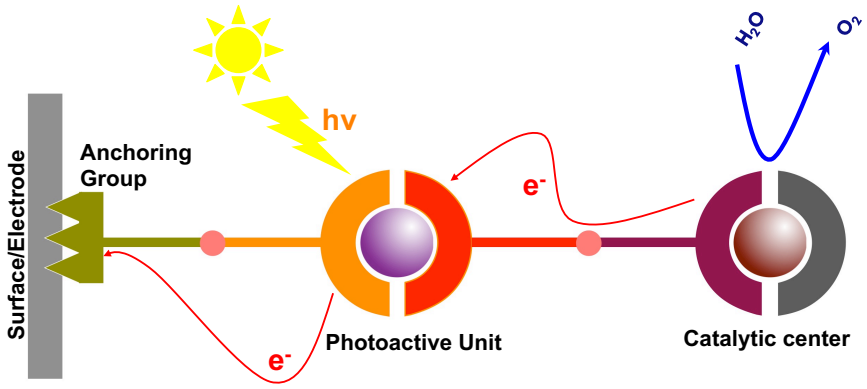

Scheme 2. 1:A schematic view of the Msc project.

After the photophysical study of the dyads was complete, some of the dyads showed evidence that they were able to activate their catalytic part through irradiation in the presence of a sacrificial electron acceptor (SA). Their capability to oxidize organic substrates was further investigated by photo-catalytic experiments.

3 Synthetic approach

3.1 Porphyrin-Ruthenium polypyridyl complex Dyads

<u>Group I</u>
The anchoring group is placed on porphyrin.

Free base porphyrin

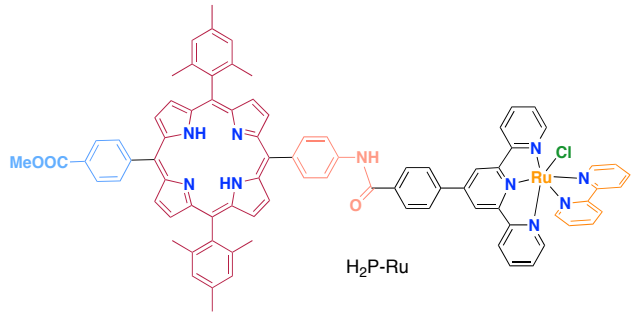

H_2P-Ru

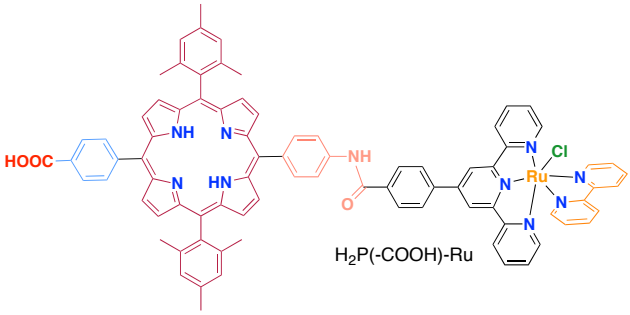

H_2P(-COOH)-Ru

Zinc porphyrin

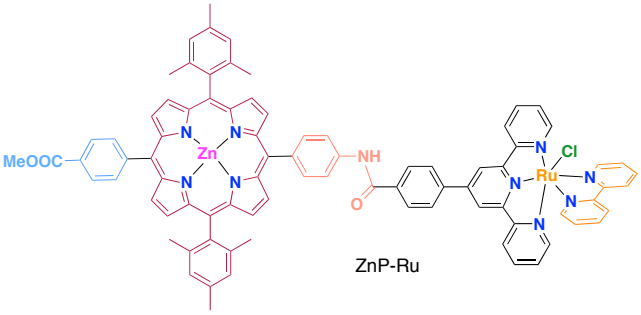

ZnP-Ru

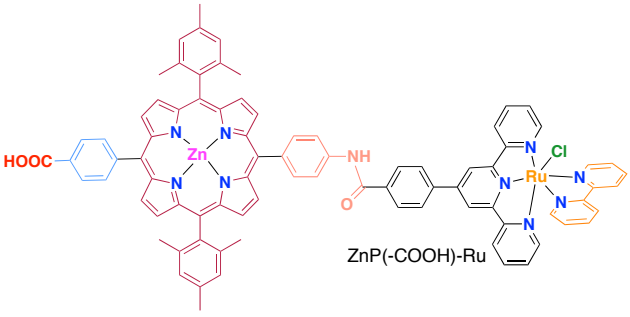

ZnP(-COOH)-Ru

Group II

The anchoring group is located on the bipyridine ligand of Ruthenium complex.

Free base porphyrin

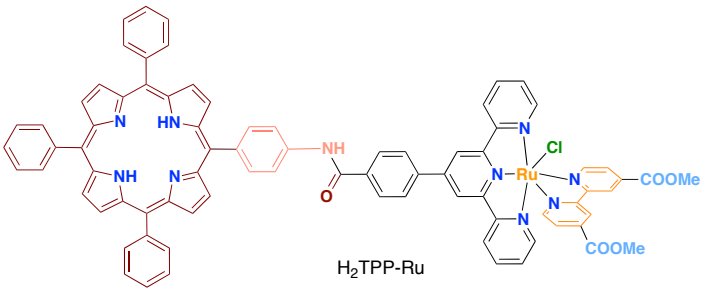

$H_2TPP\text{-}Ru$

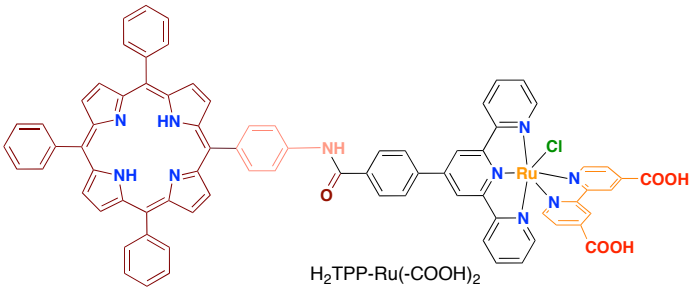

$H_2TPP\text{-}Ru(\text{-}COOH)_2$

Zinc porphyrin

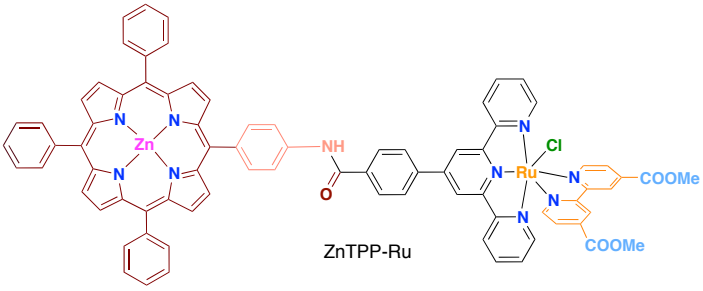

ZnTPP-Ru

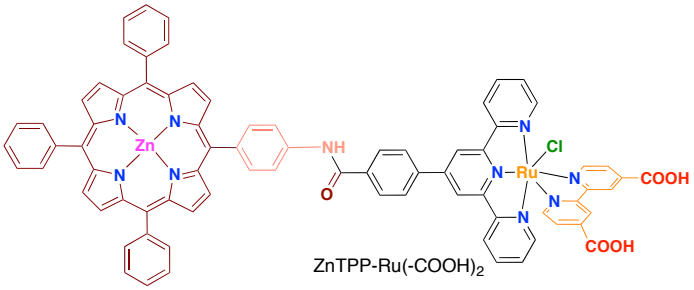

$ZnTPP\text{-}Ru(\text{-}COOH)_2$

3.2 Synthetic Methods

As mentioned before, these dyads were synthesized to investigate the capability of the porphyrin to photo-activate a ruthenium catalyst. Both the ester and carboxylic derivatives were synthesized in order to study them under irradiation in solution and also adsorbed on TiO_2 nanoparticles. Two porphyrins (5) and (7) were synthesized and covalently linked to two ruthenium complexes (9) and (10), thus, we can modify the position of the position of the anchoring group.

The Group I have the anchoring group located on the porphyrin ring. The synthesis of the porphyrin ring (Scheme 3.1) starts with 2 eq of dipyrromethane and 1 eq of each aldehyde (2: methyl 4-formylbenzoate and 3: 4-nitrobenzaldehyde) to form the porphyrin ring. The conditions of the reaction were adopted by the recent work of Balaban's and Gryko 's groups [15] in aqueous media. The porphyrin (5) is being isolated after reduction of the nitro group of the porphyrin ring.

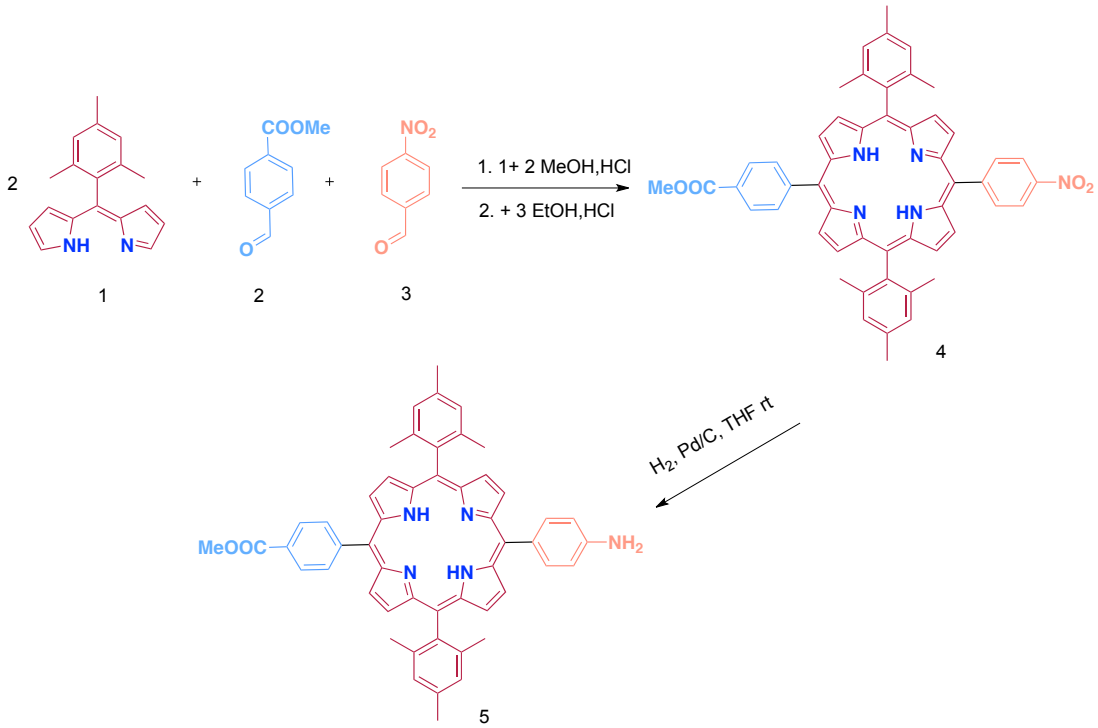

Scheme 3. 1: Synthesis of porphyrin (5).

The porphyrin derivative of Group II was synthesized through a different procedure. The initial porphyrin is a tetraphenyl porphyrin, one of the most well studied and widely synthesized. The porphyrin forms after the reflux of benzaldeyde in propionic acid. Further modification takes place by one phenyl nitration of the porphyrin leading to mono-nitro porphyrin (7) and after reduction the porphyrin (8) is isolated. (Scheme 3.2)

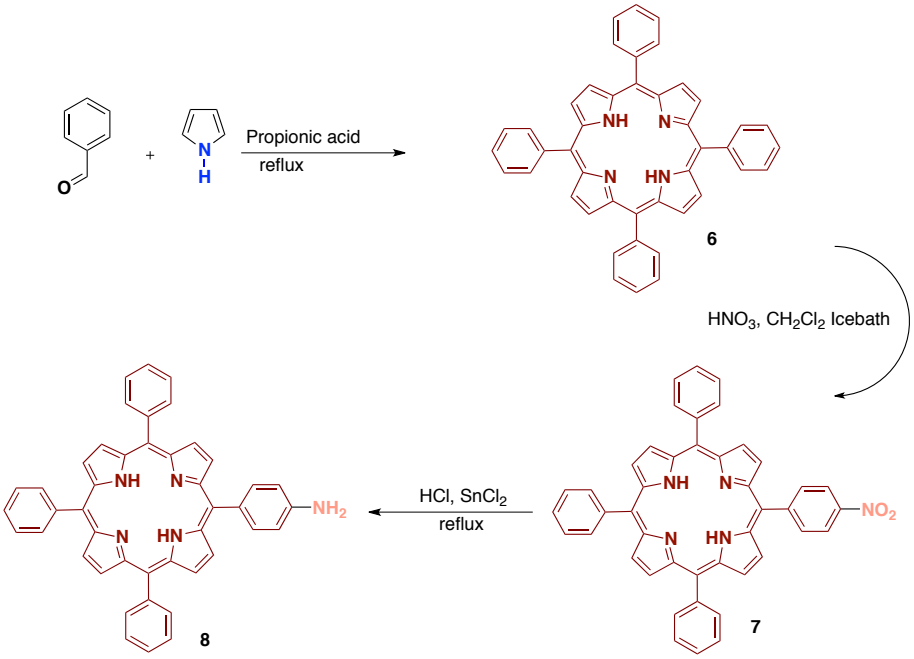

Scheme 3. 2: Synthesis of porphyrin 7.

The most popular synthesis of ruthenium polypyridyl complexes begins with the reflux of $RuCl_3 \cdot 3H_2O$ in the presence of DMSO (dimethyl sulfoxide) in order to form $Ru(DMSO)_4(Cl)_2$. The most efficient way to synthesize our polypyridyl complexes was to first mono-substitute the $Ru(DMSO)_4(Cl)_2$ with the bipyridine ligand (9) or (10) in chloroform.

For the synthesis of $Rubpy(DMSO)_2Cl_2$ the 2,2' bipyridyl and $Ru(DMSO)_4(Cl)$ are being dissolved in methanol and refluxed, then by precipitation we isolate the product (9). (Scheme 3.3)

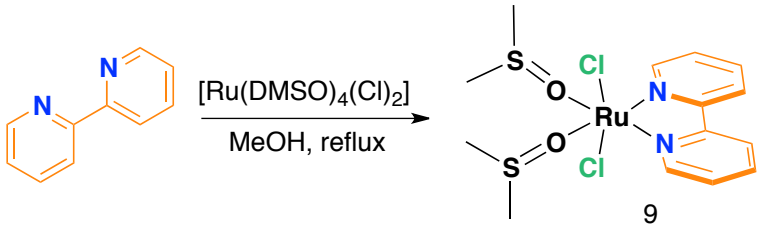

Scheme 3. 3: Synthesis of $Rubpy(DMSO)_2Cl_2$.

The synthesis of Rubpy$(MeCOO)_2(DMSO)_2Cl_2$ involved the protection of carboxylic groups of [2,2'-bipyridine]-4,4'-dicarboxylic acid, which took place in methanol in presence of H_2SO_4. We continuously isolated the product (10) according to previous coupling between Rubpy$(DMSO)_2Cl_2$ the 2,2' bipyridyl ligand. (Scheme 3.4)

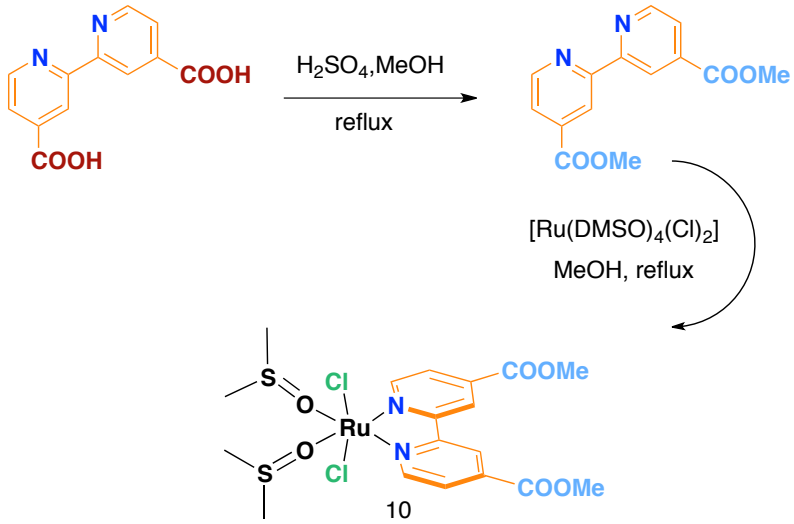

Scheme 3. 4: Synthesis of Rubpy'(DMSO)2Cl2.

The amide bond is formed between the amine-group of the porphyrin ring (5) or (8) and the carboxylic group of 4-([2,2':6',2''-terpyridin]-4'-yl)benzoic acid leading to compound (11) and (12). The reaction is a two-step process, where firstly, the alkyl chloride of 4-([2,2':6',2''-terpyridin]-4'-yl)benzoic acid is forming, and secondly, the formation of the amide bond.(Scheme 3.5)

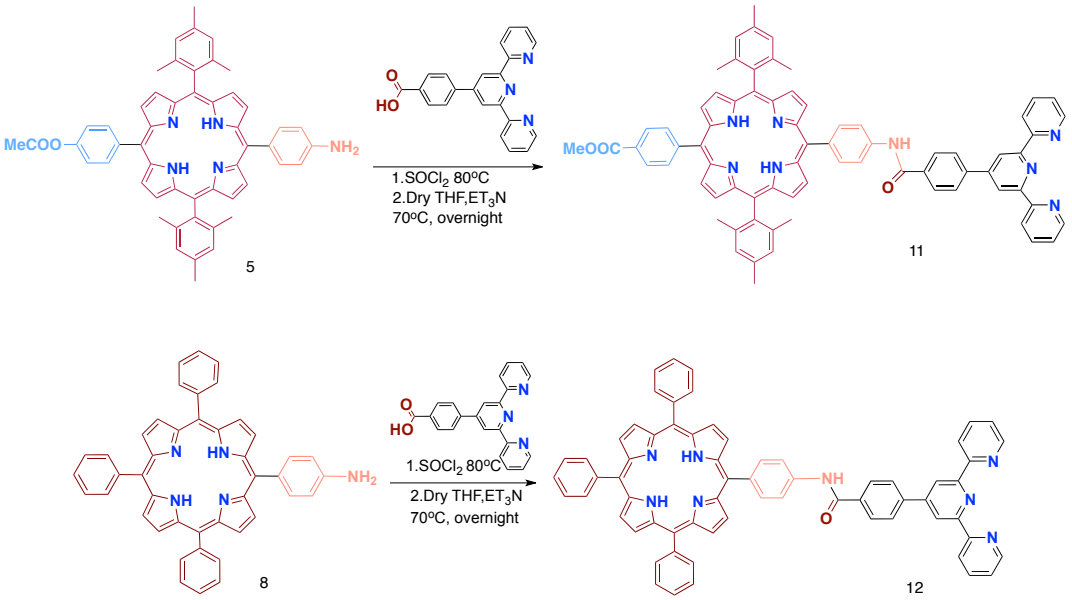

Scheme 3. 5: Amide bond between the porphyrin ring and 4-([2,2':6',2''-terpyridin]-4'yl)benzoic acid.

The coupling of the compounds (11) and (12) with the suitable ruthenium complex is taking place under the same conditions for both groups, which is under reflux with acetic acid as a solvent. (Scheme 3.6)

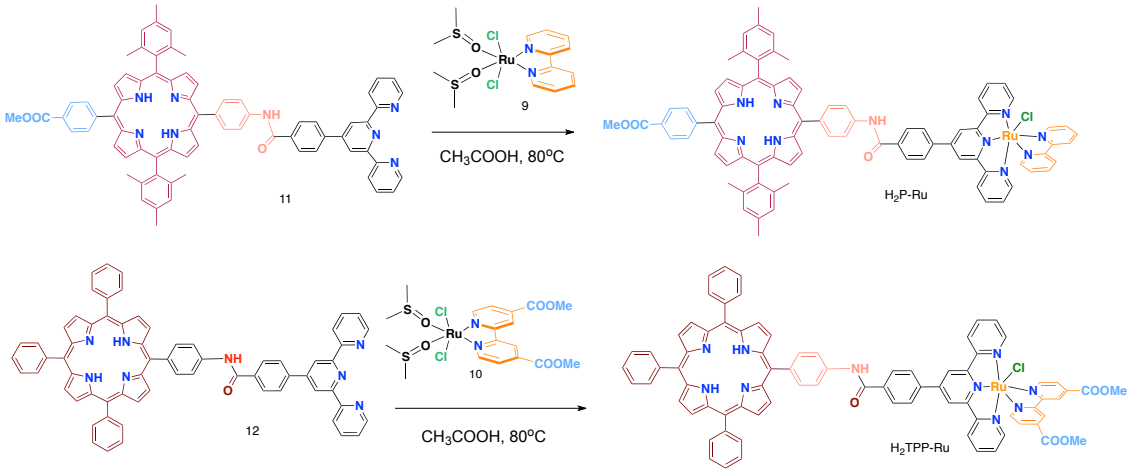

Scheme 3. 6: Synthesis of H2P-Ru and H2TPP-Ru.

At this point the porphyrins of the dyads were metallated with Zinc, allowing ZnP-Ru and ZnTPP-Ru to be isolated. (Scheme 3.7)

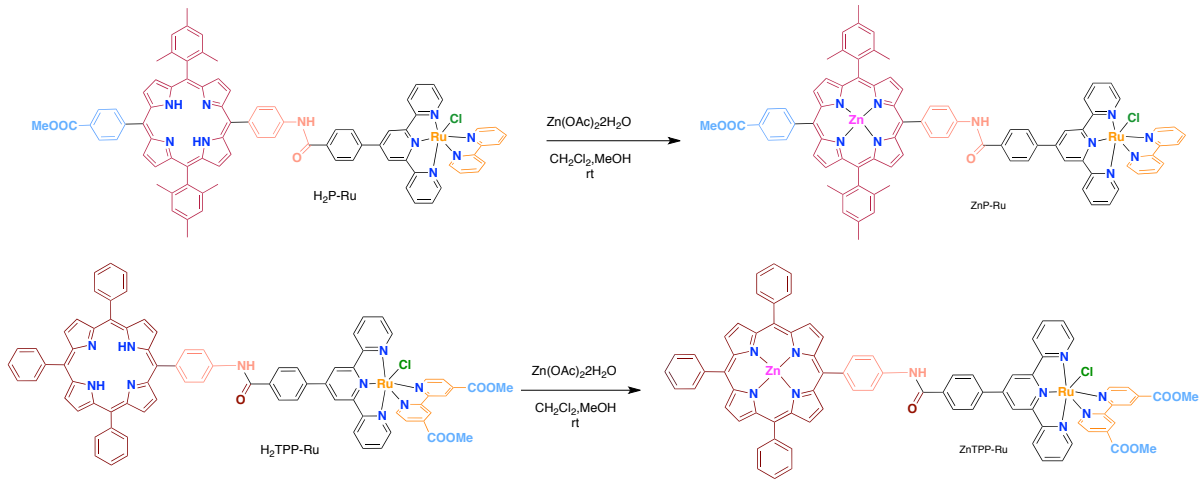

Scheme 3. 7: Synthesis of ZnP-Ru and ZnTPP-Ru.

Finally, the ester groups were hydrolyzed to carboxyl groups in order to study those systems in the presence of a semiconductor, such as TiO_2 nanoparticles. (Scheme 3.8)

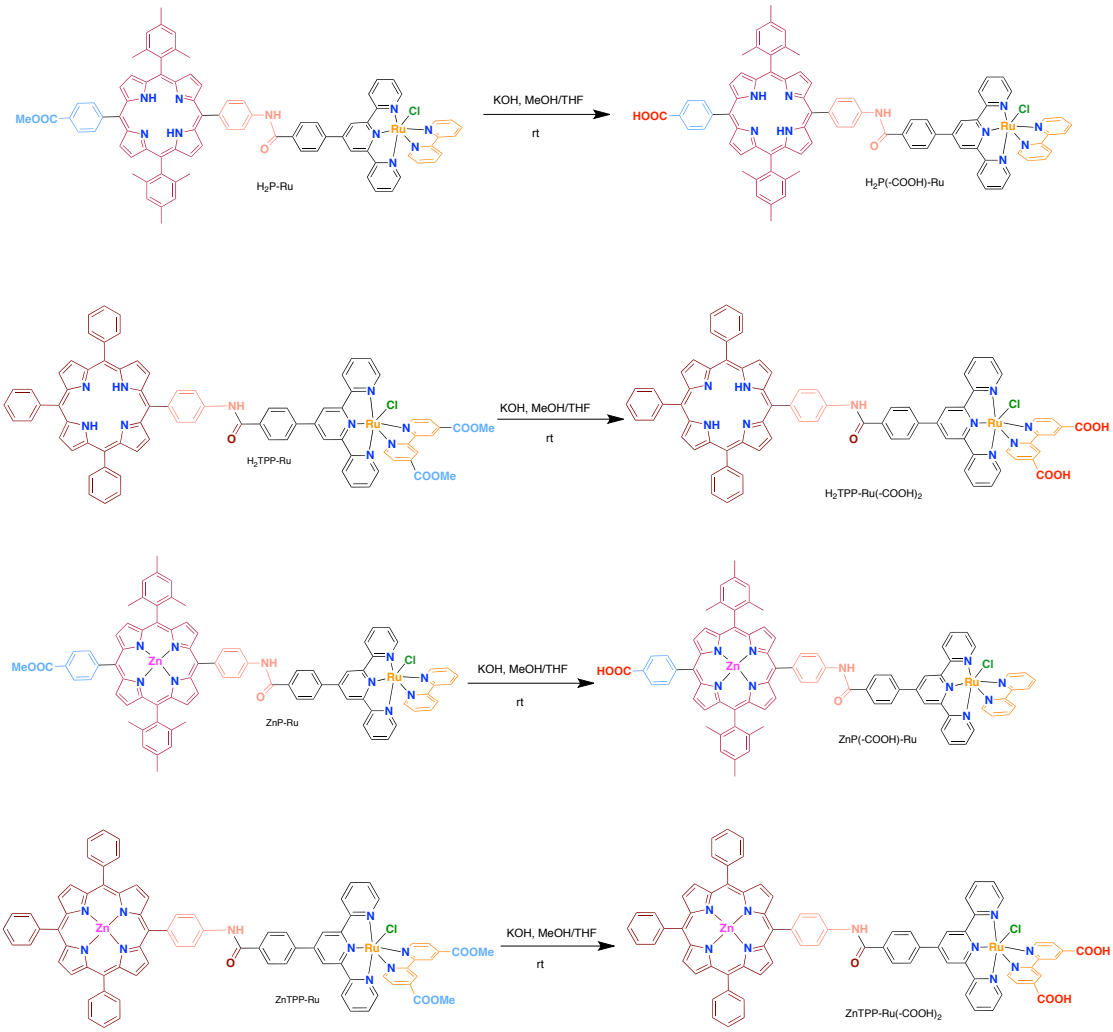

Scheme 3. 8: Hydrolysis of ester groups.

As references, porphyrin compounds H_2-P and Zn-P were synthesized for comparative purposes. An amide bond was formed between porphyrin (5) and its Zinc derivative with benzoyl chloride. (Scheme 3.9)

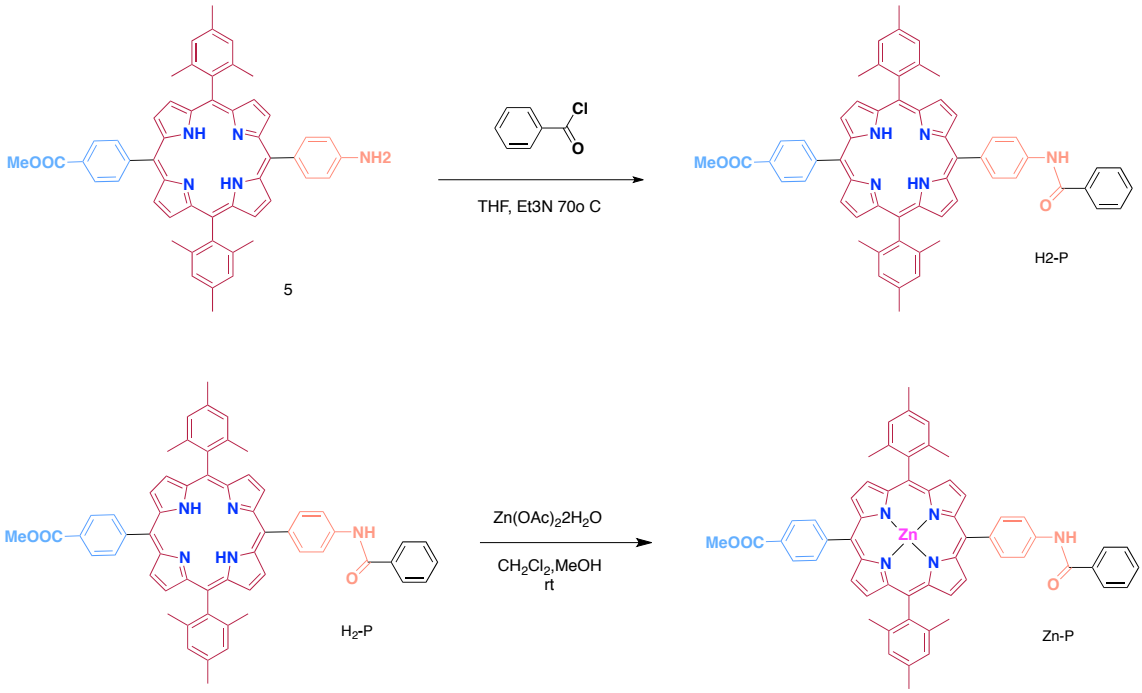

Scheme 3. 9: Synthesis of porphyrin reference compounds.

4 Discussion

As previously mentioned, these dyads were synthesized to investigate the ability of the porphyrin derivatives to act as a photosensitizer in order to activate a ruthenium polypyridyl- complex as a catalyst. Different photophysical methods were used for the comprehension of our system, such as Absorption/Emission spectroscopy, Electrochemistry and Transient/Differential Absorption. Our conclusions also agreed with Density Functional Theory (DFT) calculations and the photo-catalytic ability was further investigated through photocatalytic experiments.

Reviewing the literature[90,91] which was the inspiration behind this project, there are different ruthenium complexes which are being studied as catalysts in either electrochemical or photochemical systems. Two of the recent systems published by Rocha et al and Aukauloo et al are consisted of two ruthenium polypyridyl- complexes; the first ruthenium complex works as a photosensitizer, while the second works as an oxidative catalyst of organic substrates. (Scheme 4.1)

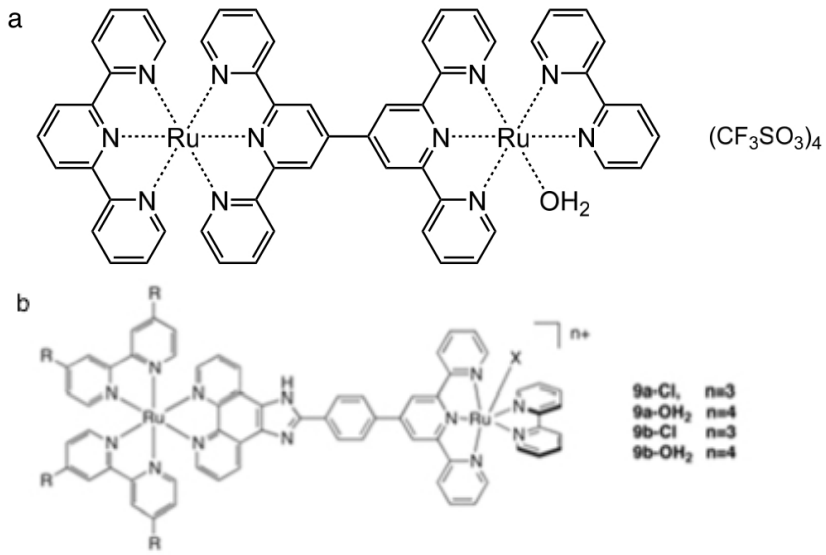

Scheme 4. 1: Binuclear Ruthenium systems (a) Rocha et al, (b) Aukauloo et al.

Throughout this discussion section we will follow the studies of the dyads and try to explain the electron transitions which take place. We will also explore the ability of photoinduced activation of the catalytic moiety of ruthenium.

4.1 Electrochemical Studies

For the investigation of the dyads' electrochemical properties, cyclic (*CV*) and square-wave(*SQ*) voltammetry were used. In both techniques the potential applied *V* is varied with time *t* and the resulting current *i* is measured. Plotting current versus potential gives a voltammogram; the analysis of which provides information about the formal potential E^0. This information includes the reduction or oxidation of an electroactive species as well as the reversibility of the process. The techniques differ in how the potential varies with time: in *CV*, *V* is linearly swept back and forth between

two set values at a prefixed rate (Fig. 4.1 (a)), while in *SQ*, a series of voltage pulses is superimposed to a linear potential sweep (Figure 4.2 (b)). The timescale of both experiments is determined by the scan rate.

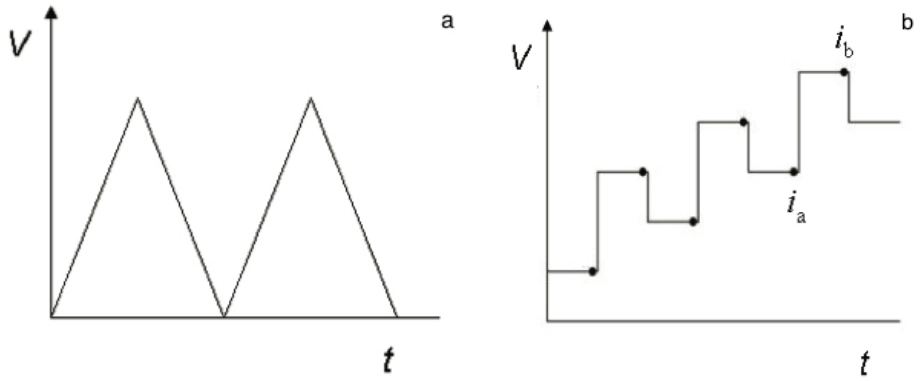

Figure 4.2: (α) CV waveform (two circles). (b) SQ waveform.

In a typical *CV* voltammogram (Fig. 4.3 a), there is a plot of the measured current *i* vs. *V*, where the oxidative current results in a positive wave with a maximum point (anodic peak, at potential E_{pa}) and the reductive current in a negative wave with a minimum point (cathodic peak, at potential E_{pc}). If the process is reversible, then the current values at the two peaks are the same and E^0 is almost identical to $E_{1/2}$ where $E_{1/2} = (E_{red} + E_{ox})/2$. In the case of *SQ* (Fig. 4.3 b) a different plot is being used; $\Delta i/V$, where Δi is the difference between currents sampled before and at the end of each potential pulse. For a reversible process, the result is a symmetrical peak which holds the relation $E_{1/2} = E_{peak} + \Delta E/2$, where ΔE is the pulse potential.

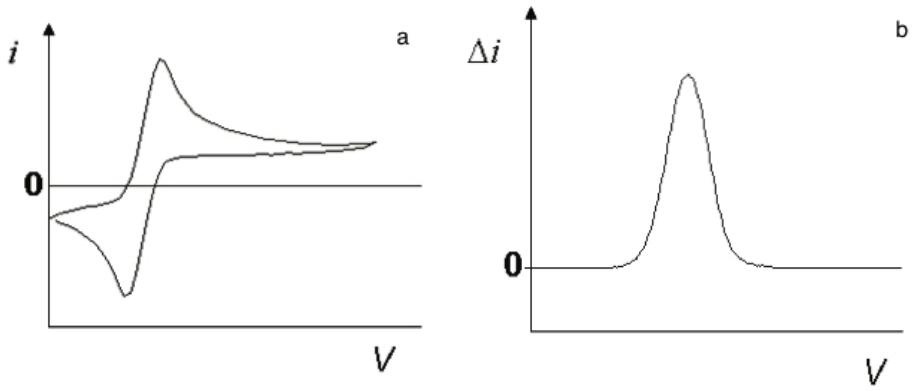

Figure 4.3: (α) CV voltammogram for a reversible process. (b) SQ voltammogram for a reversible process. $\Delta i = (i_b - i_a)$

In order to characterize the electrochemical properties of the porphyrin-ruthenium dyads, it is crucial to identify any irreversible or non-reversible process. This can be achieved through *CV* voltammograms, which are ideal to determine the type of processes occurring. Conversely, the potential is more accurately obtained from *SQ*. The *SQ* also provides a superior peak resolution, which is extremely useful in the case of two or more processes taking place at similar potentials. The *CV* and *SQ* voltammogram of two of the dyads can be seen below. (Figure 4.4)

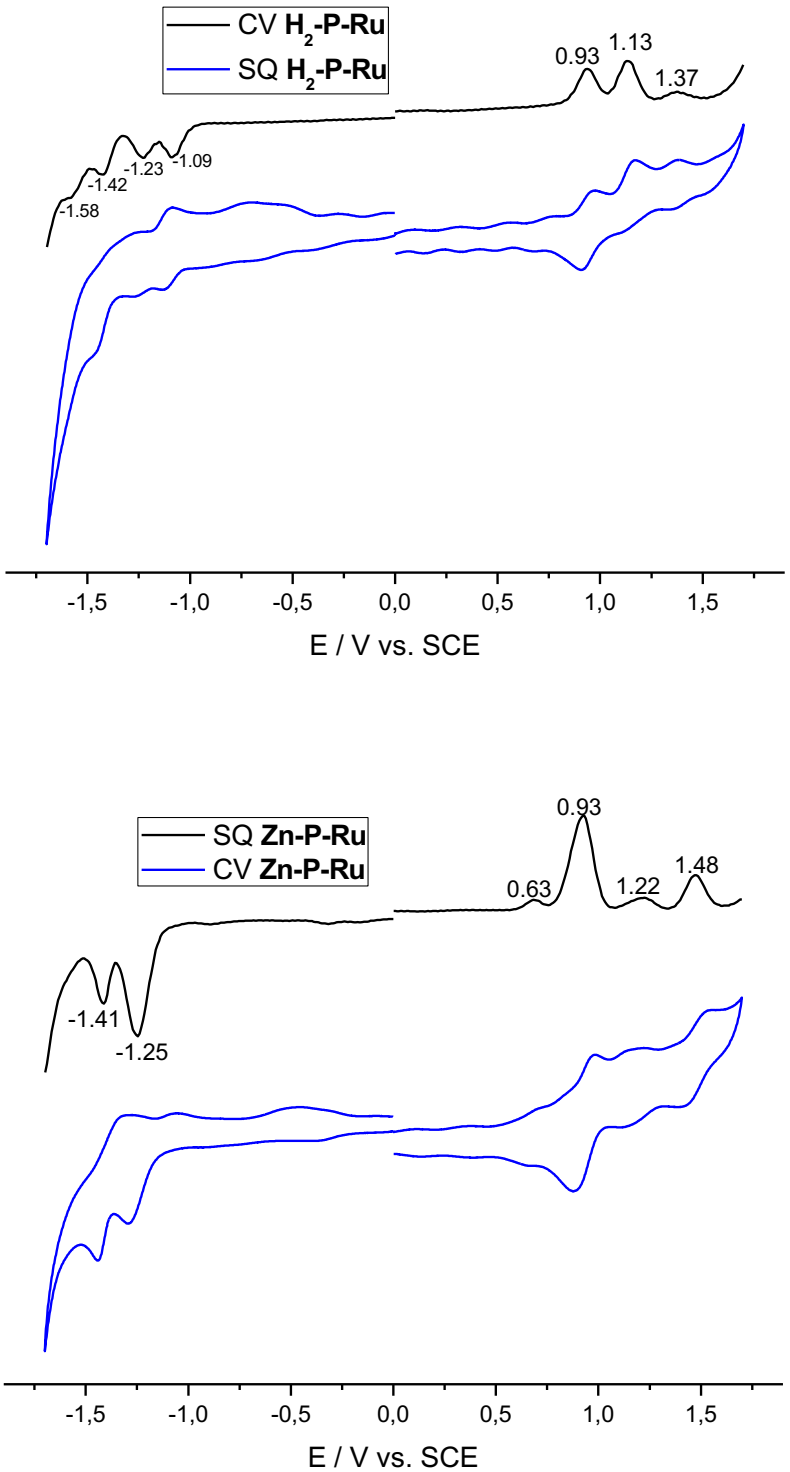

*Figure 4.4: Cyclic and square wave voltammograms of **H_2-P-Ru** and **Zn-P-Ru**.*

On the following table, the potentials of the dyads and their references are being reported. (Tab. 4.1) The voltamogramms of the dyad H_2-P-Ru shows that its electrochemical properties correspond to those obtained separately for its constitutive units H_2-P and Ru. On the anodic side, waves at 0.93 V and 1.13 V correspond to the oxidation of Ru and H_2-P moieties respectively; while on the cathodic side, peaks at -1.09 V and -1.23V originate respectively from the porphyrin and the bipyridine reduction. In the case of the dyad Zn-P-Ru, the first oxidation occurs at very similar potentials for ZnP

and Ru_{cat} components, therefore, the outcome is, in case of the dyad, a two-electron oxidation wave which is observed at 0.93 V and similarly a two-electron reduction wave at -1.25 V.

Compound	$E_{1/2}$ (P^{-}/P^{2-})	$E_{1/2}$(bpy^{-}/bpy^{2-})	$E_{1/2}$(bpy^{0}/bpy^{-})	$E_{1/2}$(P/P^{-})	$E_{1/2}$(Ru^{III}/Ru^{II})	$E_{1/2}$ (P^{+}/P)	$E_{1/2}$(P^{2+}/P^{+})
Ru_{cat}		-1.42	-1.25		0.94		
H_2-P	-1.58			-1.08		1.14	1.42
Zn-P				-1.25		0.90	1.25
H_2-P-Ru_{cat}	-1.58	-1.42	-1.23	-1.09	0.93	1.13	1.37
Zn-P-Ru_{cat}		-1.41	-1.25	-1.25	0.93	0.93	1.22

Table 4. 1: Electrochemical Data. $E_{1/2} = (E_{pa} + E_{pc})/2$ in Volts vs SCE, measured in benzonitrile, scan speed: 100 mV/s

4.2 Absorption Spectroscopy

Ultraviolet–visible spectroscopy (UV-Vis or UV/Vis) refers to absorption spectroscopy or reflectance spectroscopy in the ultraviolet-visible spectral region. This spectroscopy has different applications, one of which is based on the Beer-Lambert law[92] which associates the absorption of a molecule with its concentration and a fingerprint constant corresponding only to that molecule called molecular absorption.

$$A = \log I/I_O = \varepsilon cd$$

- A: absorption,
- Io: intensity of incident radiation I: and passing radiation
- e: molecular absorption ($lt \cdot mol^{-1} \cdot cm^{-1}$)
- c: concentration of solution (mol / lt)
- d: the optical path (cm)

Molecules containing π-electrons or non-bonding electrons (n-electrons) can absorb the energy in the form of ultraviolet or visible light to excite these electrons to higher anti-bonding molecular orbitals.

Among the porphyrin properties, it was mentioned that they have a very characteristic UV-Vis spectrum, namely the intense Soret Band at 400nm due to the delocalization of the porphyrin ring current. In the 450-800nm region, the four Q Bands, which are weaker, appear to be responsible for the rich color of porphyrins. In the early 1960s, Gouterman[93,94] studied the molecular orbitals of porphyrin rings in various electronic states. His research led to the conclusion that there are two HOMO and two LUMO molecular orbitals which are degenerate. HOMO is defined as the highest occupied molecular orbital and LUMO, respectively, the lowest unoccupied molecular orbital. The HOMO has a_{1u} and a_{2u} symmetry, while LUMO has e_g symmetry. (Fig. 4.5)

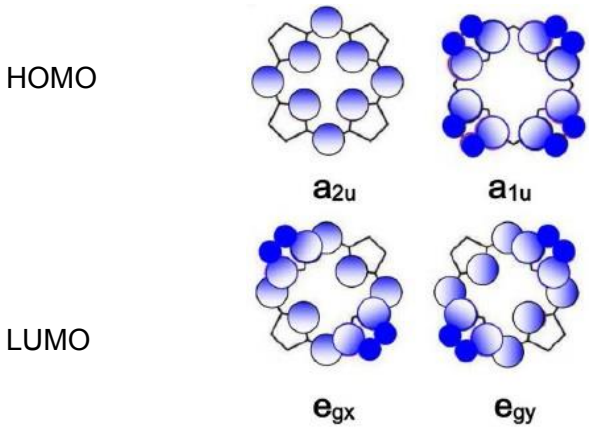

Figure 4.5: The two molecular orbitals HOMO a porphyrin ring is degenerate in symmetries a1u and a2u. Both LUMO molecular orbitals have e_g symmetry.

According to this theory, the absorption bands in porphyrin systems arise from transitions between two HOMOs and two LUMOs. The metal centre and the substituents on the ring affect the relative energies of these transitions. The permitted transitions occur between π to π *. The Soret Band results from a_{1u} to e_g transitions, while the Q Band is due to a_{2u} to e_g transitions. (Fig. 4.6)

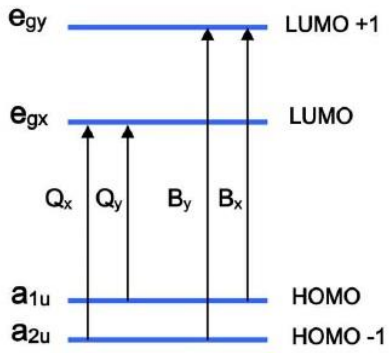

Figure 4.6: Permitted electron transitions from HOMO to LUMO orbitals.

Looking into a characteristic UV-Vis spectrum (Fig. 4.7) of a free-base porphyrin, we can observe the Soret Band around 400nm and the Q bands between 500-650nm. Different substituents on the porphyrin ring do not affect the pattern of the spectra, but they may cause redshift (moving to the right) or blueshift (moving to the left).

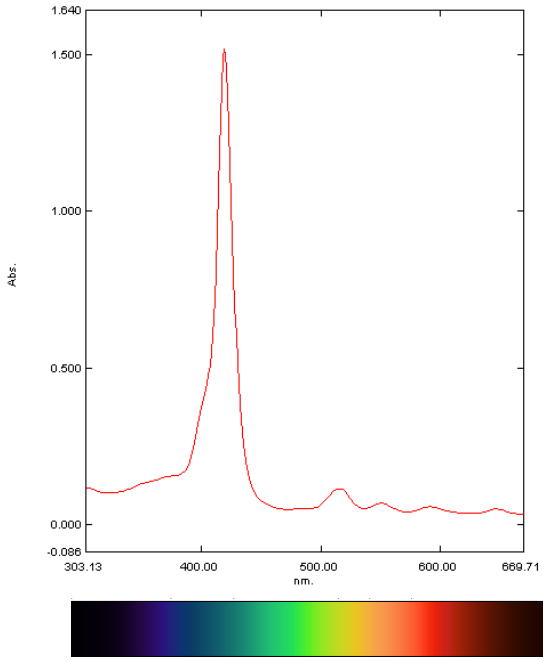

Figure 4.7: Absorption spectrum of a free base porphyrin.

In the case of metallated porphyrin, the pattern of the UV-Vis spectrum is changing. We can observe the Sorret band, but in the case of the Q bands, the identity of the metal can change the spectrum radically. Metalloporphyrins can be divided into two groups based on their UV-vis and fluorescence properties: (1) Regular metalloporphyrins contain closed-shell metal ions (d^0 or d^{10})—for example Zn II , in which the d π (dxz , dyz) metal-based orbitals are relatively low in energy. These have very little effect on the porphyrin π to π^* energy gap in porphyrin electronic spectra. (2) Hypsoporphyrins are metalloporphyrins in which the metals are of d^m (m = 6–9), having filled d π orbitals. In hypsoporphyrins there is significant metal d π to porphyrin π^* orbital interactions (metal to ligand π- backbonding). This results in an increased porphyrin π to π^* energy separation, causing the electronic absorptions to undergo blueshifts. (Fig. 4.8)

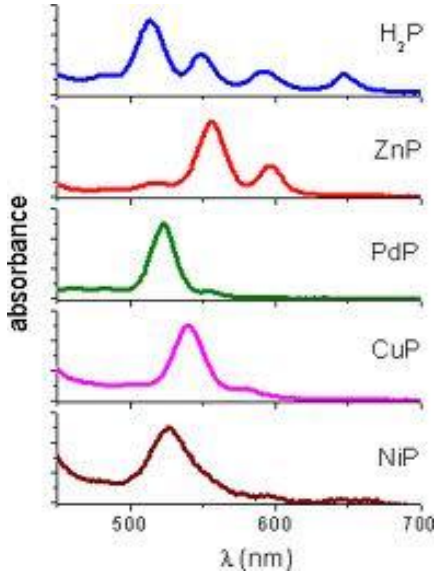

Figure 4.8: Comparison Q region spectrum of different metalloporphyrins.

The following spectrum includes the spectra of reference compounds, 1:1 eq of the reference in the same solution and also H_2P-Ru. The spectrum of the reference porphyrin is a characteristic free-base porphyrin spectrum with an intense Soret band at 421 nm and moderate Q bands at 516, 551, 591, 649 nm. The characteristic bands of the ruthenium polyripydyl complex (Ru_{cat}) can also be observed, with a band around 320 nm as result of ligand-centered (LC) $\pi \rightarrow \pi^*$ transition and a band at 515 nm as a result of metal-to-ligand charge transfer (^{1}MLCT). With regards to the dyad synthesized during this thesis: H_2P-Ru, we can observe the porphyrin's characteristic bands and also the band of the ruthenium complex. It is clear that the dyad's spectrum is the sum of its components, which means there are no interactions between the two moieties in the ground state. (Fig. 4.9)

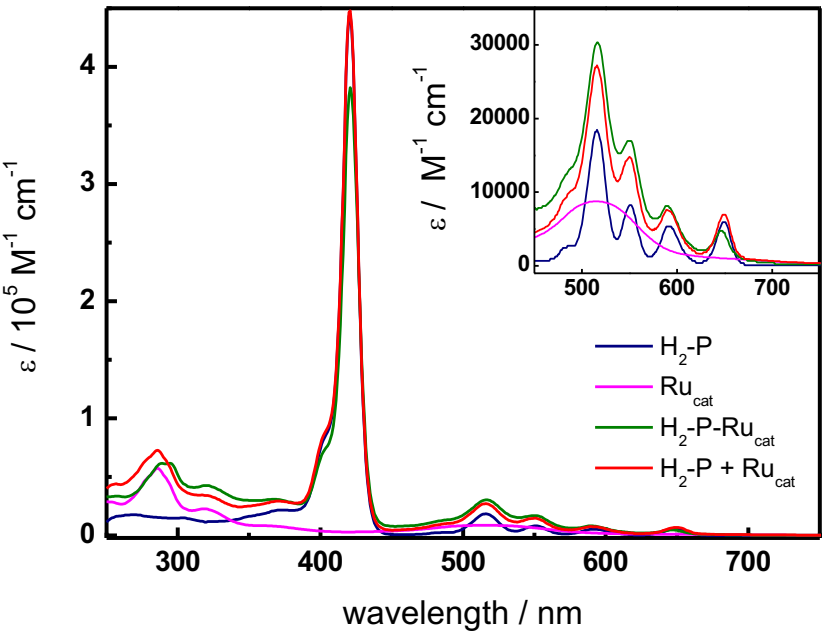

Figure 4.9: UV-vis absorption spectra for the dyad and the reference compounds. H_2-P-Ru_{cat}. Solvent was chloroform except for the Ru_{cat}. (in acetonitrile).

A similar picture was also given by the ZnP-Ru dyad. We can observe the two Q bands of the Zinc porphyrin and the characteristic Sorret. The dyad spectrum is clearly the result of the sum of the components, which indicates no interactions in the ground state too. (Fig. 4.10). It appears that the individual features of the two moieties are not significantly altered, although the Soret band is less intense in the dyads. This perturbation has previously been observed in similar systems.[95]

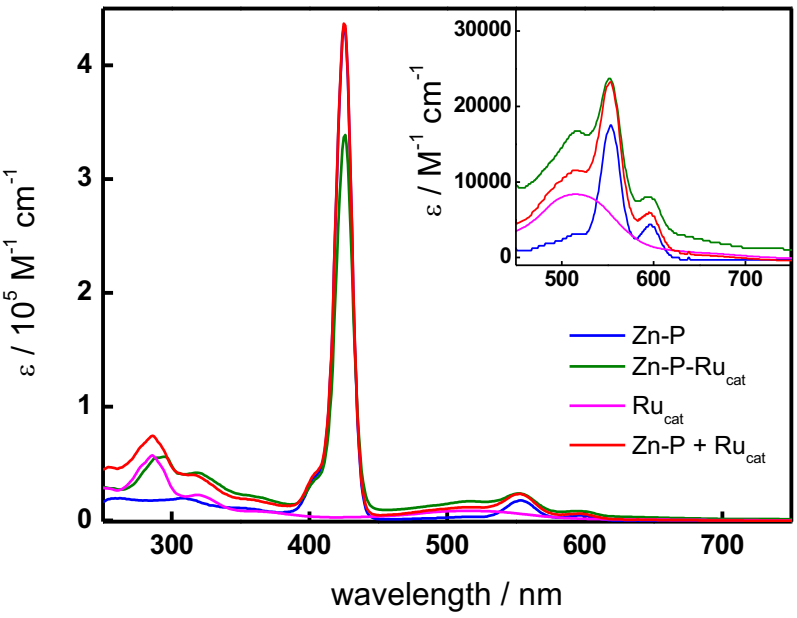

Figure 4.10: UV-vis absorption spectra for the dyad and the reference compounds. Zn-P-Ru_{cat}. Solvent was chloroform except for the Ru_{cat}. (in acetonitrile).

4.3 Emission Spectroscopy

Emission spectroscopy is another method to study the interactions between the two parts of the dyads, however, in this case they are in the excited state. Radiative transitions involve the absorption of a photon, followed by either the transition to a higher energy level or by emission. The Non-radiative transitions arise through several different mechanisms. The sum of the possible radiative or non radiative transitions are being presented in Jablonski diagram.[96] (Fig. 4.11)

Relaxation of the excited state to its lowest vibrational level is called Vibrational relaxation. This process involves the dissipation of energy from the molecule to its surroundings, and thus, it cannot occur for isolated molecules. A second type of non-radiative transitions is internal conversion (IC), which occurs when a vibrational state of an electronically excited state can couple to a vibrational state of a lower electronic state. A third type is intersystem crossing (ISC); this is a transition to a state with a different spin multiplicity. In molecules with large spin-orbit coupling, intersystem crossing is much more important than in molecules that exhibit only small spin-orbit coupling. This type of non-radiative transitions can give rise to phosphorescence.

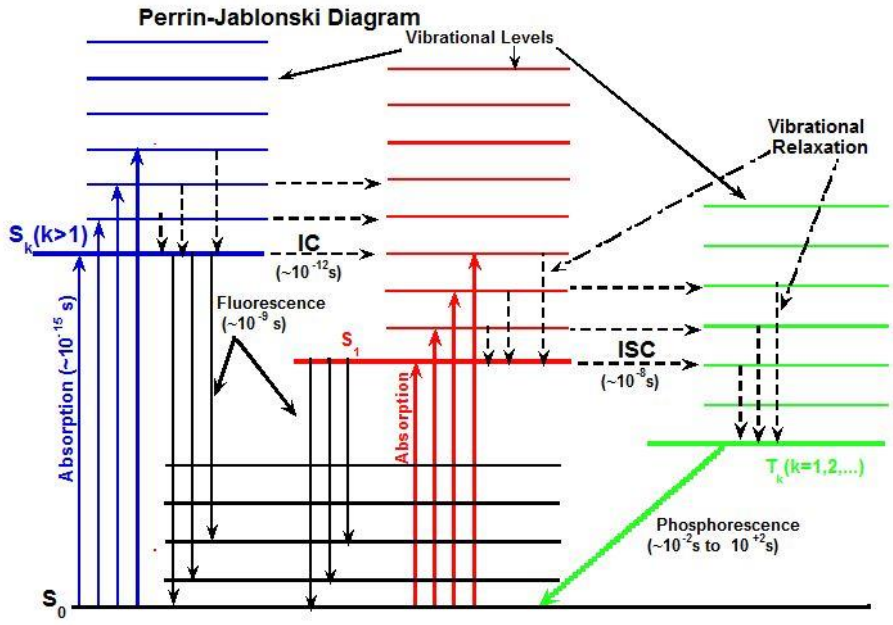

Figure 4.11: Jablonski diagram shows the sum of radiative or non radiative transitions.

The differences between the vibrational levels of the basic and excited states are similar, causing the fluorescence spectrum to often be almost identical to the first absorption band. The difference in wavenumber between the maximum absorption of the first film and the maximum fluorescence is called 'Stokes shift'. The photon emission and absorption are equally rapid processes; the excited molecules remain in the S_1 for some time, which ranges from a few picoseconds up to several nanoseconds. After the excitation of a population of molecules, the fluorescence intensity increases exponentially, reflecting the average life of the molecules in the first excited state. The quantum fluorescence yield, Φ_f, is the quotient of the number of photons emitted to the number of absorbed photons.

The fluorescence quenching refers to any process which decreases the fluorescence intensity of a given substance. Different processes can lead to quenching, such as excited state reactions, energy transfers, complex-formation and collisional quenching. Through emission spectroscopy we can compare the reference compounds' fluorescence and also that of the dyads', and investigate the electron transitions. Below we can see some representative fluorescence spectra of the dyads and their reference compounds. (Fig. 4.12 and 4.13)

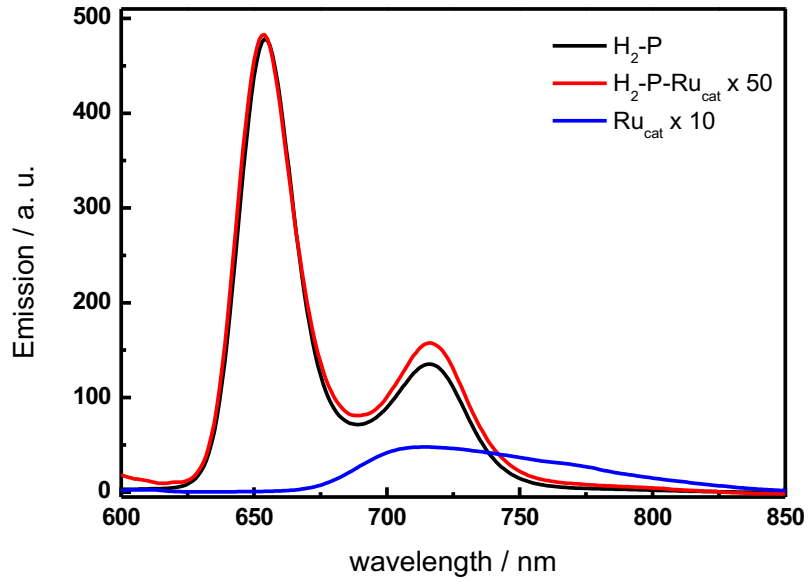

Figure 4.12: Emission spectra in chloroform (acetonitrile for Ru_{cat}) of compounds investigated. Excitation wavelength: 590 nm for H_2-P and H_2-P-Ru_{cat} and 515 nm for Ru_{cat}.

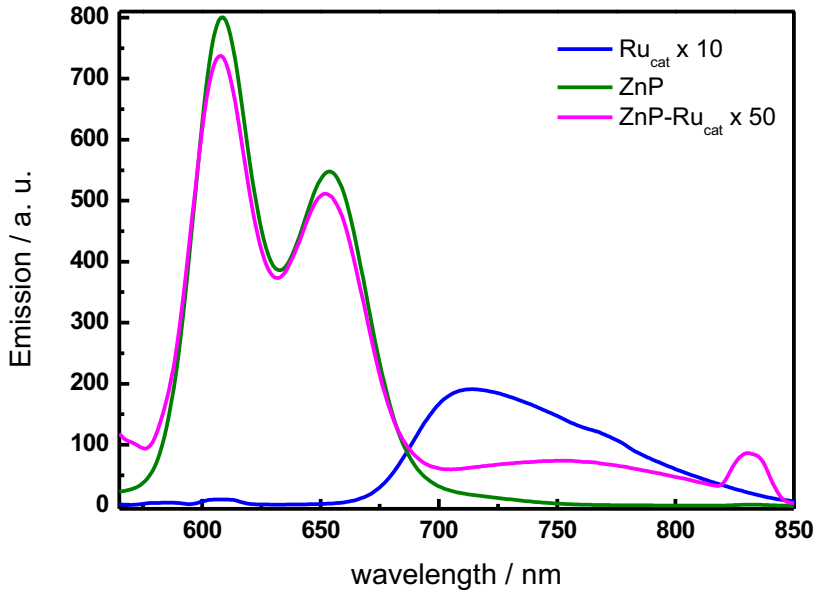

Figure 4.13: Emission spectra in chloroform (acetonitrile for Rucat) of compounds investigated. Excitation wavelength: 555 nm for Zn-P and Zn-P-Rucat and 515 nm for Rucat.

Through emission spectroscopy, it was possible to partially characterize the excited state of the dyads. Upon irradiation, the H_2P-Ru was at 590 nm, where 70% of the incident light was absorbed by the H_2-P moiety and the resulting luminescence spectrum in chloroform (Fig. 4.12) shows bands at 655 nm and 715 nm. These originate from the porphyrin fluorescence with a small contribution to the 715 nm peak coming from the Ru_{cat} luminescence. However, the emission quantum yield is significantly reduced in the dyad (Φ_f = 0.0024, Table 4.2) as compared to the reference H_2-P (Φ_f = 0.118). This behavior indicates the presence of an intramolecular reaction (energy or electron transfer) responsible for the

deactivation of the singlet excited state of the porphyrin. Upon excitation at 532 nm, only 40% of the incident light is absorbed by the H_2-P moiety and the fluorescence quantum yield accordingly decreases to Φ_f= 0.0012, suggesting that singlet-singlet energy transfer from Ru ^{1}MLCT excited state and porphyrin singlet excited state does not operate, otherwise Φ_f would have not changed. Therefore, excitation, either of the porphyrin moiety or of the ruthenium, results in the formation of a ^{3}MLCT excited state, which in ruthenium polipyridine complexes, at room temperature, decays in less than 1 ps.[97,98]

compound	Φ_f	λ_{em}/ nm	E_S /eV	Φ_{ISC}	E_T /eV	$\tau_T/\mu s$
Ru_{cat}	0.004	717		~1[a]	~1.85[b]	< 0.01
H_2-P	0.118	655, 714	1.91[c]	0.88[c]	1.51[d]	25
Zn-P	0.039	610, 655	2.06[c]	0.90[c]	1.59[d]	12
H_2-P-Ru_{cat}	0.0024	655, 714				2.5
Zn-P-Ru_{cat}	6.2 x 10^{-4}	610, 655, 750				1.9

Table 4. 2: [a] expected by analogy with $[Ru(bpy)_3]^{2+}$ and $[Ru(tpy)_2]^{2+}$ estimated according to ref. 8 (cfr SI); [c] 0-0 transition obtained from the intersection between normalised absorption and fluorescence spectra; [d] from maximum of phosphorescence at 77K (cf SI).

In the case of the Zn-P-Ru_{cat} dyad, upon excitation at 555 nm, 85% of light is absorbed by Zn-P moiety: emission quantum yield is strongly decreased as compared to the reference porphyrin and the spectrum exhibits, together with the porphyrin bands at 610 nm and 655 nm, a new broad band peaking at 750 nm (~1.65 eV), with 35 nm red-shifted as compared to the Ru_{cat} emission (Fig. 4.13), indicating the presence of a low-lying emitting excited state. This band was red-shifted and enhanced in a more polar solvent (Fig. 4.14). Decay from this excited state, possibly due to the formation of an intramolecular exciplex, which are stabilized in polar solvent, may prevent the formation of the triplet excited state.

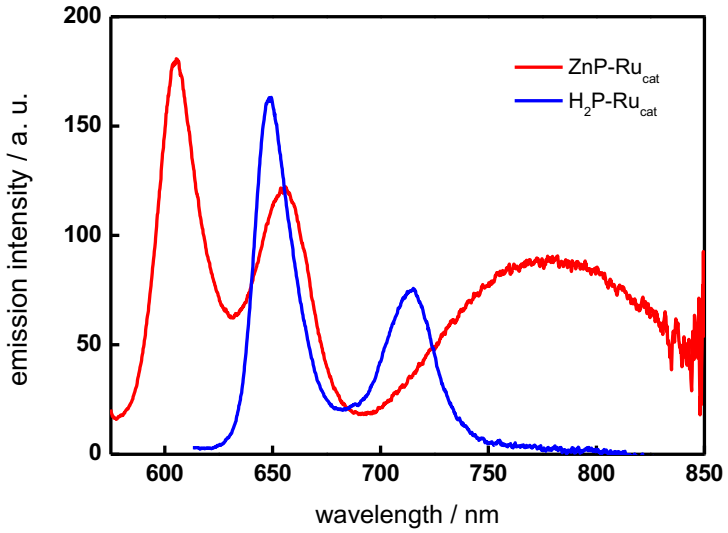

Figure 4.14: Emission in acetonitrile/acetone (50:50) solvent mixture. Excitation wavelength: 555 nm for Zn-P-Ru_{cat}, and 595 nm for H_2-P-Ru_{cat}.

From the energetics point of view, the dyads' ability for electron transfer in between the two moieties can be investigated through processing of the electrochemical data. They can provide the opportunity to estimate the thermodynamic energy change for electron transfer (Gibbs free energy change: *ΔGeT*) in such a system by using a Weller-type analysis.[99](Fig 4.15)

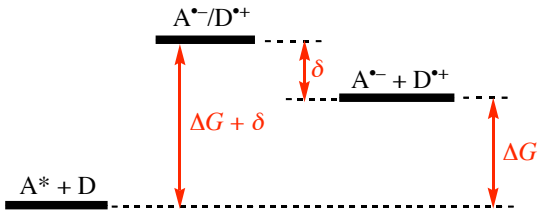

Figure 4.15: Diagram for electron transitions.

$$\Delta G = E_{ox}(D^{+}/D) - E_{red}(A/A^{-}) - E_{00}$$

In this equation, E_{ox} is the oxidation potential of the electron donor, while the reduction potential $E(D^{+}/D)$ describes the following process:

$$D_P^{+} + e \rightarrow D$$

E_{red} is the reduction potential $E(A/A^{-})$ and describes the following process:

$$A_P + e \rightarrow A_P^{-}$$

E_{00} is the energy of the S_0 to S_1 transition of the fluorophore, which can either be D_P or A_P. This can be estimated using the maximum emission of the donor at 77 K, or from the intersection between normalised absorption and fluorescence spectra.

The energy of the $^1H_2$-P excited state is not sufficient to drive the reduction (ΔG = +450 mV) or oxidation (ΔG = +110 mV) of the covalently linked ruthenium moiety. Although, the singlet excited state of the porphyrin and the triplet ^{3}MLCT of Ru_{cat} lie very close in energy. Energy transfer between these two levels is normally spin-forbidden, however, due to the strong spin–orbit coupling, induced by the ruthenium heavy atom effect, this process is most likely responsible for the quenching of the porphyrin excited state. [95,100,101] Analogously to the case of H_2-P-Ru dyad, for Zn-P-Ru the intramolecular electron transfer is endergonic (ΔG = +120 mV) for either reduction or oxidation of the appended ruthenium moiety. Thus, in this case, quenching of the porphyrin singlet excited state may occur either by singlet-triplet energy transfer, which is thermodynamically favorable, or via the formation of exciplex, which lies close (1.65 eV in chloroform, 1.59 eV in acetonitrile/acetone mixture) to the triplet porphyrin excited state.

4.4 Transient Differential Absorption

Through intricate examination and characterization of transient excited states, the photophysical influences of molecular sub-units can be defined, and one can begin to

intelligently design increasingly more effective and efficient photo-active molecules. Transient Absorption Spectroscopy is a time-resolved spectroscopy, ideal for studying dynamic processes in chemical compounds.

Transient Absorption Spectroscopy is an extension of the Absorption spectroscopy, also known as flash or pump-probe (PP) spectroscopy. The sample is being excited by a flash of light and the absorbance at a particular wavelength, or range of wavelengths, is measured as a function of time. In order to receive this kind of spectrum, the sample receives two pulses one after the other: the pump and the probe. After passing the sample, the pump is usually blocked, and the probe intensity is measured.

When the pump pulse excites the sample, some molecules leave the ground state and are transferred to the excited state (solid green arrow). This means that the concentration of ground-state molecules decreases and part of the ground state absorption signal disappears. Therefore, at the wavelengths of ground state absorption, the absorption difference becomes negative. The spectral shape of this negative contribution is identical to that of the ground state absorption spectrum measured by a spectrophotometer (this is what is missing, as some molecules are now in the excited state). This contribution to the difference absorption signal is called ground state bleaching (GSB) and is shown in Fig 4.16B by the green area curve. Over time, this signal remains until all the excited molecules return to the original ground state, from which they were excited.

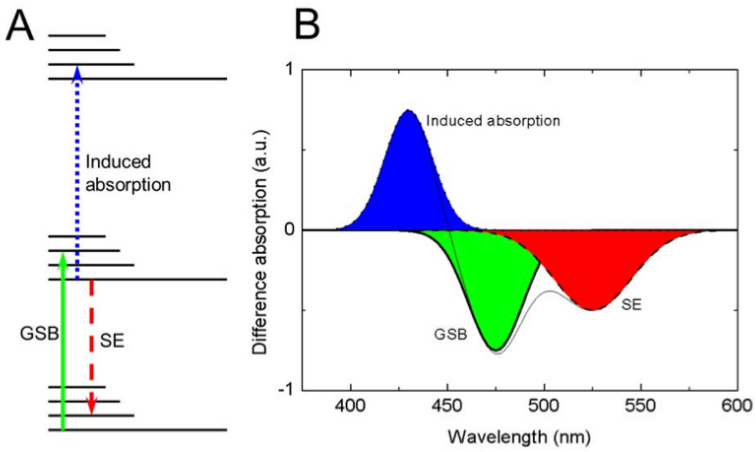

Figure 4.16: A. Energy levels of a molecule and some quantum transitions influencing the difference absorption spectrum. B: The corresponding difference absorption spectrum and with separated contributions of different transitions.

Stimulated emission (SE) arises, when the probe pulse finds some of the molecules in the excited state, and the photons of the probe pulse stimulate the emission of the sample molecules (red dashed arrow in Fig. 4.16B). This is the phenomenon underlying the principle of lasers. The photons radiated by the molecules have exactly the same polarization, direction and wavelength as the photons that 'dropped' the molecules from the excited to the ground state. It becomes apparent that this signal, similarly to the GSB signal, will be negative. When the pump pulse is blocked, the number of photons reaching the detector will be equal to the number of photons impinging on the sample (assuming no absorption). When the pump pulse is unblocked, the detector will also receive all these photons plus the photons emitted by the sample.

The induced absorption (IA) resulting from the fact that the molecules are in the excited state, can absorb another photon and go to a higher excited state (dotted blue line in Fig. 4.16A). This process can only occur in the excited molecules, therefore, after the excitation, additional absorption appears and the related contribution to ΔA signal is always

positive (blue area curve in Fig. 4.16B). However, it is noted that induced absorption can be caused not only by the singlet excited states of molecules. If, for example, the excited molecule has undergone intersystem crossing to the triplet excited state, triplet state absorption will be observed $S_1 \rightarrow T_1$, analogously to transitions $T_1 \rightarrow T_n$.

In our case, the dyads were studied in order to identify the electron transitions which were taking place. Upon excitation of H_2-P-Ru, with a 532 nm laser pulse, only typical features of the porphyrin triplet excited state[102] were observed (Fig. 4.17), as obtained for the reference H_2-P under identical experimental conditions. The amplitude of ΔA in the dyad is about 60% of ΔA in the free-base porphyrin. However, formation of the $^3H_2$-P exclusively via intersystem crossing from $^1H_2$-P state should yield only ~35% [$\Phi_{abs}(\Phi_{abs}$ (H_2-P)* $\Phi_{ISC}(H_2$-P))] of the triplet porphyrin. This also suggests that the short-lived *Ru_{cat} is involved in generating the $^3H_2$-P species, most likely by triplet-triplet energy transfer, which is a downhill reaction (ΔG = -340 mV). Surprisingly, the triplet excited state lifetime is shorter in the dyad (2.5 µs) than in the reference H_2-P (25 µs). This effect, previously observed in dyads where the ruthenium ion is in close proximity of a porphyrin moiety, has been attributed to the heavy atom effect of the ruthenium, which enhances the spin-orbit coupling interaction.[103,100] In conclusion, light absorption in the H_2-P-Ru dyad results in the formation of a triplet excited state, mainly localised on H_2-P and having a lifetime of 2.5 µs.

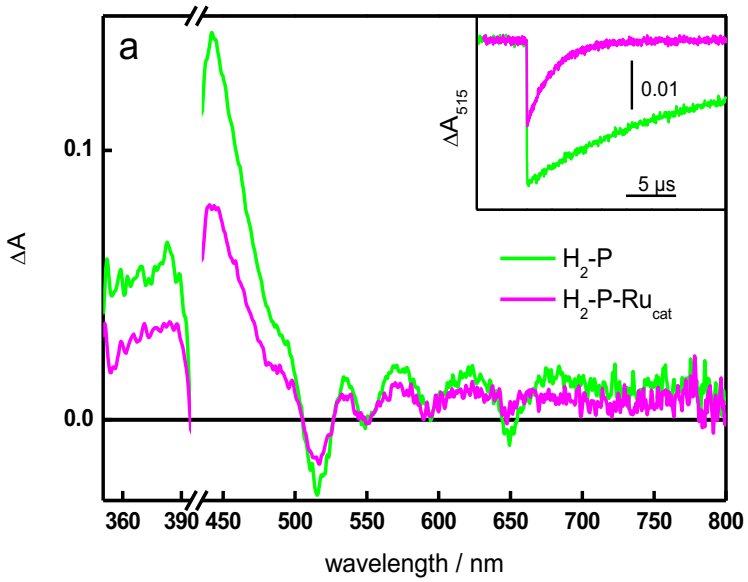

Figure 4.17: Transient absorption spectra at 100 ns after laser flash H_2-P (magenta) and H_2-P-Ru (green). Excitation wavelength: 532 nm. Absorbance: 0.1. Laser energy: 9-10 mJ. Inset: kinetic traces at 515 nm

Excitation with a laser pulse of the Zn-P-Ru dyad had the formation of the porphyrin triplet excited state (Figure 4.18) with ΔA being ~50% of that of the reference Zn-P and no other intermediate detected, suggesting that intersystem crossing from ^{1}Zn-P* excited state might be the only state to generate ^{3}Zn-P*. In conclusion, light absorption in the Zn-P-Ru dyad results in the formation of a triplet excited state, mainly localized on Zn-P, and having a lifetime of 1.9 μs.

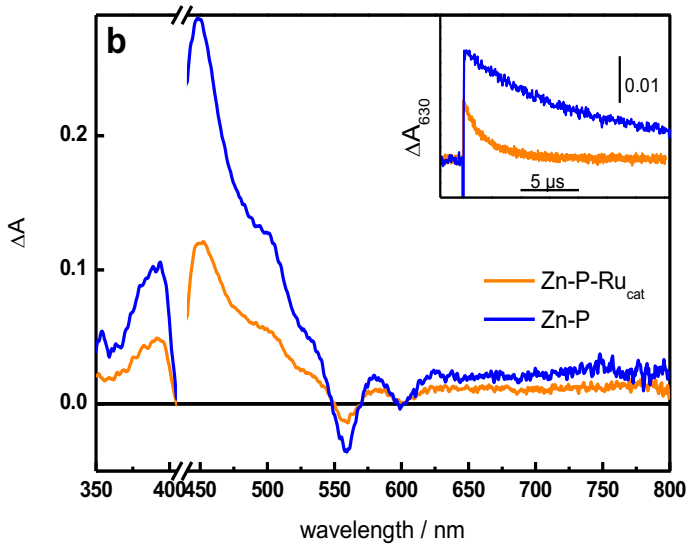

Figure 4.18: Zn-P (blue) and Zn-P-Ru (orange) in acetone/CH3CN (50:50) argon-purged solutions. Excitation wavelength: 532 nm. Absorbance: 0.1. Laser energy: 9-10 mJ. Inset: kinetic traces at 630 nm.

The following scheme (Scheme 4.1) summarizes the results of the photophysical studies and the electron transitions which take place between the porphyrin and ruthenium complex.

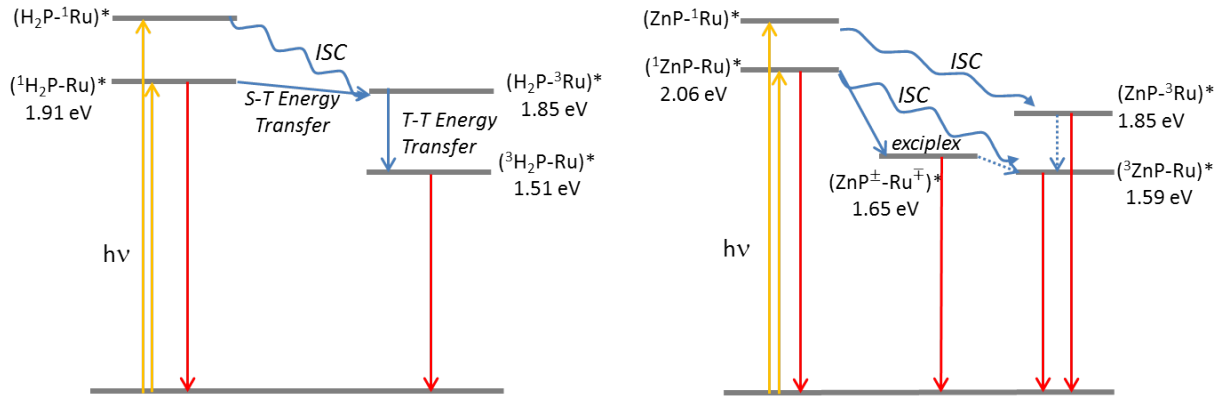

*Scheme 4. 10: Energy scheme for intramolecular reaction within the dyads **H$_2$-P-Ru** (left) and **Zn-P-Ru** (right). Yellow arrows, light absorption; red arrows, emission; blue arrows, intramolecular transitions.*

4.5 Photoinduced electron transfer

Having assessed that light absorption ultimately produces, in both dyads, a porphyrin triplet excited state lasting about 2 µs, we studied the reactions initiated in the presence of a reversible electron acceptor (methyl viologen, MV^{2+}) in order to investigate the possibility for it to oxidize Ru by an intramolecular electron transfer reaction. In both dyads, excited at 532 nm, the triplet state was quenched by MV^{2+} with a rate constant close to the diffusion limit (~10^9 M^{-1} s^{-1}). The transient spectra recorded 1 µs after the laser pulse (Fig. 4.19) indicates the formation of the radical ion pair $MV^{\bullet+}$ (positive absorption bands at 400 nm and 610 nm) and H_2-$P^{\bullet+}$-Ru or Zn-$P^{\bullet+}$-Ru respectively (broad positive absorption band between 500 and 800 nm, on which negative bands, due to the ground state depletion of the Q bands, are superimposed).

These spectral characteristics match well with those observed with the reference porphyrins H_2-$P^{\bullet+}$ or Zn-$P^{\bullet+}$ and are consistent with the literature.[104,105] However, after the initial formation of the porphyrin radical cation, a different behavior was observed for the two dyads. In the case of H_2-P-Ru, the H_2-$P^{\bullet+}$ initially formed, evolved in 1.5 µs (Fig. 4.19, inset, kinetics at 665nm and 500 nm) to yield the formation of Ru(III) characterized by an absorption depletion between 400 nm and 560 nm[106] (spectrum at 10 µs), while the absorption due to $MV^{\bullet+}$ (610 nm, inset) was only slightly decreased. Subsequent charge recombination between $MV^{\bullet+}$ and Ru(III) occurred in ~200 µs. In contrast, in the case of Zn-P-Ru, once the $MV^{\bullet+}$ and $ZnP^{\bullet+}$ radical species were formed (Fig. 4.19, right), only charge recombination in 200 µs (inset) without formation of Ru(III) was observed. The difference between the two dyads is rationalized by considering their different electrochemical properties. Due to the higher oxidation potential of the P^+/P couple in the dyad H_2-P-Ru, a driving force ΔG = -200 mV is available for H_2-$P^{\bullet+}$ to oxidize Ru(II), whereas in the dyad Zn-P-Ru, the available driving force for Zn-$P^{\bullet+}$ to oxidize Ru(II) is close to zero (table 1) and therefore an equilibrium is expected to be established between Zn-$P^{\bullet+}$ and Ru(III).

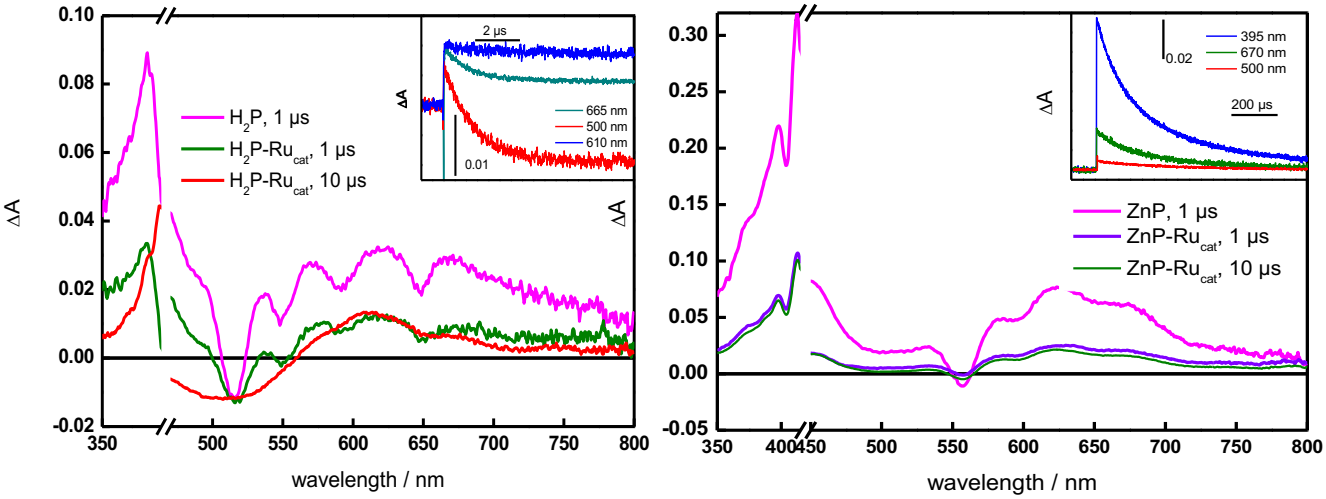

Figure 4.19: Left: differential absorption spectra of acetone/CH_3CN (50:50) solutions of H_2-P-Ru and H_2-P in the presence of 10 mM MV^{2+} (inset: kinetics at 500, 610 and 665nm). Right: Zn-P-Ru and Zn-P in the presence of 10 mM MV^{2+} (inset: kinetics at 395, 500 and 670).

4.6 Density functional theory (DFT)

Density functional theory (DFT) is a computational quantum mechanical modeling method widely used in Physics, Chemistry and Materials Science to investigate the electronic structure of molecules in the ground and excited state. Using this theory, the properties of a multi-electron system can be determined. In our case, by using functionals, the electron density of the dyads was calculated and the HOMO-LUMO gap was determined.

Firstly, the structure and the orientation of the dyads in the gas phase were determined, shown on the following figure. (Fig. 4.20) The tpy ligand of the ruthenium complex was found on the same planar as the porphyrin ring.

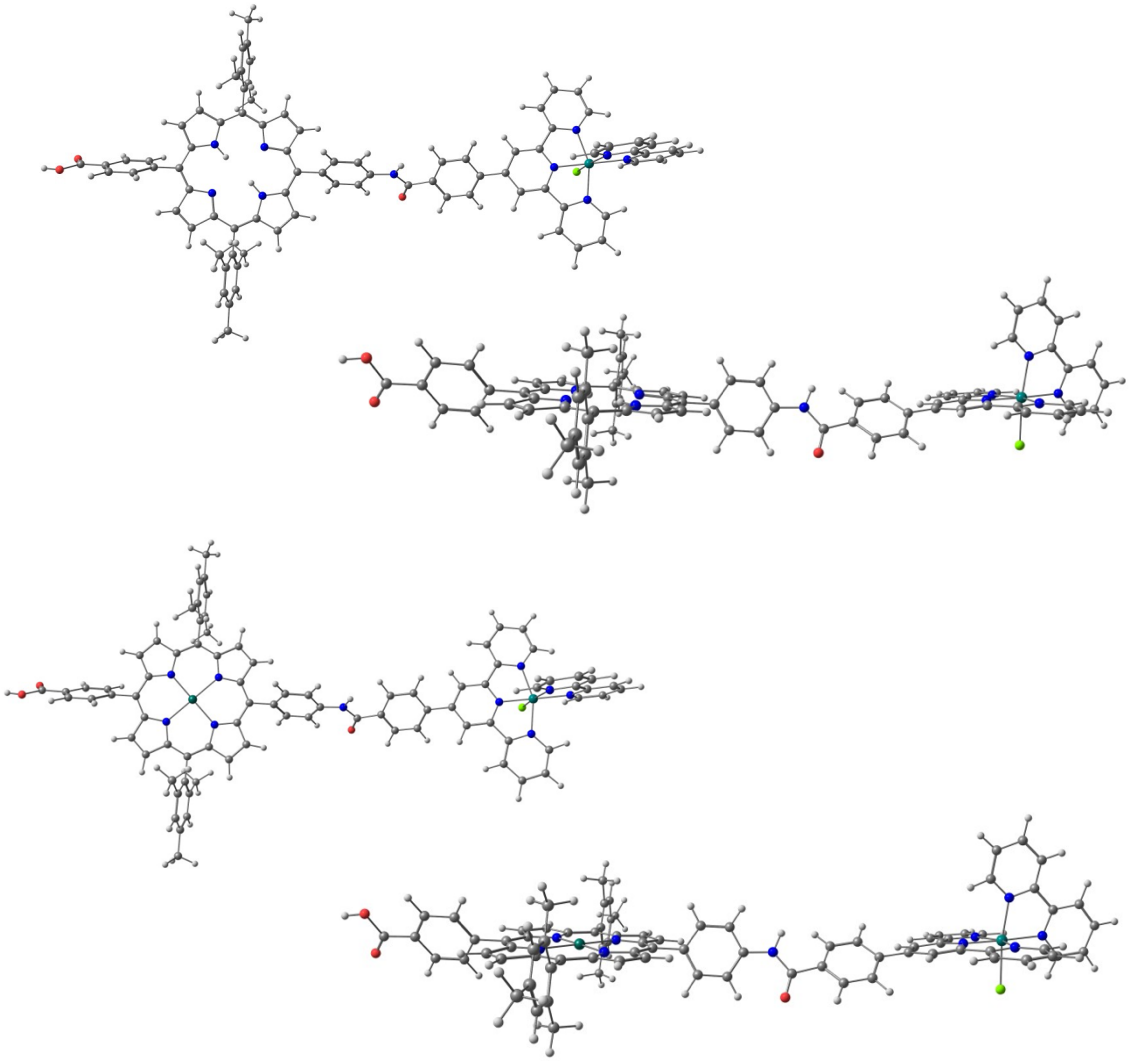

Figure 4.20: Gas phase of H2-P-Ru and Zn-P-Ru.

The HOMO and LUMO energies were then calculated. The HOMO-LUMO gap was calculated as 2,64 and 2,56 eV for the free base and Zinc dyad respectively. The HOMO-LUMO gap was calculated by electrochemical data through the following equations (Eq 4.1

for HOMO, 4.2 for LUMO) and were found to be 2,02 and 2,81 eV for the free base and Zinc dyad respectively.

$$E_{HOMO} = -(E_{onset,ox} vs [Fc^+/Fc] + 5{,}1)(eV) \qquad \textit{Equation 4. 1}$$

$$E_{LUMO} = -(E_{onset,red} vs [Fc^+/Fc] + 5{,}1)(eV) \qquad \textit{Equation 4. 2}$$

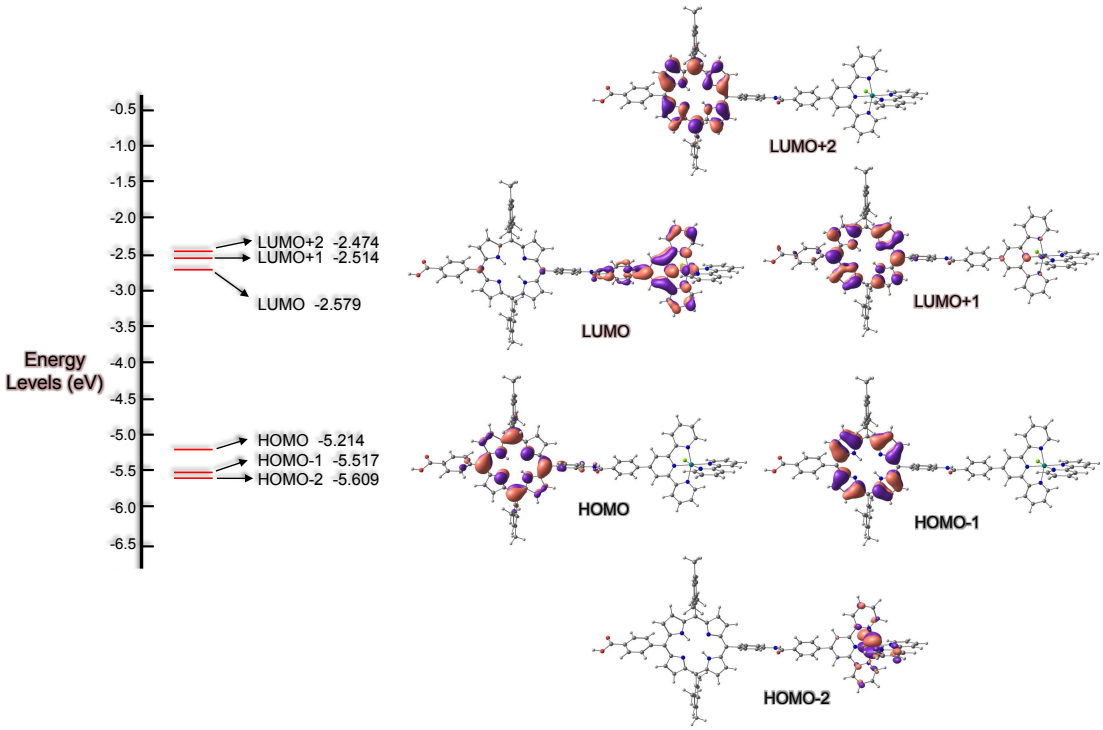

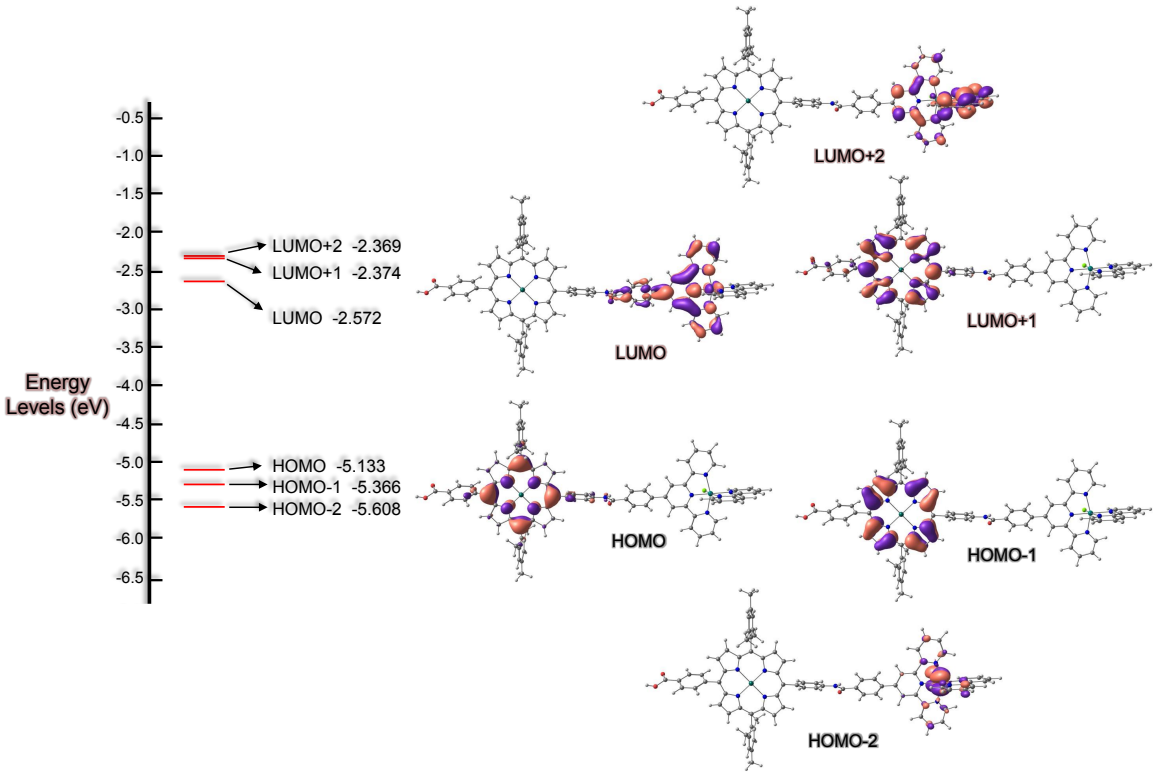

Figure 4.21: Energy Diagrams of H2P-Ru and ZnP-Ru.

4.7 Photooxidation Studies

After the previous studies, which indicated that in the case of H_2P-Ru, the chromophore (porphyrin) is able to activate the ruthenium moiety as a catalyst, the catalytic properties were then further explored. As determined from previous studies, dyads of a chromophore-catalyst can perform catalytic oxidations of different organic substrates (alcohols, methyl-sulfides etc.).(Fig 4.22)

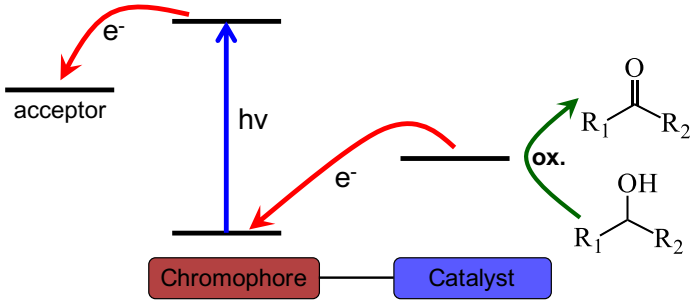

Figure 4.22: Photooxidation of alcohols.

In order to determine the catalytic ability of the dyad through light harvesting, photooxidation experiments were performed. The main protocol followed was adopted by Rocha's publication[90] even though different modifications have taken place. Sealed vials were used, containing 5.0 mL of an aqueous argon-degassed solution at pH 6.8 (0.10 M phosphate buffer) with 0.02 mM of the catalyst, 10 mM of the substrate and 20 mM of the sacrificial electron acceptor, and were then exposed to simulated visible sunlight irradiation (I > 400 nm) for 24 hours. All experiments were performed at room temperature and

atmospheric pressure while the reaction products were characterized by ^{1}H NMR spectroscopy.

Different modifications on the conditions took place concerning the solvent, the concentration of the catalyst and the substrate, the sacrificial electron acceptor and the substrate. Also, all synthesized dyads were examined for catalytic properties including those which carry carboxylic groups after they have been attached to titanium oxide (TiO_2). On the following table(Table 4.3), the results of these experiments and their modifications are summarized.

Catalyst[a]	Conc.[a]	Substrate[b]	Conc.[b]	EA	Solvent	TON[c]
H_2P-Ru(Cl)	0.02 mM	Benzyl alcohol	10.0 mM	$Na_2S_2O_8$	Phosphate buffer/Aceton	70[#]
H_2P-Ru(Cl)	0.02 mM	4-Bromo-benzyl alcohol	10.0 mM	$Na_2S_2O_8$	Phosphate buffer/Aceton	0
H_2P-Ru(Cl)	0.02 mM	4-Methoxy-benzyl alcohol	10.0 mM	$Na_2S_2O_8$	Phosphate buffer/Aceton	45
H_2P-Ru(Cl)	0.02 mM	4-Methoxy-benzyl alcohol	10.0 mM	$Na_2S_2O_8$	Phosphate buffer/$CHCl_3$	45
ZnP-Ru(Cl)	0.02 mM	4-Methoxy-benzyl alcohol	10.0 mM	$Na_2S_2O_8$	Phosphate buffer/$CHCl_3$	30
H_2P-Ru(Cl)	0.02 mM	4-Methoxy-benzyl alcohol	10.0 mM	$Na_2S_2O_8$	Phosphate buffer/$CHCl_3$	30[‡]
H_2P-Ru(Cl)	0.04 mM	4-Methoxy-benzyl alcohol	10.0 mM	$Na_2S_2O_8$	Phosphate buffer/$CHCl_3$	25
H_2P-Ru(Cl)	0.04 mM	4-Methoxy-benzyl alcohol	10.0 mM	$Na_2S_2O_8$	Phosphate buffer/$CHCl_3$	25[‡]
ZnP-Ru(Cl)	0.04 mM	4-Methoxy-benzyl alcohol	10.0 mM	$Na_2S_2O_8$	Phosphate buffer/$CHCl_3$	15
H_2P-Ru(Cl)	0.02 mM	4-Methoxy-benzyl alcohol	10.0 mM	$[Co(NH_3)_5(Cl)]Cl_2$	Phosphate buffer/$CHCl_3$	45
H_2P-Ru(Cl)	0.04 mM	4-Methoxy-benzyl alcohol	50.0 mM	$[Co(NH_3)_5(Cl)]Cl_2$	Phosphate buffer/$CHCl_3$	110
H_2P-Ru(Cl)	0.04 mM	4-Methoxy-benzyl alcohol	10.0 mM	$[Co(NH_3)_5(Cl)]Cl_2$	Phosphate buffer/$CHCl_3$	20
ZnP-Ru(Cl)	0.04 mM	4-Methoxy-benzyl alcohol	10.0 mM	$[Co(NH_3)_5(Cl)]Cl_2$	Phosphate buffer/$CHCl_3$	30
H_2P-Ru(OH)	0.04 mM	4-Methoxy-benzyl alcohol	10.0 mM	$[Co(NH_3)_5(Cl)]Cl_2$	Phosphate buffer/$CHCl_3$	20
H_2P-Ru(Cl)	0.02 mM	4-Methoxy-benzyl alcohol	10.0 mM	$[Co(NH_3)_5(Cl)]Cl_2$	Phosphate buffer*/$CHCl_3$	20
H_2P-Ru(Cl)	0.02 mM	4-Methoxy-benzyl alcohol	10.0 mM	$[Co(NH_3)_5(Cl)]Cl_2$	Phosphate buffer**/$CHCl_3$	~0
H_2P-Ru(Cl) on TiO_2	0.02 mM	4-Methoxy-benzyl alcohol	10.0 mM	-	Phosphate buffer/$CHCl_3$	70
ZnP-Ru(Cl) on TiO_2	0.02 mM	4-Methoxy-benzyl alcohol	10.0 mM	-	Phosphate buffer/$CHCl_3$	40
H_2P-Ru(Cl)	0.02 mM	4-Methoxy-benzyl alcohol	10.0 mM	4-Bromobezenediazonium tetrafluoroborate	Phosphate buffer/Aceton	45
H_2P-Ru(Cl)	0.02 mM	Thioanisole	500 mM	$[Co(NH_3)_5(Cl)]Cl_2$	H_2O/Aceton	17,500
H_2P-Ru(Cl)	0.02 mM	Thioanisole	500 mM	4-Bromobezenediazonium tetrafluoroborate	H_2O/Aceton	20,000

*Table 4. 3: [a] Concentration of the catalyst, [b] Concentration of the substrates, [c] TON= $n_{product}/n_{catalyst}$, [#] issues with work up, [‡] I>420nm, *pH=5.7, **pH=8.*

5 Research proposal

It is a crucial need to investigate the dyads under the conditions of the photooxidation experiments, using FLP (flash laser photolysis). This method is a pump-probe laboratory technique, in which a sample is firstly excited by a strong pulse (called pump pulse) of light from a laser of nanosecond, picosecond, or femtosecond pulse width or by a short-pulse light source such as a flash lamp. This first strong pulse starts a chemical reaction or leads to an increased population for energy levels other than the ground state within a sample of atoms or molecules. Typically, the absorption of light by the sample is recorded within short time intervals (by a so-called test pulses) to monitor relaxation or reaction processes initiated by the pump pulse. It will allow to explore the effect of the different sacrificial electron donors and also explain the low TONs in case of alcohols. It is also very important to repeat these experiments using labelled water H_2O^{18} in order to confirm that the oxygen atom of the substrate.

Both these methods will give insight to the mechanism of the photocatalytic reactions and may provide information in order to optimize the system. Also, they might be very constructive and promote new synthetic approach in order to construct more efficient dyads.

6 Experimental

Synthesis

Group I

Synthesis of 5(4-methoxycarbonylphenyl),15(4-nitrophenyl)-10,20-di(2,4,6- trimethylphenyl) porphyrin.

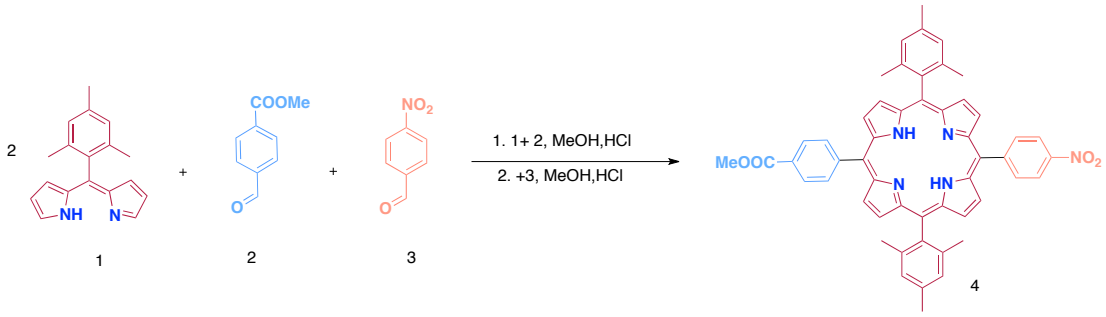

Dipyrromethane (1) (4 mmol) and aldehyde (2) (2 mmol) were dissolved in MeOH (200 mL). Subsequently a solution of HCl (36 %, 10 mL) in water (200 mL) was added and the reaction mixture was stirred at room temperature for 1 h. The precipitate formed was filtered through a Buchner funnel, washed with MeOH/water (1:1, 200 mL), and then with water (200 mL). The bilane (0.5 mmol, 1 equiv) and aldehyde (3) (0.5 mmol, 1 equiv) were added to degassed ethanol (200 mL) in a 1 L round- bottomed flask under argon. The reaction mixture was stirred for 10 min and then a solution of aqueous HCl (36 %, 1 mL) in water (50 mL) was added. The reaction mixture was stirred at room temperature for 16 h under argon in the dark. The usual work-up consisted of one extraction with chloroform (200 mL), washing with water (3 100 mL), and then with a saturated aqueous solution of NaHCO3 (100 mL). The organic layer was briefly dried on anhydrous MgSO4 and then oxidized with p-chloranil (370 mg, 1.5 mmol, 3 equiv) for 1 h by heating at reflux. . The desired compound was isolated using silica column chromatography CH_2Cl_2 to obtain compound (4) as a purple solid (316 mg, 39,4%).

1H NMR (500 MHz, $CDCl_3$):δ = 8.75 (m, 4 H), 8.72 (d, *J* = 4.5 Hz, 2 H), 8.70 (d, *J* = 5 Hz, 2H), 8.63 (d, *J* = 8.5 Hz, 2 H), 8.43 (d, *J* = 8.5 Hz, 2 H), 8.41 (d, *J*= 8.5 Hz, 2 H), 8.31 (d, *J* = 8 Hz, 2 H), 7.29 (s, 4 H), 4.11 (s, 3 H),2.63 (s, 6 H), 1.84 (s, 12 H), –2.64 (s, 2 H) ppm.

13C NMR(125 MHz, $CDCl_3$): δ = 167.5, 149.2 147.9, 146.8, 139.4, 138.2,135.2, 134.6, 130.9, 130.7, 129.8, 128.1, 128.0, 122.0, 119.3, 118.8, 116.4, 52.6, 21.8, 21.6 ppm.

HRMS (MALDI-TOF): calcd. For $C_{52}H_{43}N_5O_4$ 801.3315 [M]+; found 801.3304. $C_{52}H_{43}N_5O_4$ (801.94):calcd. C 77.88, H 5.40, N 8.73; found C 77.74, H 5.53, N 8.62.

Synthesis of 5(4-methoxycarbonylphenyl),15(4-aminophenyl)-10,20-di(2,4,6-trimethylphenyl) porphyrin.

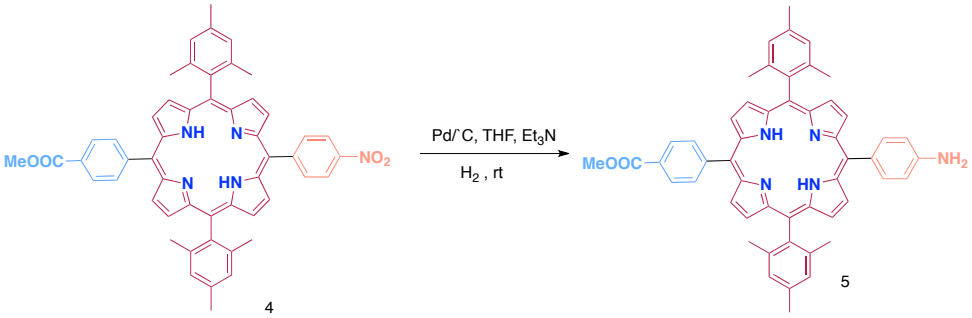

The porphyrin (4) (0.100 g, 0.125 mmol) was added in a mixture of anhydrous THF (30 mL) and anhydrous Et_3N (70 µL) containing 10% Pd / C (0.022 g, 0.22 mmol). For 3 h the reaction mixture was under constant stirring and under hydrogen atmosphere at room temperature. Then Celite pad was used to filter the reaction mixture and been distilled. For purification of porphyrin 5 column chromatography was used (silica gel, CH_2Cl_2). (0.090 g 93%)

^{1}H NMR (500 MHz, $CDCl_3$): δ =8.91 (d, J = 4.5 Hz, 2 H), 8.72 (m, 6 H), 8.44 (d, J = 8 Hz, 2 H),8.32 (d, J = 8.5 Hz, 2 H), 8.01 (d, J = 8 Hz, 2 H), 7.29 (s, 4 H),7.06 (d, J = 8 Hz, 2 H), 4.12 (s, 3 H), 2.64 (s, 6 H), 1.85 (s, 12 H),–2.58 (s, 2 H) ppm.

^{13}C NMR (125 MHz, $CDCl_3$): δ = 167.5, 147.2,146.2, 139.5, 138.6, 137.9, 135.7, 134.7, 132.3, 131.8, 130.9, 130.4,130.1, 129.6, 128.0, 127.9, 120.6, 118.5, 117.5, 113.6, 52.5, 21.8 21.6 ppm.

HRMS (MALDI-TOF): calcd. for $C_{52}H_{45}N_5O_2$ 771.3573 [M]+; found 771.3606.

Synthesis of 5(4-methoxyperoxyphenyl),15(4-terpyphenyl)-10,20-di(2,4,6- trimethylphenyl) porphyrin [compound (11)]

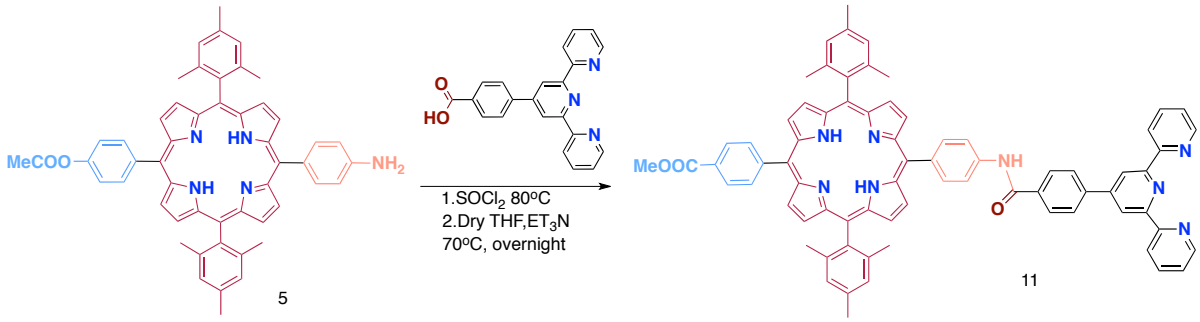

4-([2,2′:6″,2″-Terpyridin]-4′-yl)benzoic acid (terpy- COOH) (75 mg, 0.21 mmol) was dissolved in $SOCl_2$ (2.8 mL) and stirred under an argon atmosphere at 80 °C for 2 h. $SOCl_2$ was removed under reduced pressure and the resulting acyl chloride terpyridine was dried

under high vacuum at 50 °C for 1 h. The resulting solid was dissolved in anhydrous THF (9 mL) and anhydrous triethylamine (0.1 mL) and porphyrin (5) (55 mg, 0.07 mmol) were added. The reaction mixture was heated under argon at 70 °C overnight. The solvent was removed under reduced pressure, $CHCl_3$ (80 mL) was added and the mixture was washed with water (3x50 mL). The organic layer was dried with Na_2SO_4, filtered and concentrated. The desired compound was isolated using silica column chromatography CH_2Cl_2 : MeOH (100 : 6) to obtain compound (11) as a purple solid (72 mg, 91%).

^{1}H NMR (500 MHz, $CDCl_3$): δ= 8.87 (d, J = 4.7 Hz, 2H), 8.85 (s, 2H), 8.78 (m, 2H), 8.73 (m, 8H), 8.42 (d, J = 8.4 Hz, 2H), 8.36 (s, 1H), 8.31 (d,J=8.4Hz,2H),8.25 (d,J=8.5Hz,2H), 8.20 (d,J=8.5Hz, 2H), 8.13 (d,J=8.5Hz,2H), 8.10 (d,J=8.5Hz,2H), 7.93 (dt,J_1 = 7.7 Hz, J_2 = 1.8 Hz, 2H), 7.41 (m, 2H), 7.29 (s, 4H), 4.11 (s, 3H), 2.64 (s, 6H), 1.85 (s, 12H), 2.60 (s, 2H).

^{13}C NMR (75 MHz, $CDCl_3$): d 167.5, 165.7, 156.3, 156.1, 149.3, 147.1, 142.3, 139.5, 138.5, 138.4, 138.0, 137.9, 137.3, 135.5, 135.3, 134.7, 131.1, 131.0, 130.5, 129.6, 128.0, 127.9, 124.2, 121.7, 119.2, 118.8, 118.7, 117.9, 52.5, 21.8, 21.6.

HRMS (MALDI-TOF) calcd for $C_{74}H_{58}N_8O_3$ $[M]^+$ 1106.4632, found 1106.4628.

Synthesis of ruthenium complex $Ru(bpy)(DMSO)_2Cl_2$ (9)

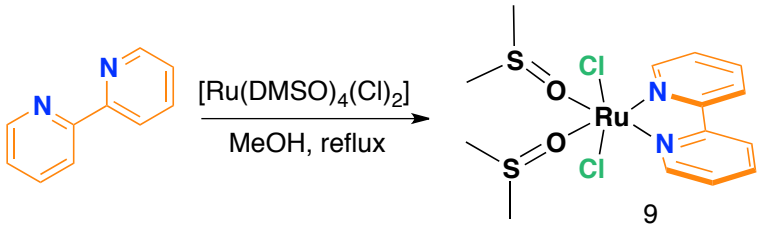

The compound (9) was synthesized according to this reference.[107]

Synthesis of 5(4-methoxyperoxyphenyl),15(4-[(RubpyterpyCl)phenyl]-10,20-di(2,4,6-trimethylphenyl) porphyrin. (compound H_2-P-Ru)

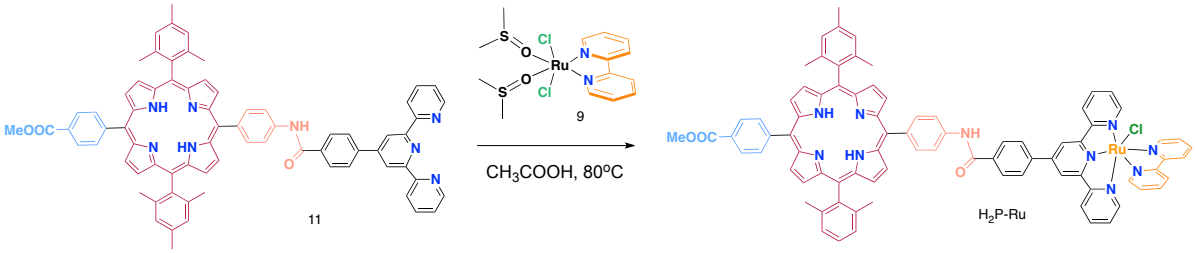

The ruthenium complex $(Ru(bpy)(DMSO)_2Cl_2)$ (55 mg, 0.11 mmol) was added to a solution of H_2-P-terpy (11) (75 mg, 0.07 mmol) in acetic acid (30 mL) and the mixture was stirred under nitrogen at 100 1C overnight. After removing the solvent, the product was purified by column chromatography on silica CH_2Cl_2 : MeOH (100 : 7) giving H_2-P-Ru as a purple solid (70 mg, 74%).

^{1}H NMR (500MHz, $CDCl_3$): δ= 11.15 (brs,1H) ,10.36 (s,1H) ,8.89 (d,J=3.5Hz,2H) ,8.83 (brs,2H) ,8.73 (d,J=4.5Hz,2H) ,8.68 (d,J=4.5Hz,4H) ,8.64 (d,J=4.5Hz,2H) ,8.52 (d,J= 6.5 Hz, 2H) , 8.42 (d, J = 7.9 Hz, 4H) , 8.30 (d, J = 7.9 Hz, 3H) , 8.19 (br s, 2H) , 8.08 (d, J = 6.5 Hz, 2H) , 7.96 (br s, 2H), 7.75 (br s, 1H), 7.47 (br s, 4H), 7.30 (br s, 1H), 7.22 (s, 4H), 7.15 (br s, 1H), 7.05 (br s, 2H), 6.78 (br s, 1H), 4.10 (s, 3H), 2.56 (s, 6H), 1.78 (s, 12H), 2.61 (s, 2H).

^{13}C NMR (125 MHz, $CDCl_3$): 167.5, 167.2, 158.7, 158.3, 157.8, 155.9, 152.8, 151.5, 147.0, 144.0, 139.5, 139.4, 138.4, 137.9, 137.3, 137.0, 136.5, 135.4, 135.2, 134.7, 131.2, 129.6, 129.5, 128.1, 127.9, 127.5, 127.2, 126.8, 126.6, 125.1, 123.3, 120.0, 119.9, 119.2, 118.6, 117.8, 52.6, 21.8, 21.6.

HRMS (MALDI-TOF) calcd for $C_{84}H_{66}Cl_2N_{10}O_3Ru$ [M Cl]$^+$ 1399.4051, found 1399.4077.

Synthesis of Zn-5(4-methoxyperoxyphenyl),15(4-[(RubpyterpyCl)phenyl]-10,20-di(2,4,6-trimethylphenyl) porphyrin. (compound Zn-P-Ru)

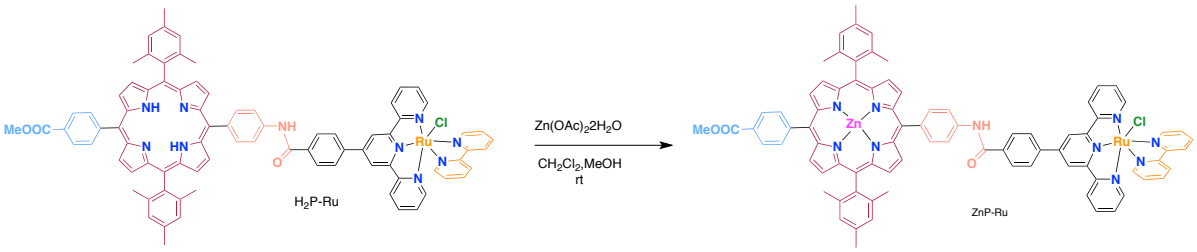

To a stirred solution of H_2-P-Ru (30 mg, 0.02 mmol) in CH_2Cl_2 (15 mL) and MeOH (3 mL) zinc acetate dihydrate (85 mg, 0.39 mmol) was added. The reaction mixture was stirred at room temperature overnight. The solvent was removed using a rotary evaporator and the desired compound was isolated by silica column chromatography CH_2Cl_2 : MeOH (100:8) to obtain Zn-P-Ru_{cat} as a purple solid (29 mg, 93%).

^{1}H NMR (500 MHz, (DMSO-d_6)): δ= 10.93 (s, 1H), 10.14 (d, J = 5.1 Hz, 1H), 9.35 (s, 2H), 9.04 (d, J = 8.1 Hz, 2H), 8.96 (d, J = 8.2 Hz, 1H), 8.83 (d, J = 4.4 Hz, 2H), 8.71 (d, J = 4.4 Hz, 2H), 8.68 (d, J = 8.5 Hz, 1H), 8.61 (m, 6H), 8.46 (d, J = 8.0 Hz, 2H), 8.36 (m, 5H), 8.31 (d, J =8.0Hz,2H),8.23(d,J=8.0Hz,2H),8.09(m,3H),7.81(t,J=7.5Hz,1H),7.67(d,J=5.4Hz,2H),7.48(d,J= 6.0 Hz, 1H), 7.43 (t, J =6.5 Hz, 2H), 7.33 (s, 4H), 7.11 (t, J = 6.5 Hz, 1H), 4.04 (s, 3H), 2.59 (s, 6H), 1.80 (s, 12H).

^{13}C NMR (125 MHz, DMSO-d_6): 166.5, 135.3, 158.6, 158.3, 158.0, 155.6, 152.0, 151.9, 149.4, 149.1, 149.0, 148.7, 147.8, 143.8, 139.3, 139.1, 138.6, 138.4, 138.0, 137.0, 136.9, 136.0, 135.7, 134.5, 134.4, 132.1, 131.6, 130.4, 130.2, 129.4, 128.8, 128.6, 127.6, 127.3, 127.0, 126.5, 124.2, 123.8, 123.6, 120.2, 119.8, 118.5, 118.2, 118.0, 52.4, 21.4, 21.0.

HRMS (MALDI-TOF) calcd for $C_{84}H_{64}ClN_{10}O_3RuZn$ [M Cl]$^+$ 1461.3186, found 1461.3171.

Synthesis of 5(4-carbooxyphenyl),15(4-[(RubpyterpyCl)phenyl]-10,20-di(2,4,6-trimethylphenyl) porphyrin. (compound H_2P(-COOH)-Ru).

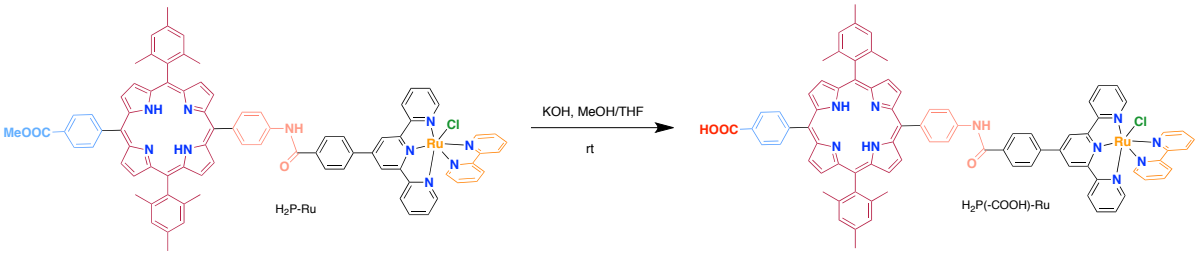

To a THF (6 mL) and MeOH (3 mL) mixed solution of H_2P-Ru (27 mg, 0.0194 mmol), an aqueous solution (3 mL) of KOH (109.06 mg, 1.9436 mmol) was added. The reaction mixture was stirred at room temperature for three days and then the solvents were evaporated under vacuum and distilled H_2O (10 mL) was added to the resulting residue. The mixture was acidified using $HCl_{(aq)}$ 1 M resulting in the precipitation of H_2P(-COOH)-Ru as a purple solid which after being filtered, washed with distilled water and dried, was collected (26,5 mg, 99%).

The ^{1}H and ^{13}C NMR spectrum could not be recorded due to its limited solubility in $CDCl_3$.

Synthesis of Zn-5(4-carbooxyphenyl),15(4-[(RubpyterpyCl)phenyl]-10,20-di(2,4,6-trimethylphenyl) porphyrin. (compound ZnP(-COOH)-Ru).

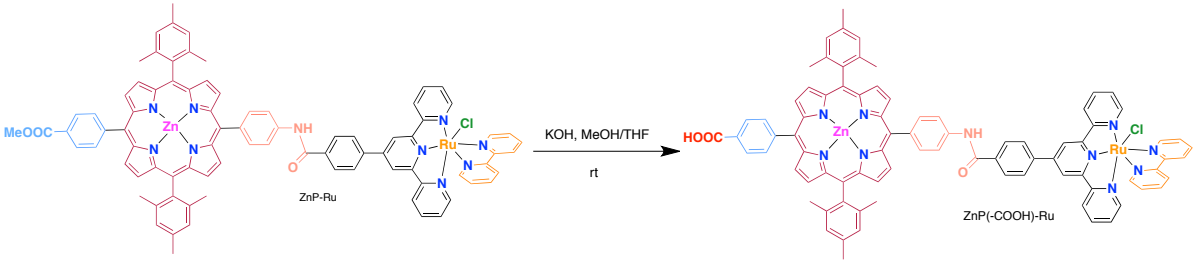

To a THF (6 mL) and MeOH (3 mL) mixed solution of ZnP-Ru (28 mg, 0.0194 mmol), an aqueous solution (3 mL) of KOH (109.06 mg, 1.9436 mmol) was added. The reaction mixture was stirred at room temperature for three days and then the solvents were evaporated under vacuum and distilled H_2O (10 mL) was added to the resulting residue. The mixture was acidified using $HCl_{(aq)}$ 1 M resulting in the precipitation of H_2P(-COOH)-Ru as a purple solid which after being filtered, washed with distilled water and dried, was collected (27,4 mg, 98%).

The ^{1}H and ^{13}C NMR spectrum could not be recorded due to its limited solubility in $CDCl_3$.

Group II

Synthesis of 5-10-15-20-Tetraphenyl porphyrin (6)

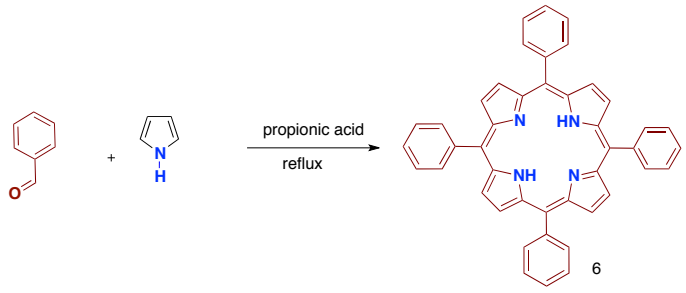

The porphyrin (6) was synthesized according to this Adler and Longo's work.[16]

Synthesis of 5,10,20(triphenyl-)-15(4-nitrophenyl-) porphyrin (7) and 15(4-amino)-5,10,20(triphenyl-) porphyrin (8).

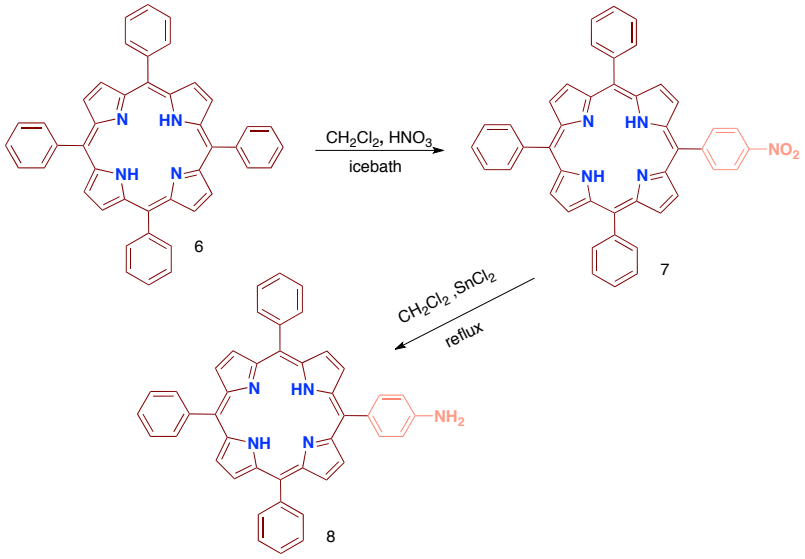

The porphyrin derivatives (7) and (8) were synthesized according to this reference.[108]

Synthesis of 5,10,20(triphenyl-)-15(4-terpyphenyl) porphyrin (12).

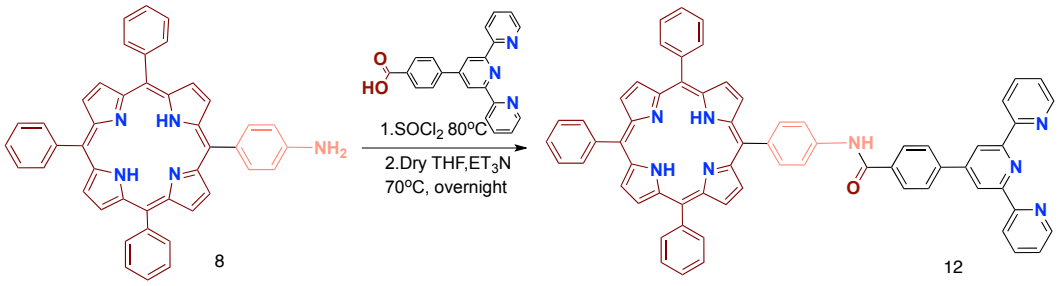

4-([2,2′:6′′,2′′-Terpyridin]-4′-yl)benzoic acid (terpy -COOH) (75 mg, 0.21 mmol) was dissolved in $SOCl_2$ (2.8 mL) and stirred under an argon atmosphere at 80 °C for 2 h. $SOCl_2$ was removed under reduced pressure and the resulting acyl chloride terpyridine was dried under high vacuum at 50 °C for 1 h. The resulting solid was dissolved in anhydrous THF (9 mL) and anhydrous triethylamine (0.1 mL) and porphyrin (8) (44 mg, 0.07 mmol) were added. The reaction mixture was heated under argon at 70 °C overnight. The solvent was removed under reduced pressure, $CHCl_3$ (80 mL) was added and the mixture was washed with water (3x50 mL). The organic layer was dried with Na_2SO_4, filtered and concentrated. The desired compound was isolated using silica column chromatography CH_2Cl_2 : MeOH (100 : 6) to obtain compound (11) as a purple solid (60 mg, 90%).

NMR

Synthesis of 2,2′-Bipyridine-4,4′-dicarboxylic ester

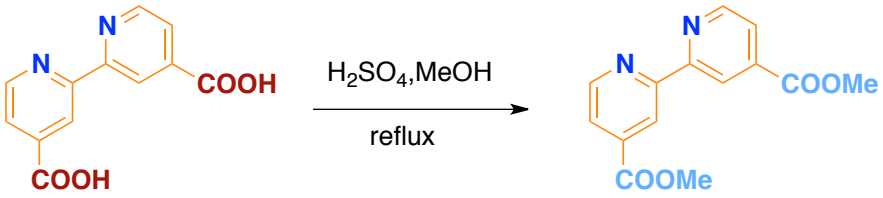

2,2′-Bipyridine-4,4′-dicarboxylic acid (200mg,) was dissolved in MeOH (1,2ml) and (0,4ml) H_2SO_4 and stirred at 100 °C for 24 h. MeOH was removed under reduced pressure, Diethyl ether (40 mL) was added and the mixture was washed with water (3x50 mL). The organic layer was dried with Na_2SO_4, filtered and concentrated. (mg,96%)

Synthesis of ruthenium complex $Ru(bpy(-COOH)_2)(DMSO)_2Cl_2$ (10)

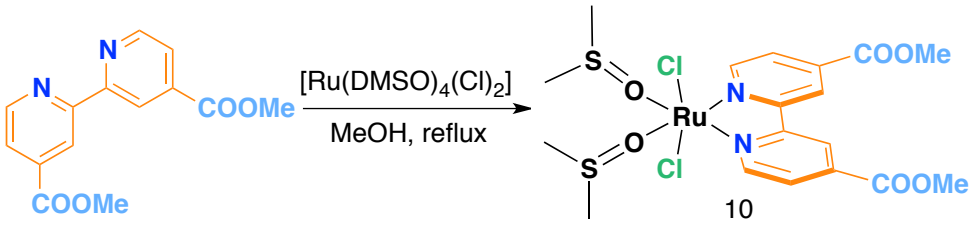

The compound (9) was synthesized according to this reference.[107]

Synthesis of 5,10,20(triphenyl-)-15-[(Rubpy(MeCOO)$_2$terpyCl)phenyl-] porphyrin (H_2-TPP-Ru).

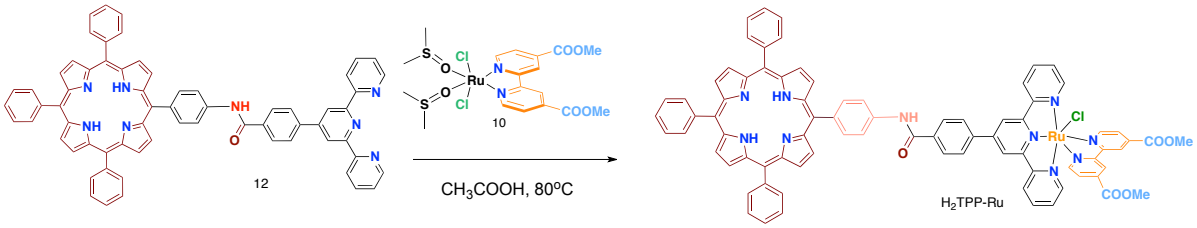

The ruthenium complex (Ru(bpy(-COOH)$_2$)(DMSO)$_2$Cl$_2$) (10) (55 mg, 0.11 mmol) was added to a solution of H_2-TPP-terpy (12) (65 mg, 0.07 mmol) in acetic acid (30 mL) and the mixture was stirred under nitrogen at 100 1C overnight. After removing the solvent, the product was purified by column chromatography on silica CH_2Cl_2 : MeOH (100 : 7) giving H_2-TPP-Ru as a purple solid (73 mg, 76%).

Synthesis of Zn-5,10,20(triphenyl-)-15-[(Rubpy(MeCOO)$_2$terpyCl)phenyl-] porphyrin (Zn-TPP-Ru).

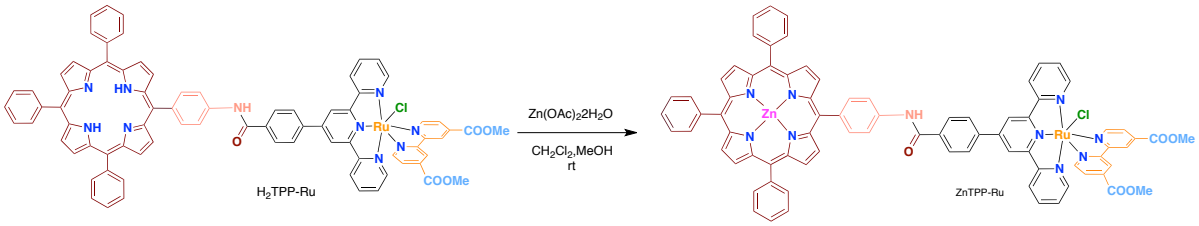

To a stirred solution of H_2-TPP-Ru (27 mg, 0.02 mmol) in CH_2Cl_2 (15 mL) and MeOH (3 mL) zinc acetate dihydrate (85 mg, 0.39 mmol) was added. The reaction mixture was stirred at room temperature overnight. The solvent was removed using a rotary evaporator and the desired compound was isolated by silica column chromatography CH_2Cl_2 : MeOH (100:8) to obtain Zn-TPP-Ru as a purple solid (27 mg, 95%).

The ^{1}H and ^{13}C NMR spectrum could not be recorded due to its limited solubility in $CDCl_3$.

Synthesis of 5,10,20(triphenyl-)-15-[(Rubpy(HCOO)$_2$terpyCl)phenyl-] porphyrin (H_2-TPP-Ru(COOH)$_2$).

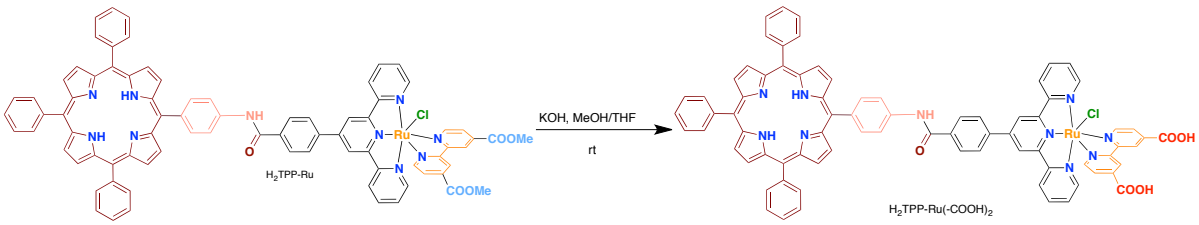

To a THF (6 mL) and MeOH (3 mL) mixed solution of H_2P-Ru (23.5 mg, 0.0170 mmol), an aqueous solution (3 mL) of KOH (95mg, 1.70 mmol) was added. The reaction mixture was stirred at room temperature for three days and then the solvents were evaporated under vacuum and distilled H_2O (10 mL) was added to the resulting residue. The mixture was acidified using $HCl_{(aq)}$ 1 M resulting in the precipitation of H_2P-Ru(-COOH)$_2$ as a purple solid which after being filtered, washed with distilled water and dried, was collected (26,5 mg, 99%).

The ^{1}H and ^{13}C NMR spectrum could not be recorded due to its limited solubility in $CDCl_3$.

Synthesis of Zn-5,10,20(triphenyl-)-15-[(Rubpy(MeCOO)$_2$terpyCl)phenyl-] porphyrin (Zn-TPP-Ru(-COOH)$_2$).

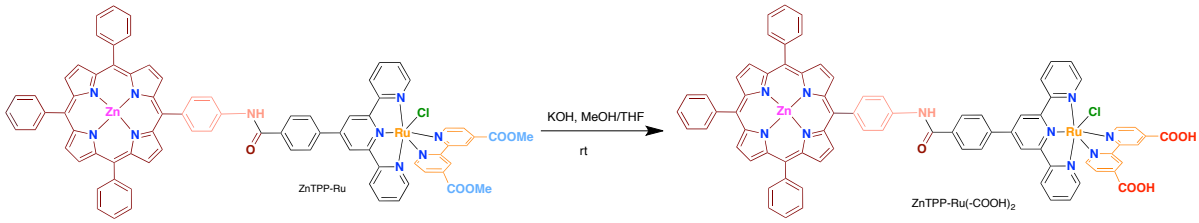

To a THF (6 mL) and MeOH (3 mL) mixed solution of H_2P-Ru (26 mg, 0.0180 mmol), an aqueous solution (3 mL) of KOH (101 mg, 1.80 mmol) was added. The reaction mixture was stirred at room temperature for three days and then the solvents were evaporated under vacuum and distilled H_2O (10 mL) was added to the resulting residue. The mixture was acidified using $HCl_{(aq)}$ 1 M resulting in the precipitation of Zn-TPP-Ru(-COOH)$_2$ as a purple solid which after being filtered, washed with distilled water and dried, was collected (24 mg, 97%).

The ^{1}H and ^{13}C NMR spectrum could not be recorded due to its limited solubility in $CDCl_3$.

Synthesis of 5(4-methoxyperoxyphenyl),15(4-[phenylCHONHphenyl]-10,20-di(2,4,6-trimethylphenyl) porphyrin (H_2-P)

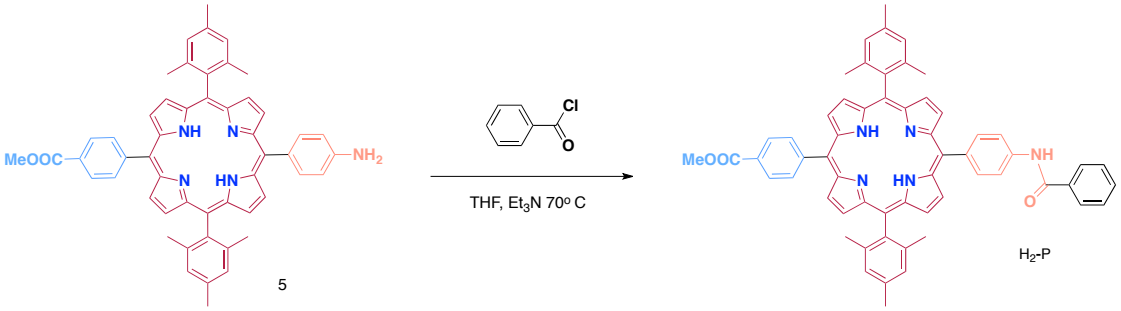

Benzoyl chloride (32 mL, 0.27 mmol) and porphyrin (5) (35 mg, 0.05 mmol) were dissolved in dry THF (4 mL) and dry triethylamine (50 mL) and the reaction mixture was stirred under argon at 70 1C overnight. At this time the solvent was removed under reduced pressure and the desired product was isolated by silica column chromatography CH_2Cl_2 : EtOH (98 : 2) to obtain the desired product as a purple solid (31 mg, 78%)

^{1}H NMR (500 MHz, $CDCl_3$): δ= 8.86 (d, J = 4.7 Hz, 2H), 8.74 (d, J = 4.7 Hz, 2H), 8.72 (m, 4H), 8.43 (d, J = 8.4 Hz, 2H), 8.32 (d, J = 8.4 Hz, 2H), 8.25 (d, J = 8.5 Hz, 2H), 8.18 (s, 1H), 8.05 (m, 4H), 7.63 (m, 3H), 7.29 (s, 4H), 4.11 (s, 3H), 2.64 (s, 6H), 1.85 (s, 12H), 2.61 (s, 2H).

^{13}C NMR (75 MHz, $CDCl_3$): 167.5, 166.2, 147.0, 139.5, 138.5, 138.3, 138.0, 137.8, 135.3, 135.2, 134.7, 132.3, 131.2, 131.0, 130.4, 129.6, 129.1, 128.0, 127.9, 127.3, 119.2, 118.7, 118.5, 117.9, 52.6, 21.8, 21.6.

HRMS (MALDI-TOF) calcd for $C_{59}H_{49}N_5O_3$ $[M]^+$ 875.3835, found 875.3841.

Synthesis of Zn5(4-methoxyperoxyphenyl),15(4-[phenylCHONHphenyl]-10,20-di(2,4,6-trimethylphenyl) porphyrin (Zn-P).

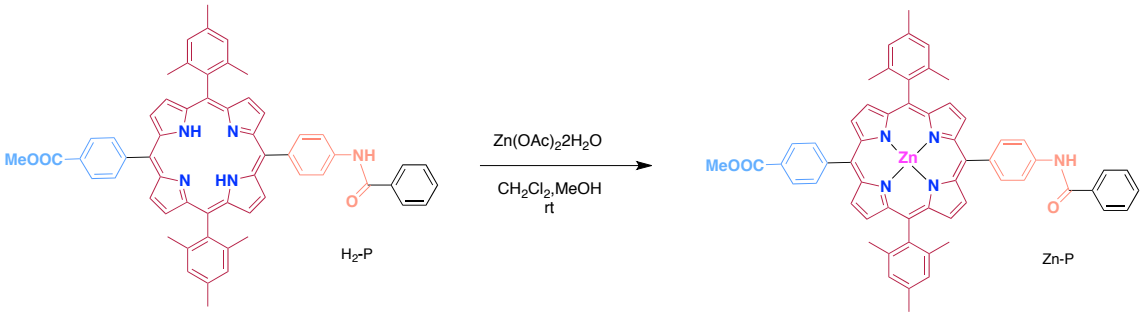

A mixture of H_2-P (27 mg, 0.03 mmol) and zinc acetate dihydrate (67 mg, 0.30 mmol) in CH_2Cl_2 (8 mL) and MeOH (2 mL) was stirred at room temperature overnight. The solvent

was removed using a rotary evaporator and the desired com- pound was isolated by silica column chromatography CH_2Cl_2 : EtOH (98:2) to obtain Zn-P as a brown solid (26 mg, 92%).

^{1}H NMR (500 MHz, $CDCl_3$): δ= 8.94 (d, J = 4.6 Hz, 2H), 8.82 (d, J = 4.6 Hz, 2H), 8.79 (m, 4H), 8.42 (d, J = 8.0 Hz, 2H), 8.32 (d, J = 8.0 Hz, 2H), 8.25 (d, J = 8.1 Hz, 2H), 8.16 (s, 1H), 8.03 (d, J = 7.4 Hz, 4H), 7.61 (m, 3H), 7.28 (s, 4H), 4.10 (s, 3H), 2.63 (s, 6H), 1.83 (s, 12H).

The ^{13}C NMR spectrum could not be recorded due to its limited solubility in $CDCl_3$. HRMS (MALDI-TOF) calcd for $C_{59}H_{47}N_5O_3$ $[M]^+$ 937.2970, found 937.2963.

7 References

(1) Smith, K. M. **1975**.

(2) Becker, E. D.; Bradley, R. B.; Watson, C. J. **2002**.

(3) Kadish, K.; Guilard, R.; Smith, K. M. In *The Porphyrin Handbook: Phthalocyanines: Properties and Materials*; 2012; pp 134–135.

(4) Yujiang Song, †, ‡; Raid E. Haddad, †, ‡; Song-Ling Jia, †, ‡; Saphon Hok, §; Marilyn M. Olmstead, §; Daniel J. Nurco, §; Neal E. Schore, §; Jun Zhang, †, ‡; Jian-Guo Ma, †, ‡; Kevin M. Smith, ‖; Stéphanie Gazeau, ⊥; Jacques Pécaut, ⊥; Jean-Claude Marchon, ⊥; Craig J. Medforth, *, †, § and; John A. Shelnutt*, †, #. **2005**.

(5) Retsek, J. L.; Drain, C. M.; Kirmaier, C.; Nurco, D. J.; Medforth, C. J.; Smith, K. M.; Sazanovich, I. V; Chirvony, V. S.; Fajer, J.; Holten, D. *J. Am. Chem. Soc.* **2003**, *125* (32), 9787–9800.

(6) Banfi, S.; Caruso, E.; Caprioli, S.; Mazzagatti, L.; Canti, G.; Ravizza, R.; Gariboldi, M.; Monti, E. *Bioorg. Med. Chem.* **2004**, *12* (18), 4853–4860.

(7) Screen, T. E. O.; Thorne, J. R. G.; Denning, R. G.; Bucknall, D. G.; Anderson, H. L. *J. Mater. Chem.* **2003**, *13* (11), 2796–2808.

(8) Charalambidis, G.; Daphnomili, D. .

(9) Borgström, M.; Blart, E.; Boschloo, G.; Mukhtar, E.; Hagfeldt, A.; Hammarström, L.; Odobel, F. *J. Phys. Chem. B* **2005**, *109* (48), 22928–22934.

(10) Maufroy, A.; Favereau, L.; Anne, F. B.; Pellegrin, Y.; Blart, E.; Hissler, M.; Jacquemin, D.; Odobel, F. *J. Mater. Chem. A* **2015**, *3* (7), 3908–3917.

(11) Fukuzumi, S. *Eur. J. Inorg. Chem.* **2008**, No. 9, 1351–1362.

(12) Tebo, A.; Herrero, C.; Aukauloo, A. *Handb. Porphyr. Sci.* **2014**, 196–233.

(13) Vincente, M. G. H.; Smith, K. M. *ChemInform* **2000**, *31* (37).

(14) Liem T. Nguyen; Mathias O. Senge, † and; Kevin M. Smith*, ‡. **1996**.

(15) Nowak-Król, A.; Plamont, R.; Canard, G.; Edzang, J. A.; Gryko, D. T.; Balaban, T. *Chem. - A Eur. J.* **2015**, *21* (4), 1488–1498.

(16) Adler, A. D.; Longo, F. R.; Finarelli, J. D.; Goldmacher, J.; Assour, J.; Korsakoff, L. *J. Org. Chem.* **1967**, *32* (2), 476–476.

(17) Adler, A. D.; Sklar, L.; Longo, F. R.; Finarelli, J. D.; Finarelli, M. G. *J. Heterocycl. Chem.* **1968**, *5* (5), 669–678.

(18) Lindsey, J. S.; Schreiman, I. C.; Hsu, H. C.; Kearney, P. C.; Marguerettaz, A. M. *J. Org. Chem.* **1987**, *52* (5), 827–836.

(19) Kincaid, J. R. Academic Press 2000.

(20) MacDonald, F.; Arsenault, P.; Bullock, E. *Am Chem Soc* **1960**, *82*, 4384–4389.

(21) Sessler, J. L.; Johnson, M. R.; Lynch, V. *J. Org. Chem.* **1987**, *52* (19), 4394–4397.

(22) Sessler, J. L.; Cyr, M. J.; Lynch, V.; McGhee, E.; Ibers, J. A. *J. Am. Chem. Soc.* **1990**, *112* (7), 2810–2813.

(23) Smith, K. M. *Porphyr. Handb.* **2003**, *1*, 1–43.

(24) Juris, A.; Balzani, V.; Barigelletti, F.; Campagna, S.; Belser, P. l; Von Zelewsky, A. *Coord. Chem. Rev.* **1988**, *84*, 85–277.

(25) Kalyanasundaram, K. *Photochemistry of polypyridine and porphyrin complexes*; Academic Press, 1991.

(26) Kalyanasundaram, K. *Coord. Chem. Rev.* **1982**, *46*, 159–244.

(27) Meijer, M. D.; van Klink, G. P. M.; van Koten, G. *Coord. Chem. Rev.* **2002**, *230* (1), 141–163.

(28) Meyer, T. J. *Acc. Chem. Res.* **1989**, *22* (5), 163–170.

(29) Sun, L.; Hammarström, L.; Åkermark, B.; Styring, S. *Chem. Soc. Rev.* **2001**, *30* (1), 36–49.

(30) Campagna, S.; Di Pietro, C.; Loiseau, F.; Maubert, B.; McClenaghan, N.; Passalacqua, R.; Puntoriero, F.; Ricevuto, V.; Serroni, S. *Coord. Chem. Rev.* **2002**, *229* (1), 67–74.

(31) Dürr, H.; Bossmann, S. *Acc. Chem. Res.* **2001**, *34* (11), 905–917.

(32) Barigelletti, F.; Flamigni, L. *Chem. Soc. Rev.* **2000**, *29* (1), 1–12.

(33) Robertson, N.; McGowan, C. A. *Chem. Soc. Rev.* **2003**, *32* (2), 96–103.

(34) Ziessel, R.; Hissler, M.; El-ghayoury, A.; Harriman, A. *Coord. Chem. Rev.* **1998**, *178*, 1251–1298.

(35) De Silva, A. P.; Gunaratne, H. Q. N.; Gunnlaugsson, T.; Huxley, A. J. M.; McCoy, C. P.; Rademacher, J. T.; Rice, T. E. *Chem. Rev.* **1997**, *97* (5), 1515–1566.

(36) Metcalfe, C.; Thomas, J. A. *Chem. Soc. Rev.* **2003**, *32* (4), 215–224.

(37) Prier, C. K.; Rankic, D. A.; MacMillan, D. W. C. *Chem. Rev.* **2013**, *113* (7), 5322–5363.

(38) Xuan, J.; Xiao, W. *Angew. Chemie Int. Ed.* **2012**, *51* (28), 6828–6838.

(39) Kärkäs, M. D.; Verho, O.; Johnston, E. V.; Åkermark, B. *Chem. Rev.* **2014**, *114* (24), 11863–12001.

(40) Lay, P. A.; Sargeson, A. M.; Taube, H.; Chou, M. H.; Creutz, C. *Inorg. Synth. Vol. 24* **1986**, 291–299.

(41) Evans, I. P.; Spencer, A.; Wilkinson, G. *J. Chem. Soc. Dalt. Trans.* **1973**, No. 2, 204–209.

(42) Hayoz, P.; Von Zelewsky, A.; Stoeckli-Evans, H. *J. Am. Chem. Soc.* **1993**, *115* (12), 5111–5114.

(43) Anderson, P. A.; Deacon, G. B.; Haarmann, K. H.; Keene, F. R.; Meyer, T. J.; Reitsma, D. A.; Skelton, B. W.; Strouse, G. F.; Thomas, N. C. *Inorg. Chem.* **1995**, *34* (24), 6145–6157.

(44) Strouse, G. F.; Anderson, P. A.; Schoonover, J. R.; Meyer, T. J.; Keene, F. R. *Inorg. Chem.* **1992**, *31* (14), 3004–3006.

(45) Treadway, J. A.; Moss, J. A.; Meyer, T. J. *Inorg. Chem.* **1999**, *38* (20), 4386–4387.

(46) Freedman, D. A.; Evju, J. K.; Pomije, M. K.; Mann, K. R. *Inorg. Chem.* **2001**, *40* (22), 5711–5715.

(47) Zakeeruddin, S. M.; Nazeeruddin, M. K.; Humphry-Baker, R.; Grätzel, M.; Shklover, V. *Inorg. Chem.* **1998**, *37* (20), 5251–5259.

(48) Cargill Thompson, A. M. W. W. *Coord. Chem. Rev.* **1997**, *160*, 1–52.

(49) Fallahpour, R.-A. *Synthesis (Stuttg).* **2003**, *2003* (2), 0155–0184.

(50) Hagelin, H.; Hedman, B.; Orabona, I.; Åkermark, T.; Åkermark, B.; Klug, C. A. *J. Mol. Catal. A Chem.* **2000**, *164* (1), 137–146.

(51) Pomerantz, M.; Amarasekara, A. S.; Dias, H. V. R. *J. Org. Chem.* **2002**, *67* (20), 6931–6937.

(52) Tiecco, M.; Testaferri, L.; Tingoli, M.; Chianelli, D.; Montanucci, M. *Synthesis (Stuttg).* **1984**, *1984* (9), 736–738.

(53) Uenishi, J.; Tanaka, T.; Wakabayashi, S.; Oae, S.; Tsukube, H. *Tetrahedron Lett.* **1990**, *31* (32), 4625–4628.

(54) Lehmann, U.; Henze, O.; Schlüter, A. D. *Chem. Eur. J.* **1999**, *5* (3), 854–859.

(55) Schubert, U. S.; Eschbaumer, C.; Hien, O.; Andres, P. R. *Tetrahedron Lett.* **2001**, *42* (28), 4705–4707.

(56) Savage, S. A.; Smith, A. P.; Fraser, C. L. *J. Org. Chem.* **1998**, *63* (26), 10048–10051.

(57) Kroehnke, F. *Synthesis (Stuttg).* **1976**, *1976* (1), 1–24.

(58) Potts, K. T.; Cipullo, M. J.; Ralli, P.; Theodoridis, G. *J. Org. Chem.* **1982**, *47* (16), 3027–3038.

(59) Potts, K. T.; Usifer, D. A.; Guadalupe, A.; Abruna, H. D. *J. Am. Chem. Soc.* **1987**, *109* (13), 3961–3967.

(60) Jameson, D. L.; Guise, L. E. *Tetrahedron Lett.* **1991**, *32* (18), 1999–2002.

(61) Lewis, N. S.; Nocera, D. G. *Proc. Natl. Acad. Sci.* **2006**, *103* (43), 15729–15735.

(62) Armaroli, N.; Balzani, V. *Angew. Chemie Int. Ed.* **2007**, *46* (1-2), 52–66.

(63) Herrero, C.; Quaranta, A.; Leibl, W.; Rutherford, A. W.; Aukauloo, A. *Energy Environ. Sci.* **2011**, *4* (7), 2353–2365.

(64) Gust, D.; Moore, T. A.; Moore, A. L. *Acc. Chem. Res.* **2009**, *42* (12), 1890–1898.

(65) Ferreira, K. N.; Iverson, T. M.; Maghlaoui, K.; Barber, J.; Iwata, S. *Science (80-.).* **2004**, *303* (5665), 1831–1838.

(66) Herrero, C.; Lassalle-Kaiser, B.; Leibl, W.; Rutherford, A. W.; Aukauloo, A. *Coord. Chem. Rev.* **2008**, *252* (3), 456–468.

(67) Rutherford, A. W.; Boussac, A. *Science (80-.).* **2004**, *303* (5665), 1782–1784.

(68) Loll, B.; Kern, J.; Saenger, W.; Zouni, A.; Biesiadka, J. *Nature* **2005**, *438* (7070), 1040–1044.

(69) Barber, J.; Ferreira, K.; Maghlaoui, K.; Iwata, S. *Phys. Chem. Chem. Phys.* **2004**, *6* (20), 4737–4742.

(70) Yano, J.; Kern, J.; Irrgang, K.-D.; Latimer, M. J.; Bergmann, U.; Glatzel, P.; Pushkar, Y.; Biesiadka, J.; Loll, B.; Sauer, K. *Proc. Natl. Acad. Sci. U. S. A.* **2005**, *102* (34), 12047–12052.

(71) Lavergne, J.; Junge, W. *Photosynth. Res.* **1993**, *38* (3), 279–296.

(72) Umena, Y.; Kawakami, K.; Shen, J.-R.; Kamiya, N. *Nature* **2011**, *473* (7345), 55–60.

(73) Ke, B. *Photosynthesis photobiochemistry and photobiophysics*; Springer Science & Business Media, 2001; Vol. 10.

(74) Alibabaei, L.; Brennaman, M. K.; Norris, M. R.; Kalanyan, B.; Song, W.; Losego, M. D.; Concepcion, J. J.; Binstead, R. A.; Parsons, G. N.; Meyer, T. J. *Proc. Natl. Acad. Sci.* **2013**, *110* (50), 20008–20013.

(75) Inoue, H.; Shimada, T.; Kou, Y.; Nabetani, Y.; Masui, D.; Takagi, S.; Tachibana, H. *ChemSusChem* **2011**, *4* (2), 173–179.

(76) Weinberg, D. R.; Gagliardi, C. J.; Hull, J. F.; Murphy, C. F.; Kent, C. A.; Westlake, B. C.;

Paul, A.; Ess, D. H.; McCafferty, D. G.; Meyer, T. J. *Chem. Rev.* **2012**, *112* (7), 4016–4093.

(77) Gagliardi, C. J.; Vannucci, A. K.; Concepcion, J. J.; Chen, Z.; Meyer, T. J. *Energy Environ. Sci.* **2012**, *5* (7), 7704–7717.

(78) Meyer, T. J.; Huynh, M. H. V; Thorp, H. H. *Angew. Chemie Int. Ed.* **2007**, *46* (28), 5284–5304.

(79) Gersten, S. W.; Samuels, G. J.; Meyer, T. J. *J. Am. Chem. Soc.* **1982**, *104* (14), 4029–4030.

(80) Gilbert, J. A.; Eggleston, D. S.; Murphy Jr, W. R.; Geselowitz, D. A.; Gersten, S. W.; Hodgson, D. J.; Meyer, T. J. *J. Am. Chem. Soc.* **1985**, *107* (13), 3855–3864.

(81) Collin, J. P.; Sauvage, J. P. *Inorg. Chem.* **1986**, *25* (2), 135–141.

(82) Nagoshi, K.; Yamashita, S.; Yagi, M.; Kaneko, M. *J. Mol. Catal. A Chem.* **1999**, *144* (1), 71–76.

(83) Zong, R.; Thummel, R. P. *J. Am. Chem. Soc.* **2005**, *127* (37), 12802–12803.

(84) Campbell, W. M.; Burrell, A. K.; Officer, D. L.; Jolley, K. W. *Coord. Chem. Rev.* **2004**, *248* (13), 1363–1379.

(85) Windle, C. D.; Câmpian, M. V; Duhme-Klair, A.-K.; Gibson, E. A.; Perutz, R. N.; Schneider, J. *Chem. Commun.* **2012**, *48* (66), 8189–8191.

(86) Lazarides, T.; Delor, M.; Sazanovich, I. V; McCormick, T. M.; Georgakaki, I.; Charalambidis, G.; Weinstein, J. A.; Coutsolelos, A. G. *Chem. Commun.* **2014**, *50* (5), 521–523.

(87) Natali, M.; Argazzi, R.; Chiorboli, C.; Iengo, E.; Scandola, F. *Chem. Eur. J.* **2013**, *19* (28), 9261–9271.

(88) Song, L.-C.; Tang, M.-Y.; Mei, S.-Z.; Huang, J.-H.; Hu, Q.-M. *Organometallics* **2007**, *26* (7), 1575–1577.

(89) Song, L.-C.; Wang, L.-X.; Tang, M.-Y.; Li, C.-G.; Song, H.-B.; Hu, Q.-M. *Organometallics* **2009**, *28* (13), 3834–3841.

(90) Chen, W.; Rein, F. N.; Rocha, R. C. *Angew. Chemie - Int. Ed.* **2009**, *48* (51), 9672–9675.

(91) Herrero, C.; Quaranta, A.; Fallahpour, R.-A.; Leibl, W.; Aukauloo, A. *J. Phys. Chem.* **2013**, *117* (19), 9605–9612.

(92) Boyce, M.; Bertozzi, C. R. *Nat. Methods* **2011**, *8* (8), 638.

(93) Gouterman, M. *J. Mol. Spectrosc.* **1961**, *6*, 138–163.

(94) Gouterman, M.; Wagnière, G. H.; Snyder, L. C. *J. Mol. Spectrosc.* **1963**, *11* (1–6), 108–127.

(95) Benniston, A. C.; Chapman, G. M.; Harriman, A.; Mehrabi, M. *J. Phys. Chem. A* **2004**, *108* (42), 9026–9036.

(96) Valeur, B. *Molecular Fluorescence: Principles and Applications*; 2001; Vol. 8.

(97) Damrauer, N. H.; Cerullo, G.; Yeh, A.; Boussie, T. R.; Shank, C. V.; McCusker, J. K. *Science (80-.).* **1997**, *275* (5296), 54–57.

(98) Hammarström, L.; Barigelletti, F.; Flamigni, L.; Indelli, M. T.; Armaroli, N.; Calogero, G.; Guardigli, M.; Sour, A.; Collin, J.-P.; Sauvage, J.-P. *J. Phys. Chem. A* **1997**, *101* (48), 9061–9069.

(99) Lakowicz, J. R. *Principles of Fluorescence Spectroscopy*; Lakowicz, J. R., Ed.; Springer US: Boston, MA, 2006.

(100) Flamigni, L.; Armaroli, N.; Barigelletti, F.; Balzani, V.; Collin, J.-P.; Dalbavie, J.-O.; Heitz, V.; Sauvage, J.-P. *J. Phys. Chem. B* **1997**, *101* (31), 5936–5943.

(101) Flamigni, L.; Barigelletti, F.; Armaroli, N.; Collin, J.-P.; Sauvage, J.-P.; Williams, J. A. G. *Chem. – A Eur. J.* **1998**, *4* (9), 1744–1754.

(102) Pekkarinen, L.; Linschitz, H. *J. Am. Chem. Soc.* **1960**, *82* (10), 2407–2411.

(103) Benniston, A. C.; Harriman, A.; Pariani, C.; Sams, C. A. *Phys. Chem. Chem. Phys.* **2006**, *8* (17), 2051–2057.

(104) Gasyna, Z.; Browett, W. R.; Stillman, M. J. *Inorg. Chem.* **1984**, *23* (3), 382–384.

(105) Fajer, J.; Borg, D. C.; Forman, A.; Dolphin, D.; Felton, R. H. *J. Am. Chem. Soc.* **1970**, *92* (11), 3451–3459.

(106) Herrero, C.; Quaranta, A.; Fallahpour, R.-A.; Leibl, W.; Aukauloo, A. *J. Phys. Chem. C* **2013**, *117* (19), 9605–9612.

(107) Tong, L.; Inge, A. K.; Duan, L.; Wang, L.; Zou, X.; Sun, L. *Inorg. Chem.* **2013**, *52* (5), 2505–2518.

(108) Ladomenou, K.; Lazarides, T.; Panda, M. K.; Charalambidis, G.; Daphnomili, D.; Coutsolelos, A. G. *Inorg. Chem.* **2012**, *51* (20), 10548–10556.

Appendix

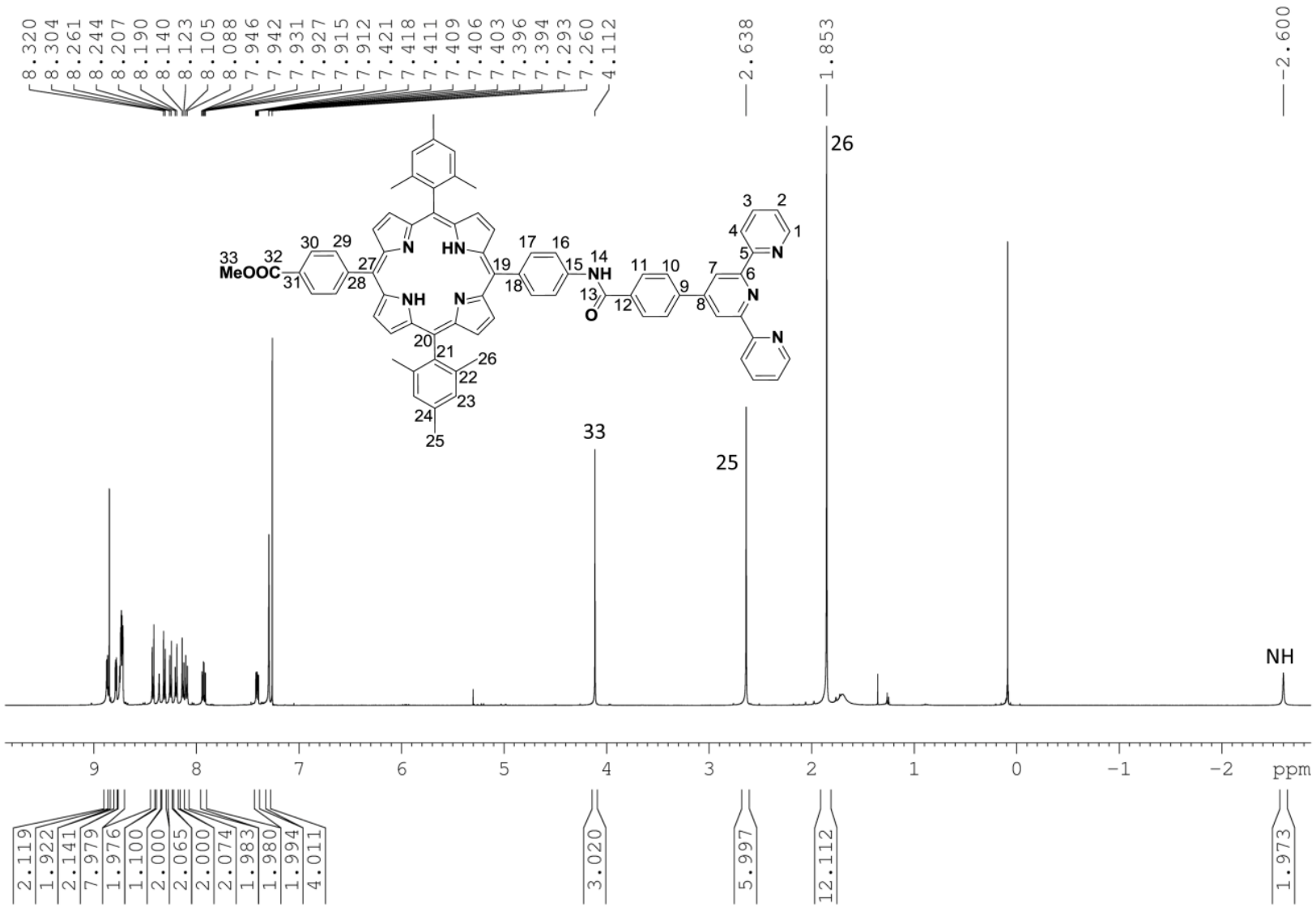

*Figure 1: ^{1}H NMR spectrum of compound **H_2-P-terpy** in $CDCl_3$*

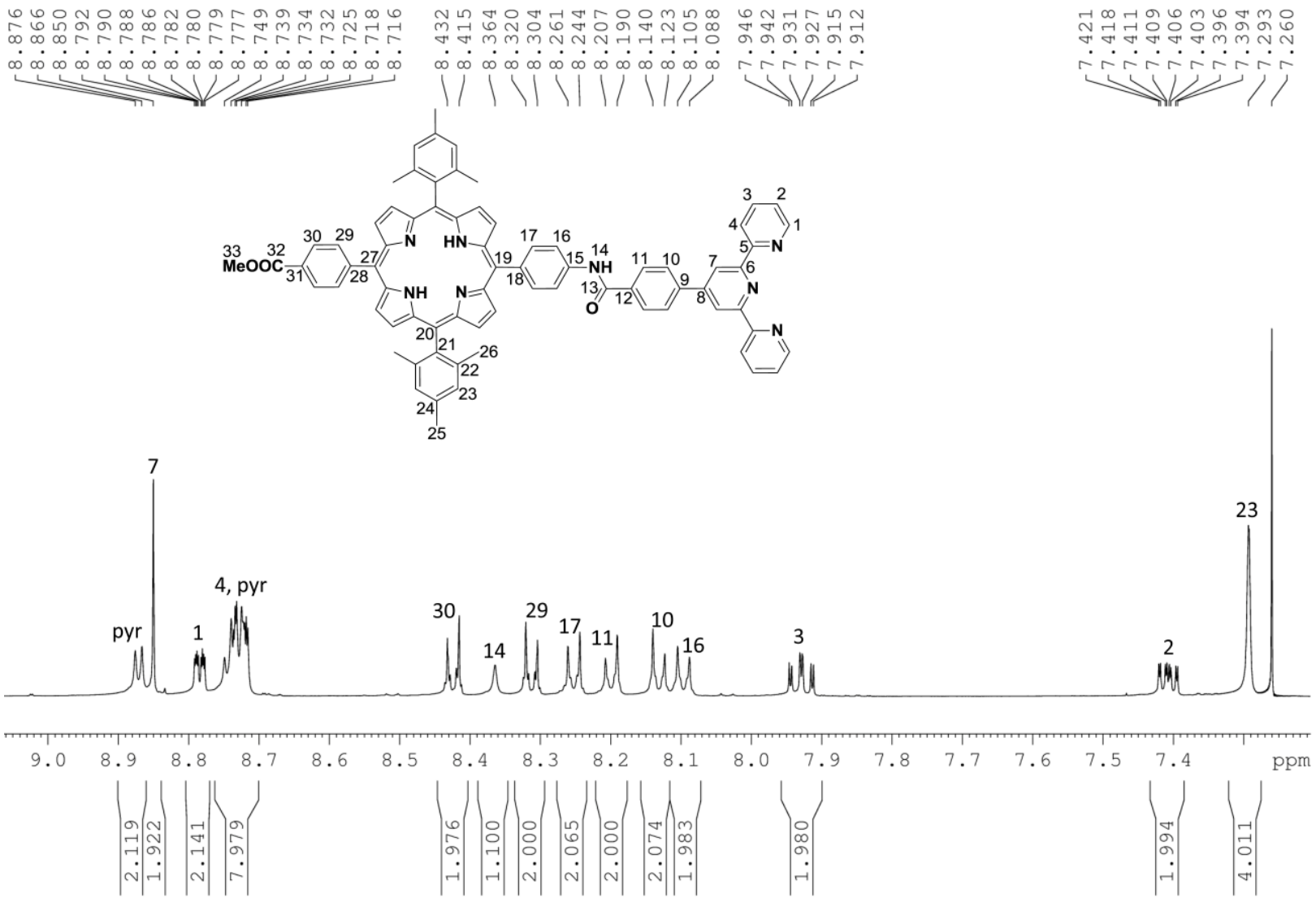

*Figure 2: Aromatic region of ^{1}H NMR spectrum of compound **H_2-P-terpy** in $CDCl_3$.*

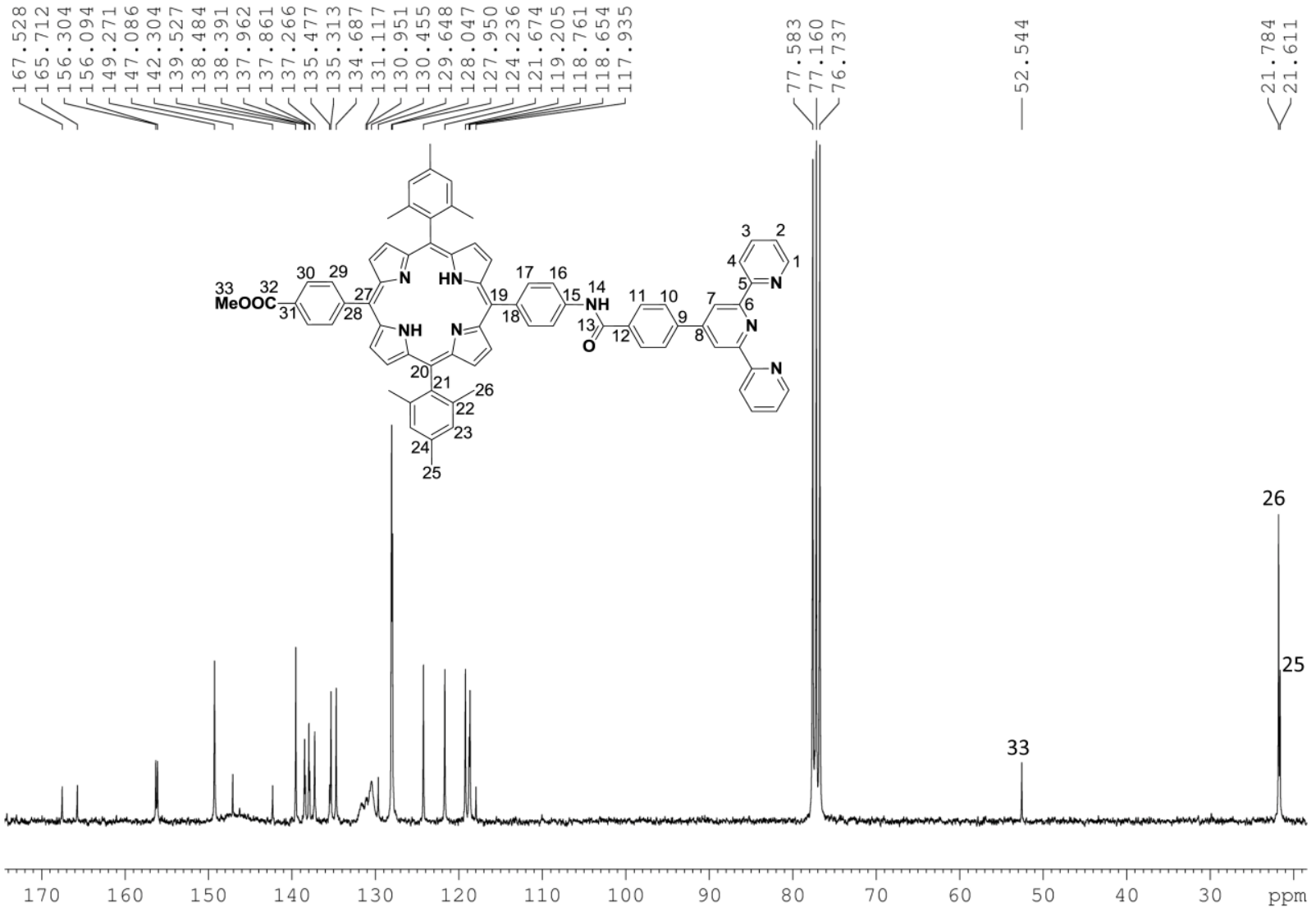

*Figure 3: ^{13}C NMR spectrum of compound **H_2-P-terpy** in $CDCl_3$.*

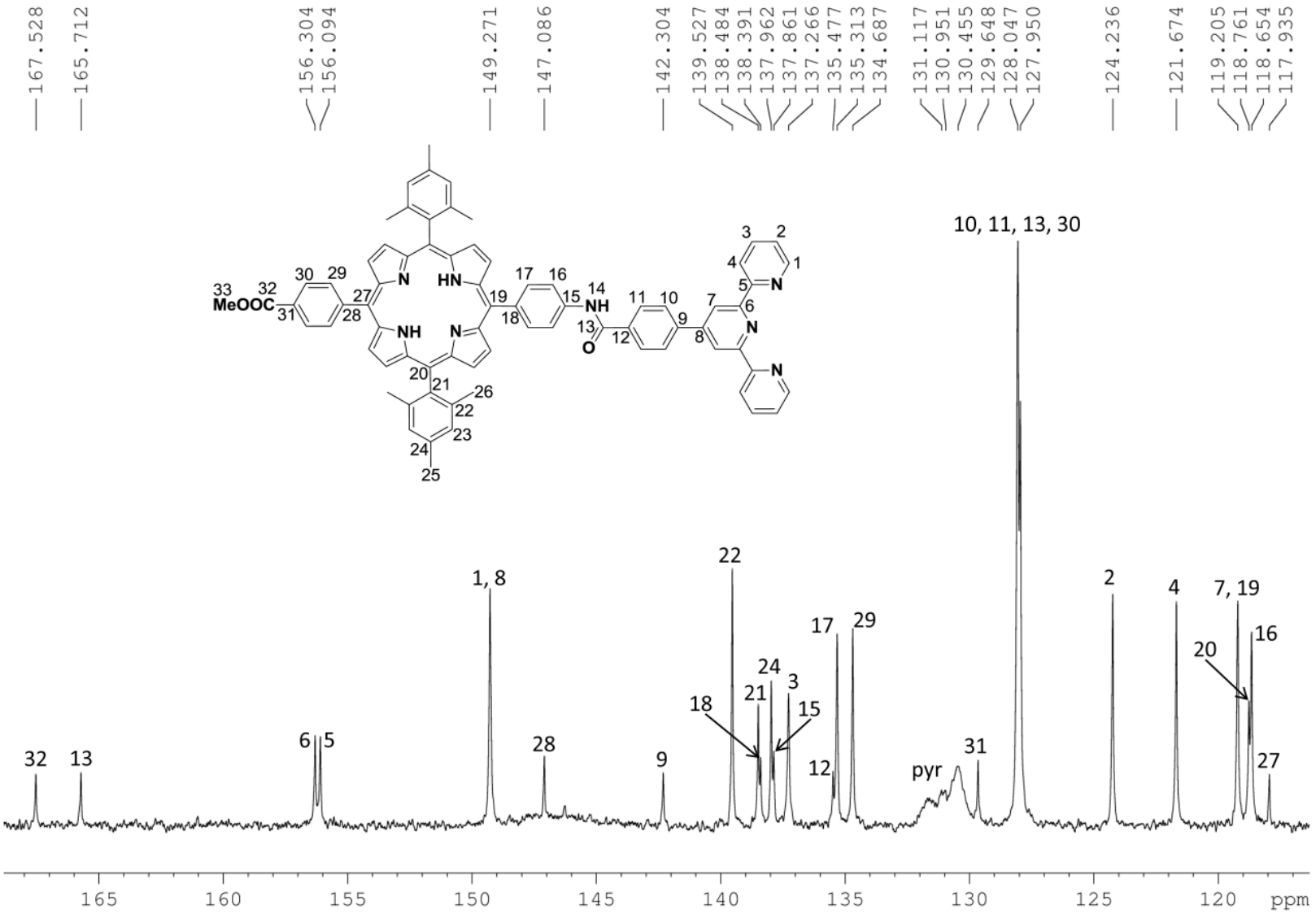

*Figure 4: Aromatic region of ^{13}C NMR spectrum of compound **H_2-P-terpy** in $CDCl_3$.*

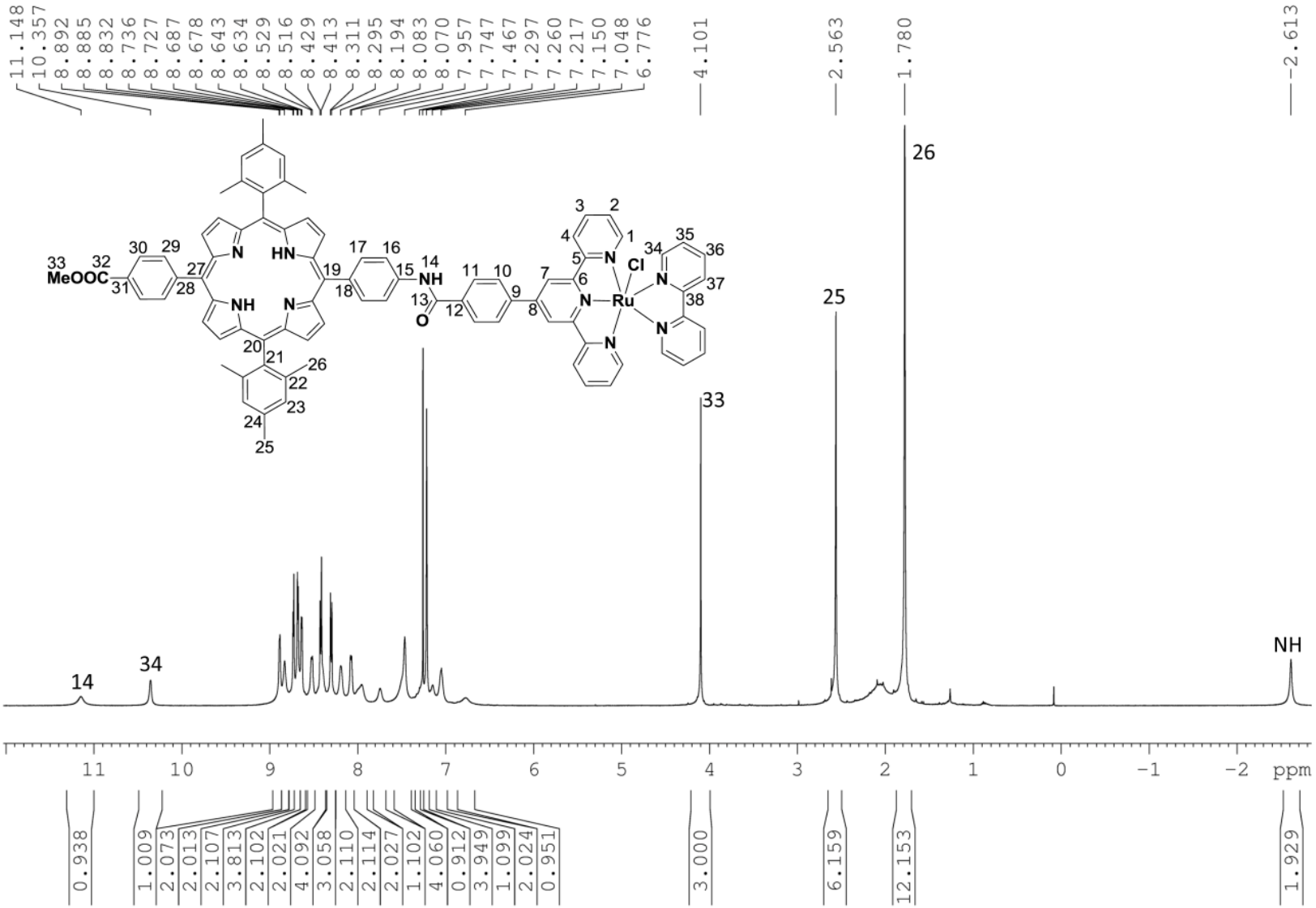

*Figure 5: ^{1}H NMR spectrum of compound **H_2-P-Ru** in $CDCl_3$.*

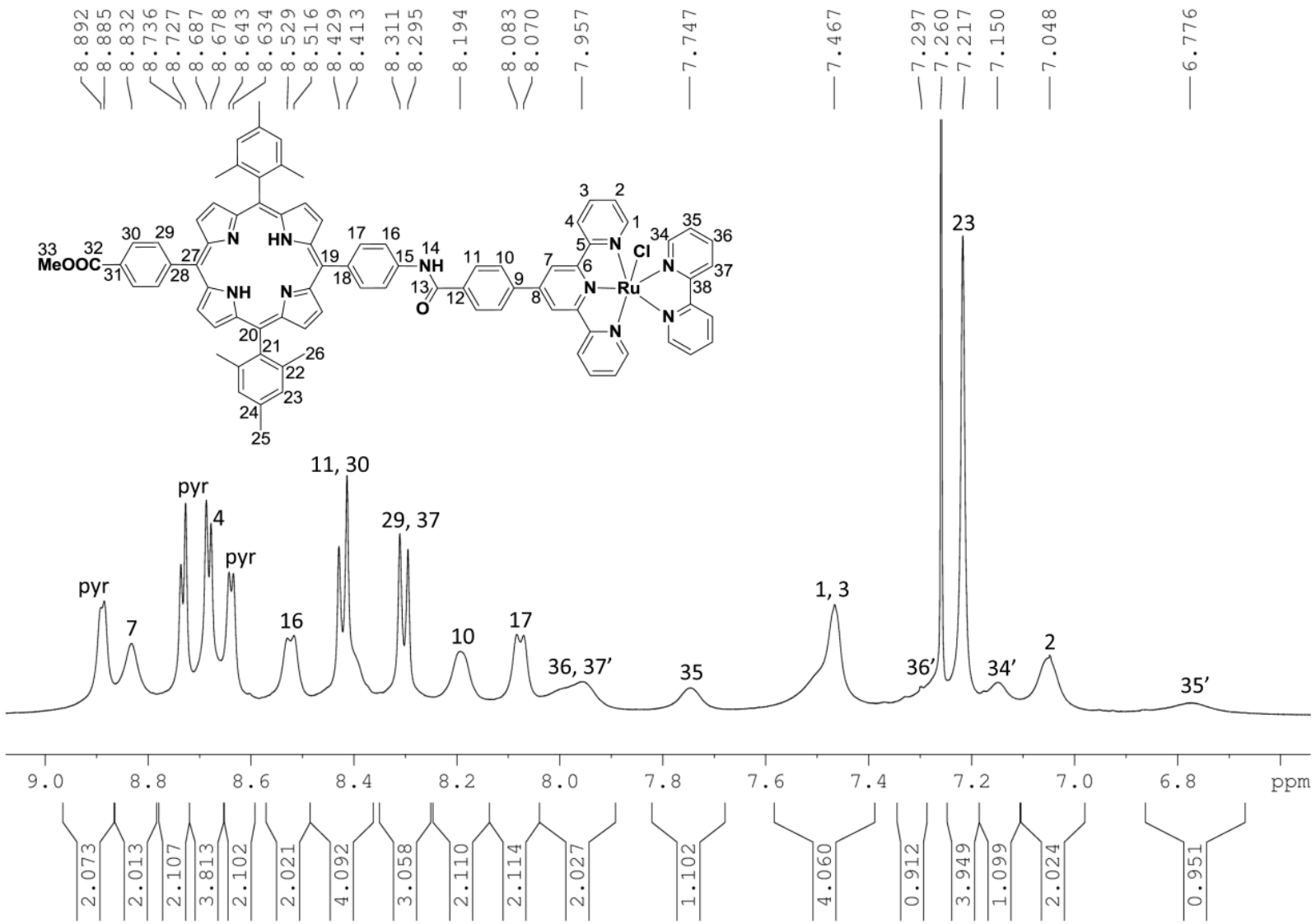

*Figure 6: Aromatic region of ^{1}H NMR spectrum of compound **H_2-P-Ru** in $CDCl_3$.*

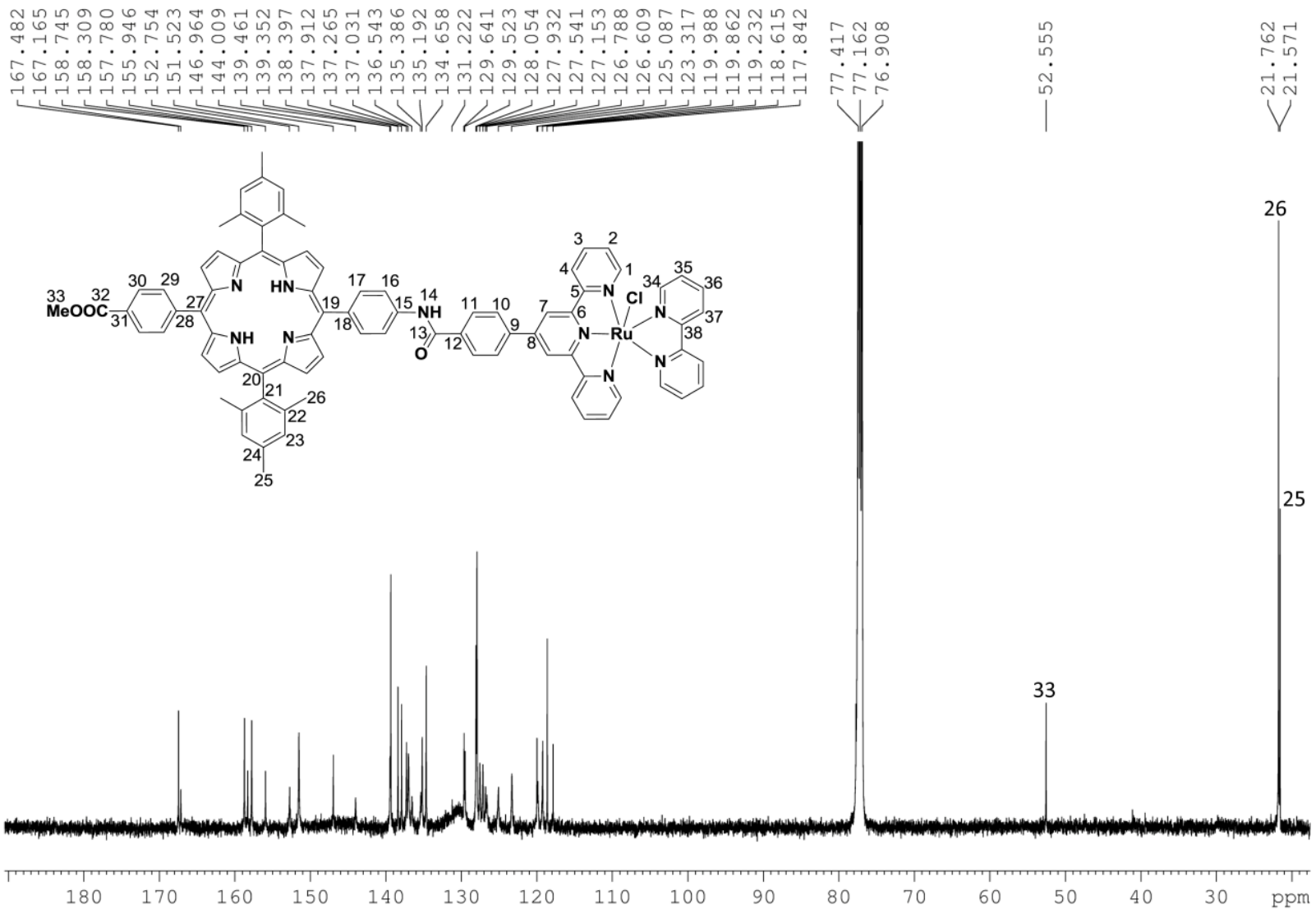

*Figure 7: ^{13}C NMR spectrum of compound **H_2-P-Ru** in $CDCl_3$.*

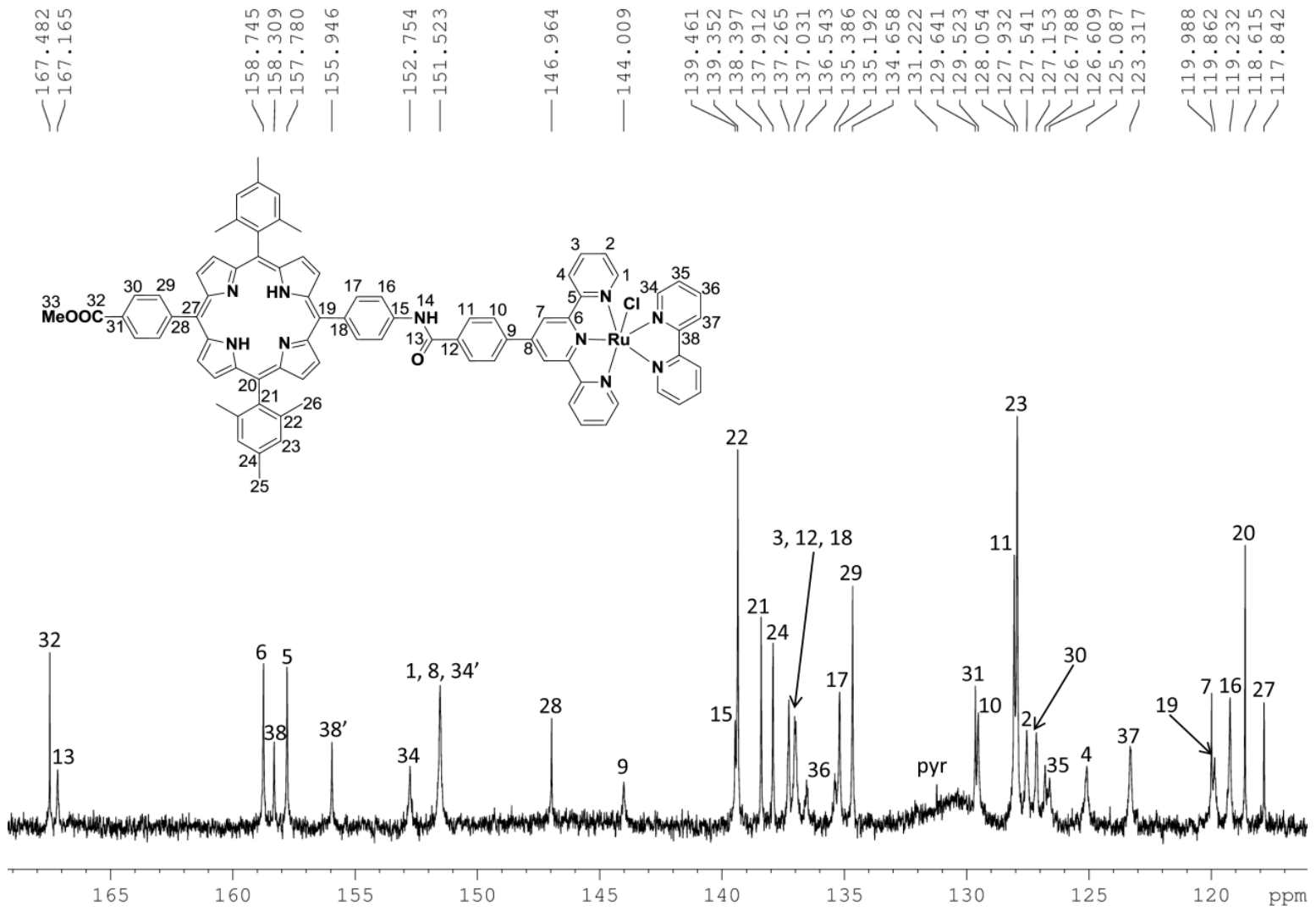

*Figure 8: Aromatic region of ^{13}C NMR spectrum of compound **H_2-P-Ru** in $CDCl_3$.*

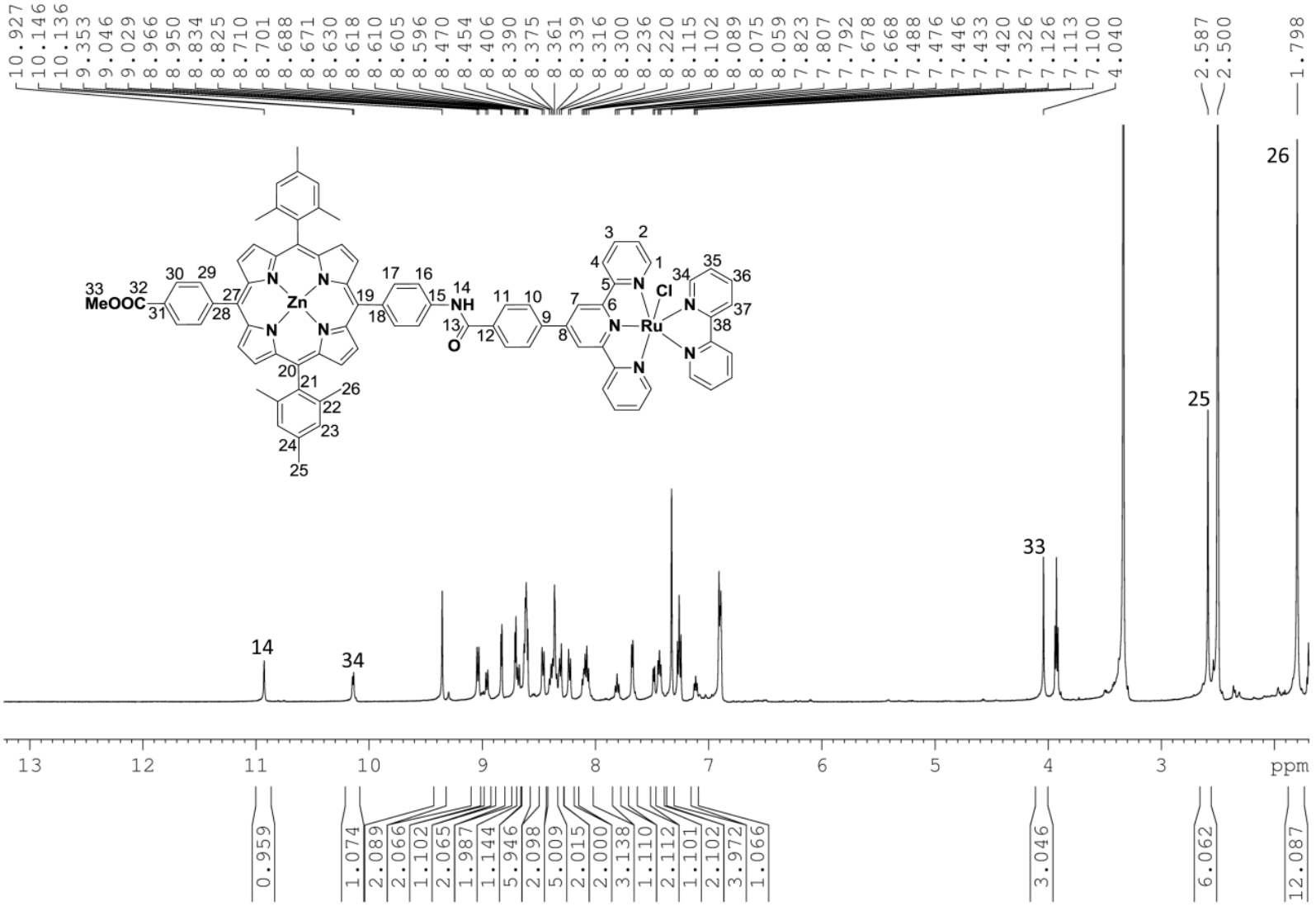

*Figure 9: ^{1}H NMR spectrum of compound **Zn-P-Ru** in DMSO-*d_6.

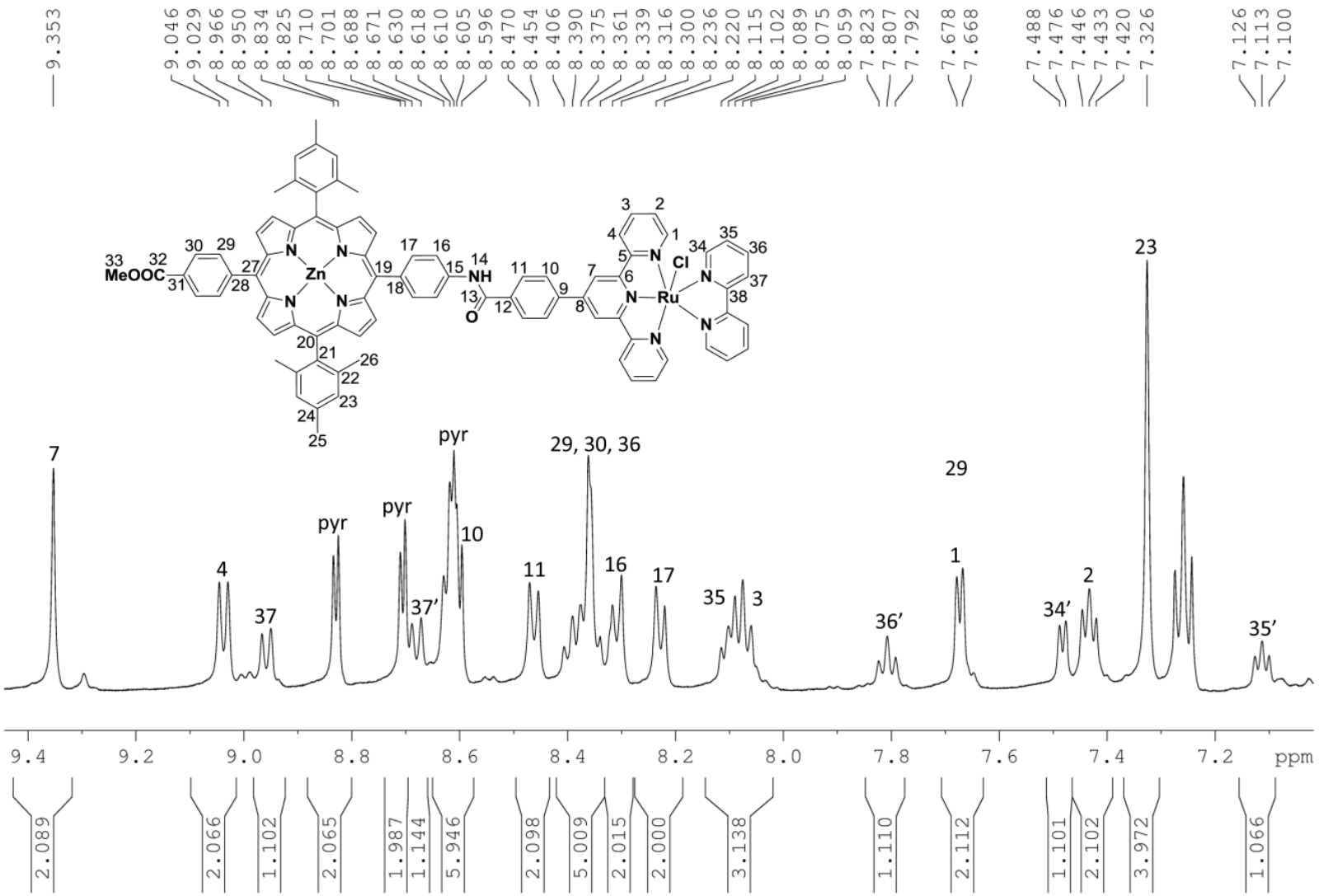

*Figure 10: Aromatic region of ^{1}H NMR spectrum of compound **Zn-P-Ru** in DMSO-d_6.*

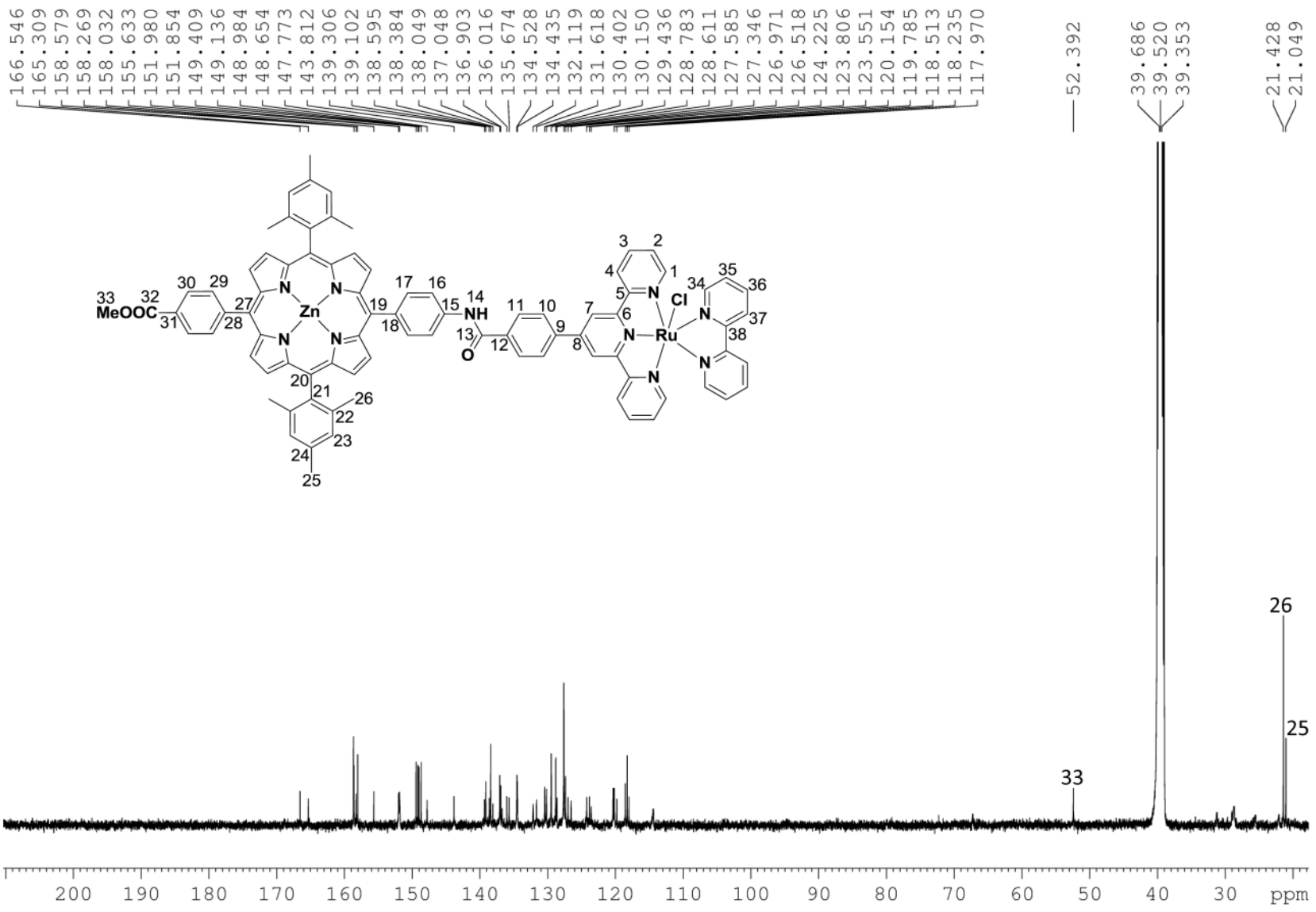

*Figure 11: ^{13}C NMR spectrum of compound **Zn-P-Ru** in DMSO-d_6.*

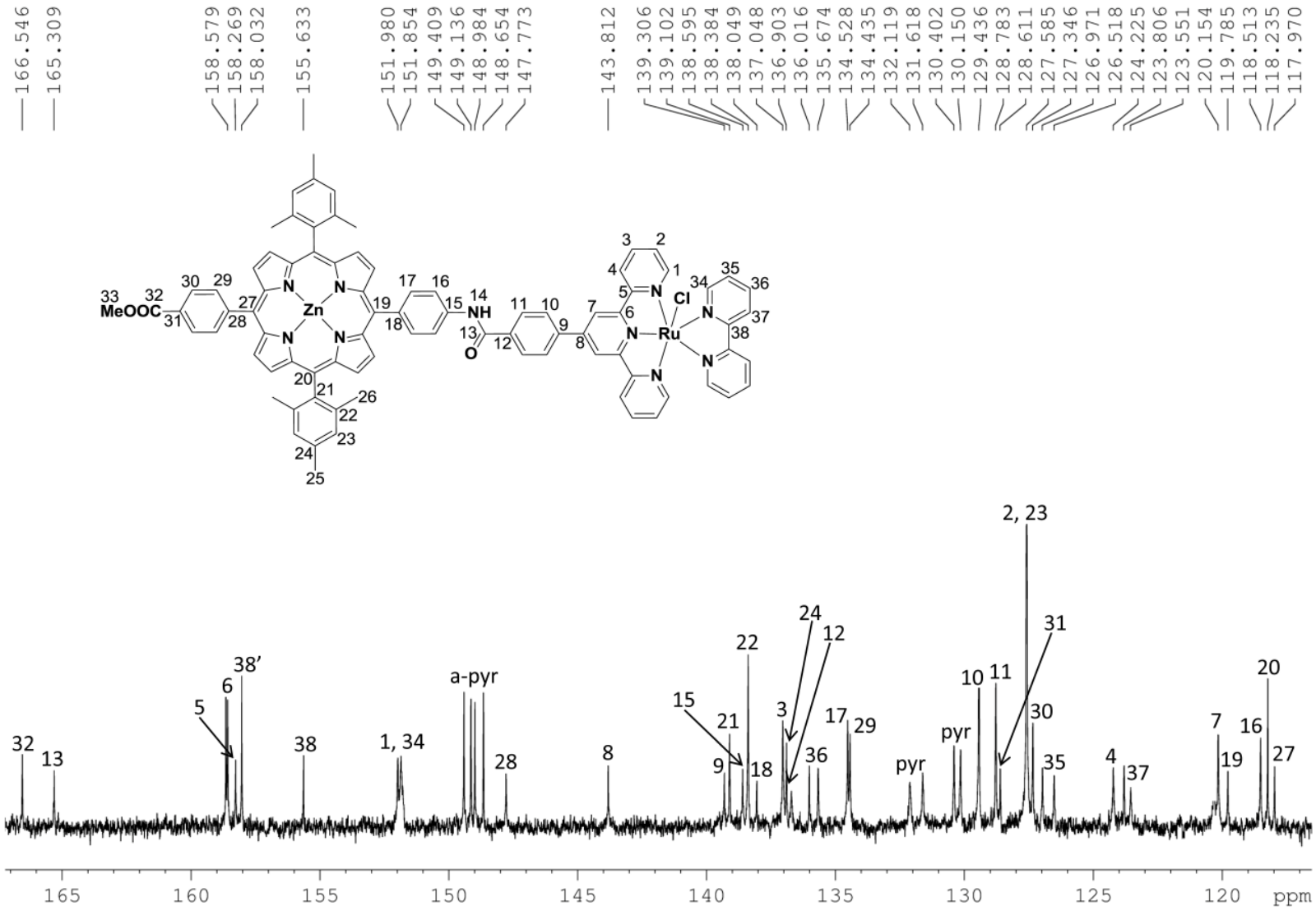

*Figure 12: Aromatic region of ^{13}C NMR spectrum of compound **Zn-P-Ru** in DMSO-d_6.*

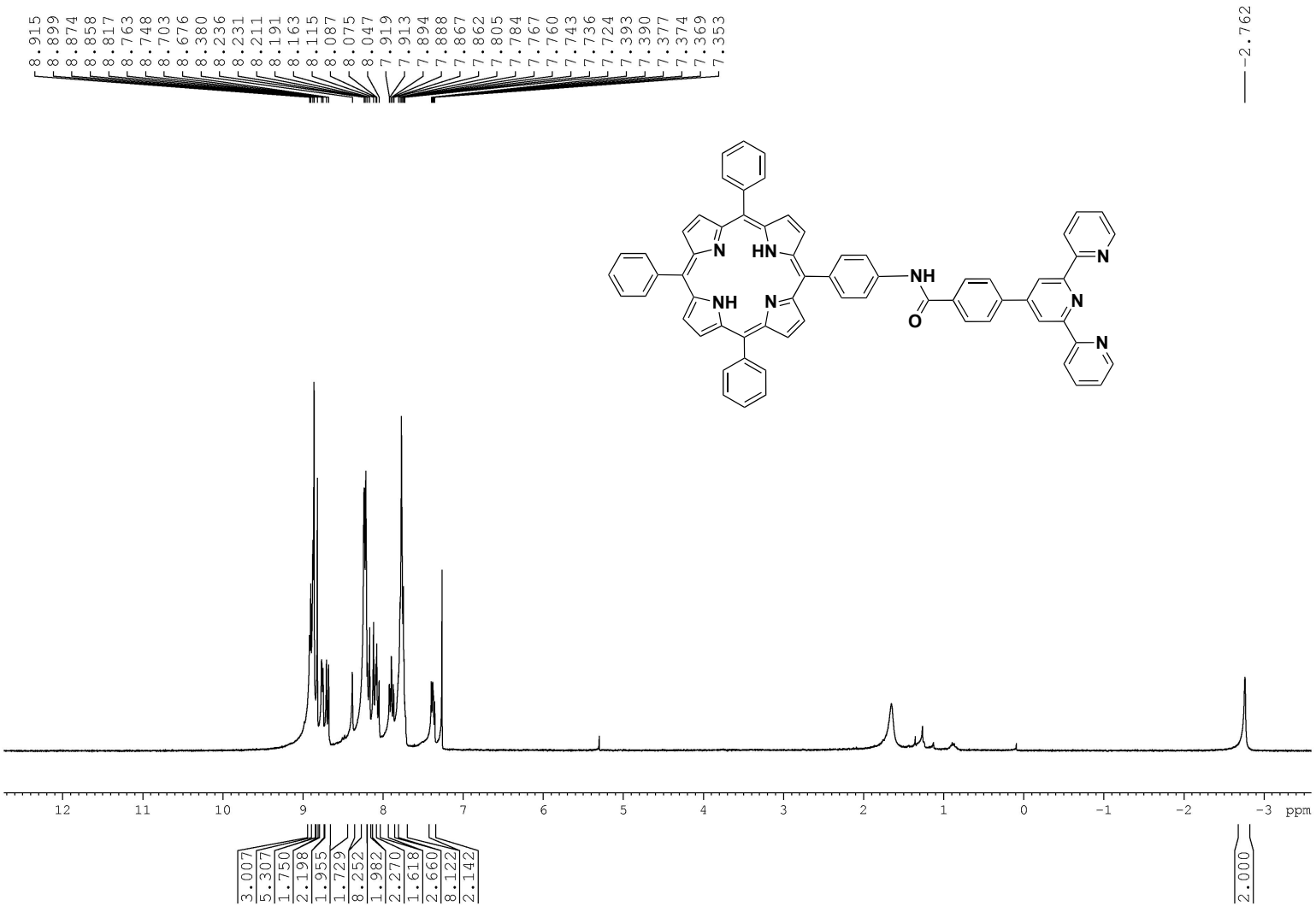

*Figure 13: : ^{1}H NMR spectrum of compound **H_2-TPP-terpy** in $CDCl_3$.*

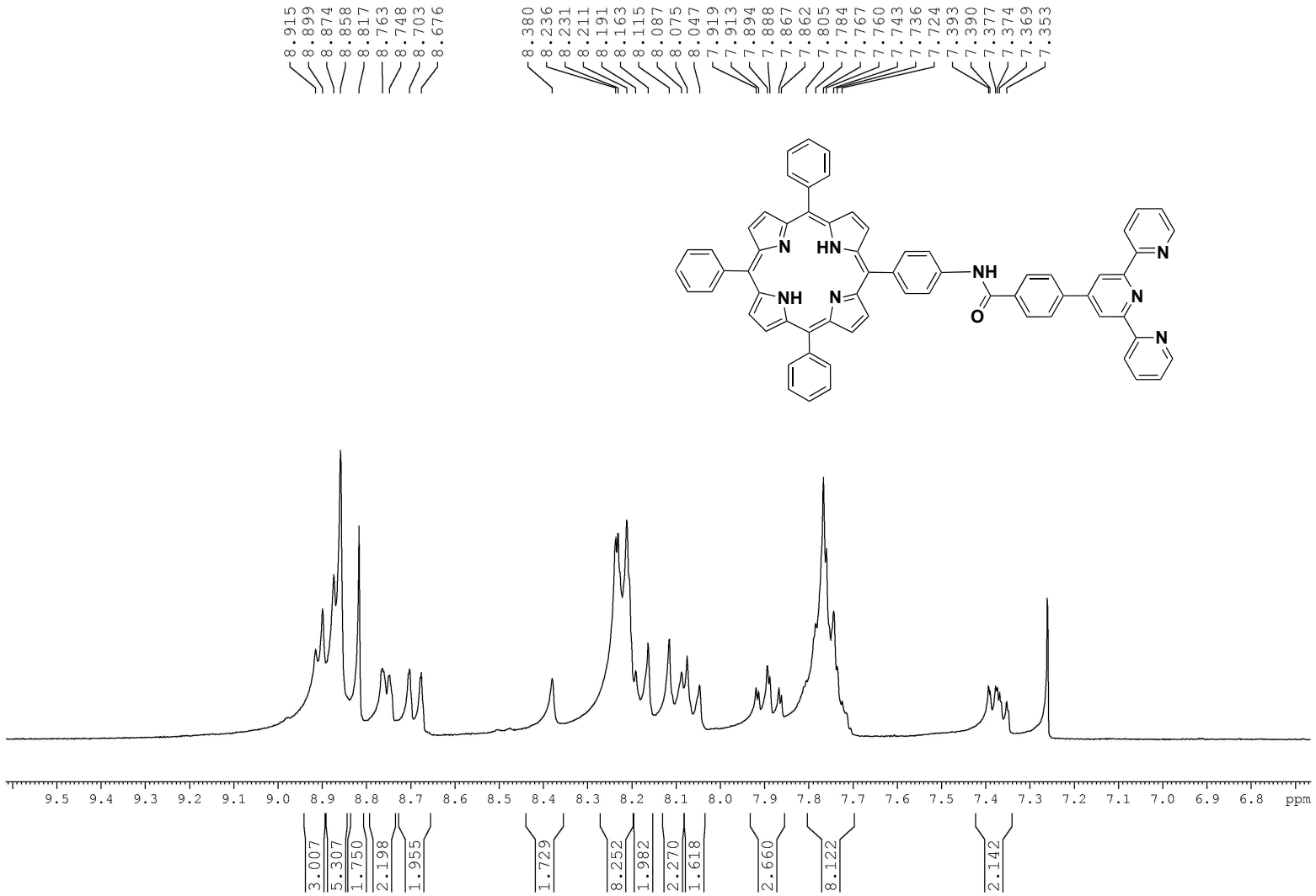

Figure 14: Aromatic region of ^{1}H NMR spectrum of compound H_2-TPP-terpy in $CDCl_3$.

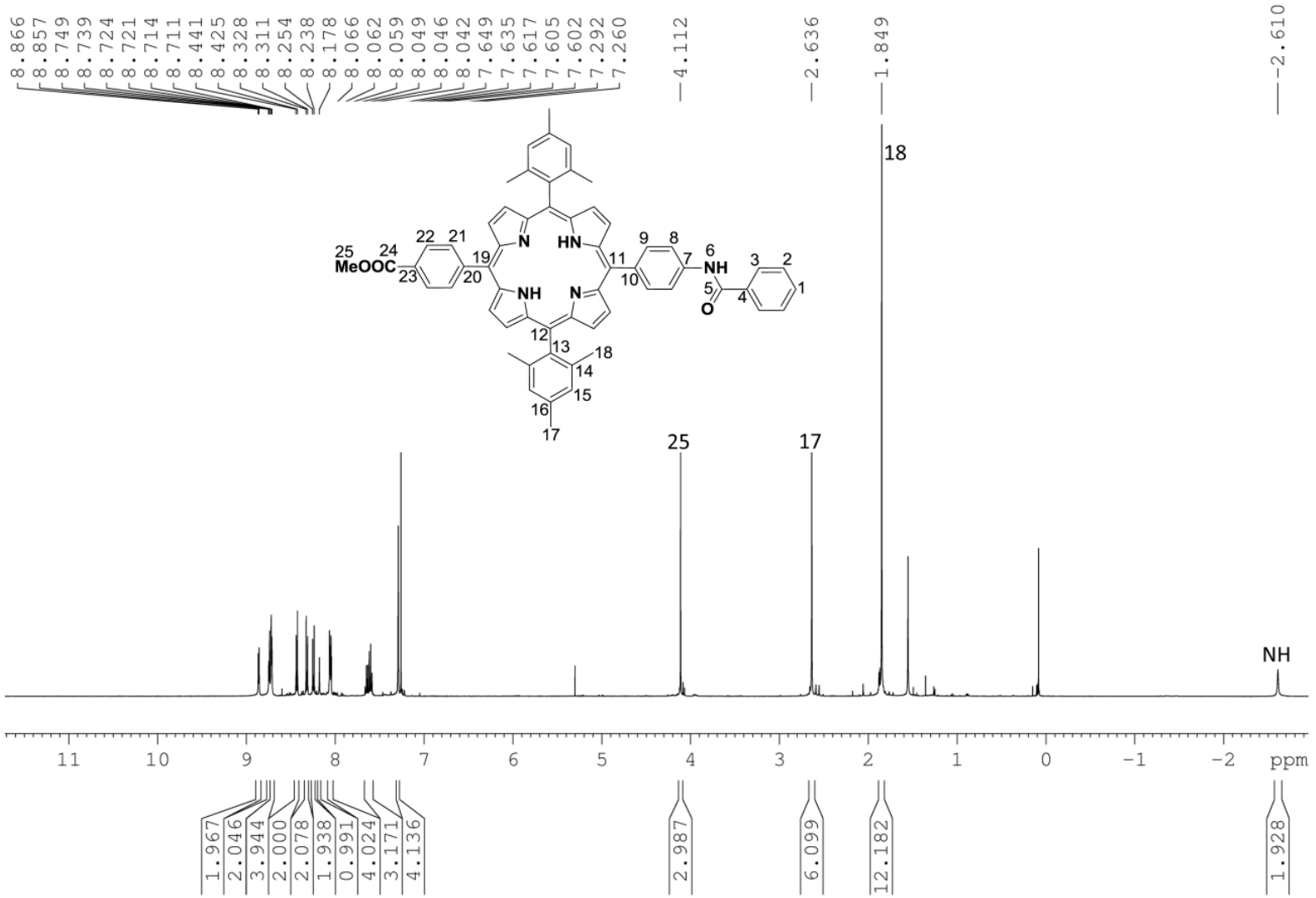

*Figure 15: ^{1}H NMR spectrum of compound **H_2-P** in $CDCl_3$.*

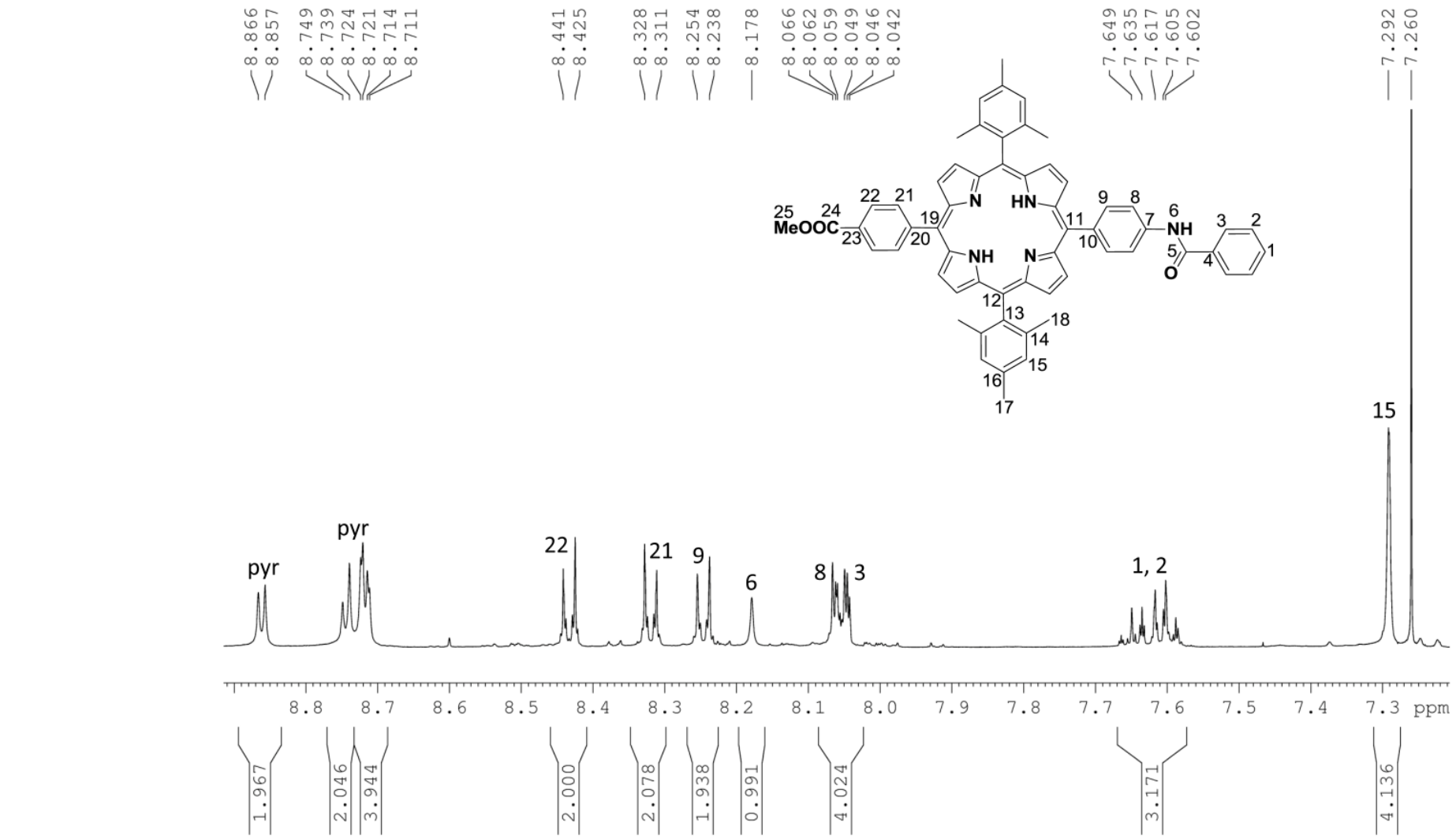

*Figure 16: Aromatic region of ^{1}H NMR spectrum of compound **H_2-P** in $CDCl_3$.*

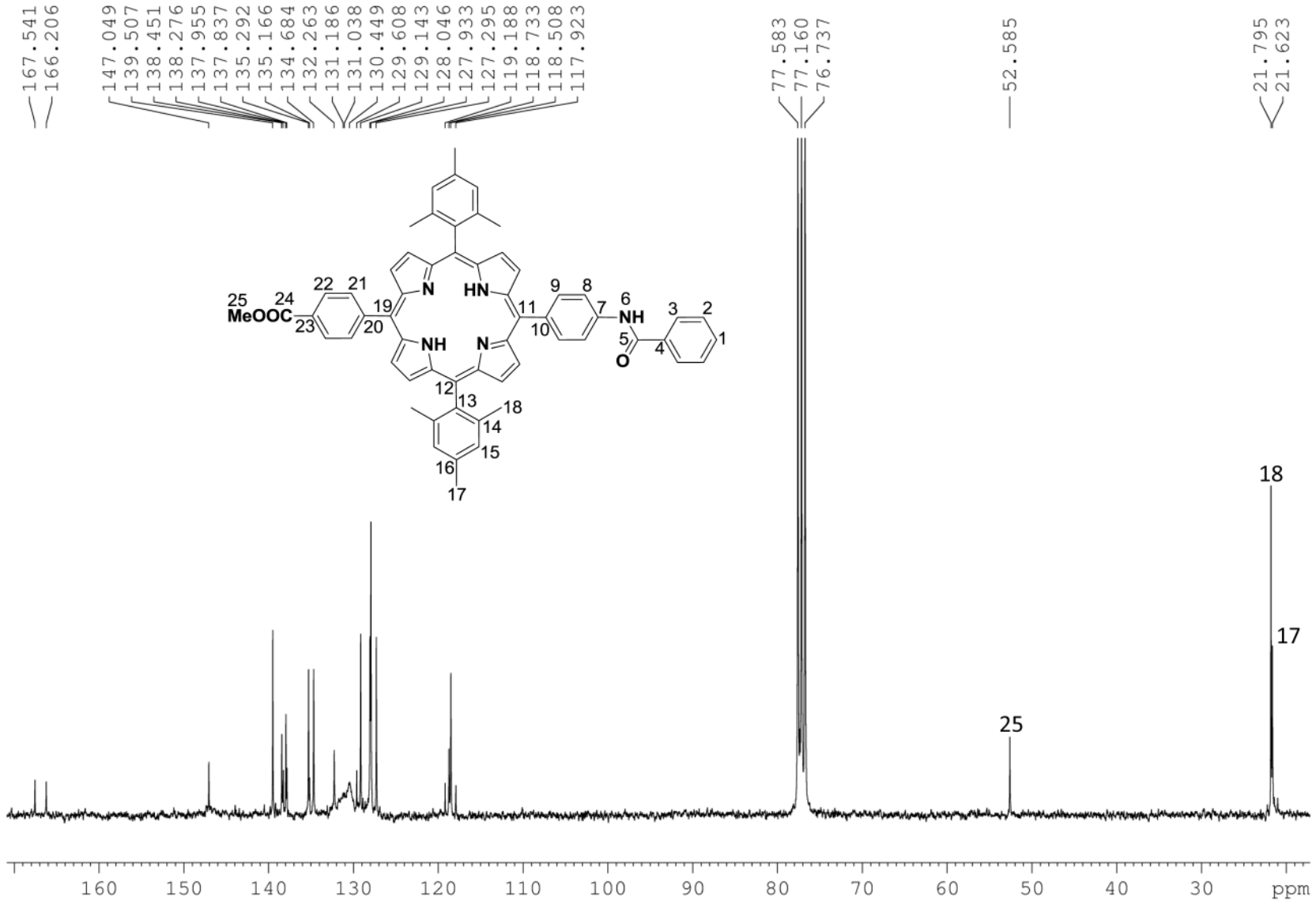

*Figure 17: ^{13}C NMR spectrum of compound **H_2-P** in $CDCl_3$.*

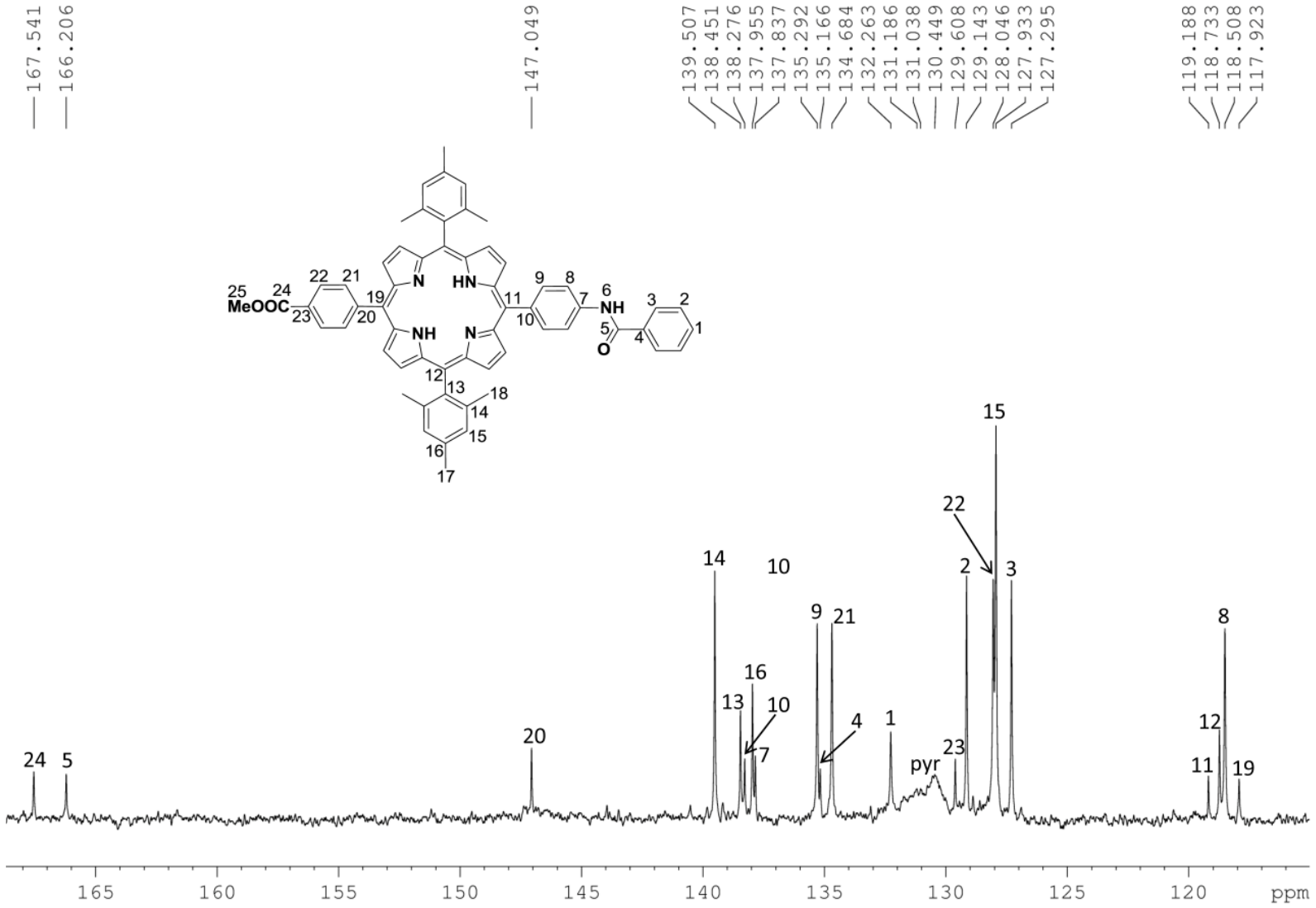

*Figure 18: Aromatic region of ^{13}C NMR spectrum of compound **H_2-P** in $CDCl_3$.*

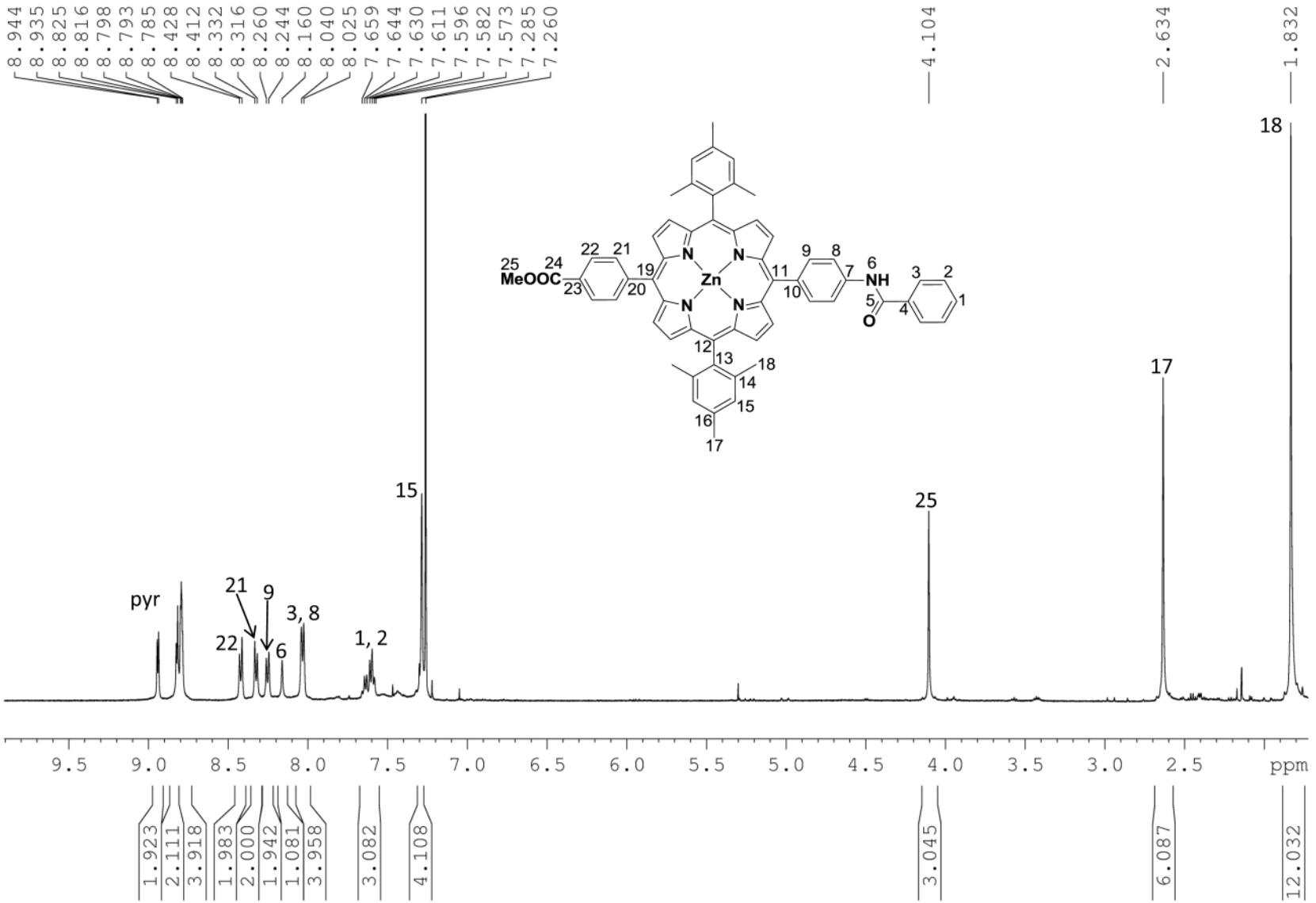

*Figure 19: ^{1}H NMR spectrum of compound **Zn-P** in $CDCl_3$.*